ME346 – Introduction to Molecular Simulations – Stanford University – Winter 2007

Handout 1. An Overview of Molecular Simulation

Wei Cai

September 26, 2005

Contents

1 Examples of molecular simulations

Pictures and movies of modern large scale molecular simulations can be downloaded from the course web site `http://micro.stanford.edu/~me346` (click "Course Materials"). Examples include plastic deformation in metals containing a crack, phase transformation induced by shock waves, nano-indentation of metal film, laser ablation on metal surface, etc. In each of these examples, molecular simulations not only produce beautiful pictures, but they also offer new understanding on the behavior of materials at the nano-scale. Many times such understanding provides new insights on how the materials would behave at the micro-scale and nano-scale. With unique capabilities to offer, molecular simulation has become a widely used tool for scientific investigation that complements our traditional way of doing science: experiment and theory. **The purpose of this course** is to provide the first introduction to molecular level simulations — how do they work, what questions can they answer, and how much can we trust their results — so that the simulation tools are no longer *black boxes* to us.

Students will develop a set of simulation codes in `Matlab` by themselves. (A simple Matlab tutorial written by Sigmon [5] may help you refresh your memory.) We will also give tutorial and exercise problems based on MD++, a molecular simulation package used in my research group. MD++ will be used for illustration in class as well as tools to solve homework problems.

2 What consists of a molecular dynamics?

In a molecular simulation, we view materials as a collection of discrete atoms. The atoms interact by exerting forces on each other and they follow the Newton's equation of motion. Based on the interaction model, a simulation compute the atoms' trajectories numerically. Thus a molecular simulation necessarily contains the following ingredients.

- The model that describes the interaction between atoms. This is usually called the interatomic potential: $V(\{\mathbf{r}_i\})$, where $\{\mathbf{r}_i\}$ represent the position of all atoms.
- Numerical integrator that follows the atoms equation of motion. This is the heart of the simulation. Usually, we also need auxiliary algorithms to set up the initial and boundary conditions and to monitor and control the systems state (such as temperature) during the simulation.
- Extract useful data from the *raw* atomic trajectory information. Compute materials properties of interest. Visualization.

We will start our discussion with a simple but complete example that illustrates a lot of issues in simulation, although it is not on the molecular scale. We will simulate the orbit of the Earth around the Sun. After we have understood how this simulation works (in a couple of lectures), we will then discuss how molecular simulations differ from this type of "macro"-scale simulations.

3 Newton's equation of motion

Throughout this course, we limit our discussions to classical dynamics (no quantum mechanics). The dynamics of classical objects follow the three laws of Newton. Let's review the Newton's laws.

Figure 1: Sir Isaac Newton (1643-1727 England).

First law: Every object in a state of uniform motion tends to remain in that state of motion unless an external force is applied to it. This is also called the *Law of inertia*.

Second law: An object's mass m, its acceleration $\mathbf{a}$, and the applied force $\mathbf{F}$ are related by

$\mathbf{F} = m\mathbf{a}$. The bold font here emphasizes that the acceleration and force are vectors. Here they point to the same direction. According to Newton, a force causes only a change in velocity ($\mathbf{v}$) but is not needed to maintain the velocity as Aristotle claimed (erroneously).

Third law: For every action there is an equal and opposite reaction.

The *second law* gives us the equation of motion for classical particles. Consider a particle (be it an atom or the Earth! depending on which scale we look at the world), its position is described by a vector $\mathbf{r} = (x, y, z)$. The velocity is how fast $\mathbf{r}$ changes with time and is also a vector: $\mathbf{v} = d\mathbf{r}/dt = (v_x, v_y, v_z)$. In component form, $v_x = dx/dt$, $v_y = dy/dt$, $v_z = dz/dt$. The acceleration vector is then time derivative of velocity, i.e., $\mathbf{a} = d\mathbf{v}/dt$. Therefore the particle's equation of motion can be written as

$$\frac{d^2\mathbf{r}}{dt^2} = \frac{\mathbf{F}}{m} \tag{1}$$

To complete the equation of motion, we need to know how does the force $\mathbf{F}$ in turn depends on position $\mathbf{r}$.

As an example, consider the Earth orbiting around the Sun. Assume the Sun is fixed at origin (0,0,0). The gravitational force on the Earth is,

$$\mathbf{F} = -\frac{GmM}{|\mathbf{r}|^2} \cdot \hat{\mathbf{e}}_r \tag{2}$$

where $\hat{\mathbf{e}}_r = \mathbf{r}/|\mathbf{r}|$ is the unit vector along $\mathbf{r}$ direction. $|\mathbf{r}| = \sqrt{x^2 + y^2 + z^2}$ is the magnitude of $\mathbf{r}$. m is the mass of the Earth (5.9736×10^{24}kg), M is mass of the Sun (1.9891×10^{30}kg), and $G = 6.67259 \times 10^{-11}\mathrm{N} \cdot \mathrm{m}^2/\mathrm{kg}^2$ is gravitational constant. If we introduce a potential field (the gravitational field of the Sun),

$$V(\mathbf{r}) = -\frac{GmM}{|\mathbf{r}|} \tag{3}$$

Then the gravitational force can be written as minus the spatial derivative of the potential,

$$\mathbf{F} = -\frac{dV(\mathbf{r})}{d\mathbf{r}} \tag{4}$$

In component form, this equation should be interpreted as,

$$\begin{aligned} F_x &= -\frac{dV(x,y,z)}{dx} \\ F_y &= -\frac{dV(x,y,z)}{dy} \\ F_z &= -\frac{dV(x,y,z)}{dz} \end{aligned}$$

Now we have the complete equation of motion for the Earth:

$$\frac{d^2\mathbf{r}}{dt^2} = -\frac{1}{m}\frac{dV(\mathbf{r})}{d\mathbf{r}} \tag{5}$$

in component form, this reads,

$$\begin{aligned}\frac{d^2x}{dt^2} &= -\frac{GMx}{|\mathbf{r}|^3} \\ \frac{d^2y}{dt^2} &= -\frac{GMy}{|\mathbf{r}|^3} \\ \frac{d^2z}{dt^2} &= -\frac{GMz}{|\mathbf{r}|^3}\end{aligned}$$

In fact, most of the system we will study has a interaction potential $V(\mathbf{r})$, from which the equation of motion can be specified through Eq. (5). $V(\mathbf{r})$ is the *potential energy* of the system. On the other hand, the *kinetic energy* is given by the velocity,

$$E_{\text{kin}} = \frac{1}{2}m|\mathbf{v}|^2 \tag{6}$$

The total energy is the sum of *potential* and *kinetic* energy contributions,

$$E_{\text{tot}} = E_{\text{kin}} + V \tag{7}$$

When we express the total energy as a function of particle position $\mathbf{r}$ and momentum $\mathbf{p} = m\mathbf{v}$, it is called the *Hamiltonian* of the system,

$$H(\mathbf{r}, \mathbf{p}) = \frac{|\mathbf{p}|^2}{2m} + V(\mathbf{r}) \tag{8}$$

The Hamiltonian (i.e. the total energy) is a conserved quantity as the particle moves. To see this, let us compute its time derivative,

$$\begin{aligned}\frac{dE_{\text{tot}}}{dt} &= m\mathbf{v}\cdot\frac{d\mathbf{v}}{dt} + \frac{dV(\mathbf{r})}{d\mathbf{r}}\cdot\frac{d\mathbf{r}}{dt} \\ &= m\frac{d\mathbf{r}}{dt}\cdot\left[-\frac{1}{m}\frac{dV(\mathbf{r})}{d\mathbf{r}}\right] + \frac{dV(\mathbf{r})}{d\mathbf{r}}\cdot\frac{d\mathbf{r}}{dt} \\ &= 0\end{aligned} \tag{9}$$

Therefore the total energy is conserved if the particle follows the Newton's equation of motion in a conservative force field (when force can be written in terms of spatial derivative of a potential field), while the kinetic energy and potential energy can interchange with each other. The Newton's equation of motion can also be written in the Hamiltonian form,

$$\frac{d\mathbf{r}}{dt} = \frac{\partial H(\mathbf{r}, \mathbf{p})}{\partial \mathbf{p}} \tag{10}$$

$$\frac{d\mathbf{p}}{dt} = -\frac{\partial H(\mathbf{r}, \mathbf{p})}{\partial \mathbf{r}} \tag{11}$$

Hence,

$$\frac{dH}{dt} = \frac{\partial H(\mathbf{r}, \mathbf{p})}{\partial \mathbf{r}}\cdot\frac{d\mathbf{r}}{dt} + \frac{\partial H(\mathbf{r}, \mathbf{p})}{\partial \mathbf{p}}\cdot\frac{d\mathbf{p}}{dt} = 0 \tag{12}$$

Figure 2: Sir William Rowan Hamilton (1805-1865 Ireland).

4 A simple numerical integrator: Verlet algorithm

A dynamical simulation computes the particle position as a function of time (i.e. its trajectory) given its initial position and velocity. This is called the initial value problem (IVP). Because the Newton's equation of motion is second order in $\mathbf{r}$, the initial condition needs to specify both particle position and velocity.

To solve the equation of motion on a computer, the first thing we need is to discretize the time. In other words, we will solve for $\mathbf{r}(t)$ on a series of time instances t_i. Usually the time axis is discretized uniformly: $t_i = i \cdot \Delta t$, where Δt is called the *time step*. Again, the task of the simulation algorithm is to find $\mathbf{r}(t_i)$ for $i = 1, 2, 3, \cdots$ given $\mathbf{r}(0)$ and $\mathbf{v}(0)$.

The Verlet algorithm begins by approximating $d^2\mathbf{r}(t)/dt^2$,

$$\frac{d^2\mathbf{r}(t)}{dt^2} \approx \frac{\mathbf{r}(t+\Delta t) - 2\mathbf{r}(t) + \mathbf{r}(t-\Delta t)}{\Delta t^2} \tag{13}$$

Thus

$$\frac{\mathbf{r}(t+\Delta t) - 2\mathbf{r}(t) + \mathbf{r}(t-\Delta t)}{\Delta t^2} = -\frac{1}{m}\frac{dV(\mathbf{r}(t))}{dr} \tag{14}$$

$$\mathbf{r}(t+\Delta t) = 2\mathbf{r}(t) - \mathbf{r}(t-\Delta t) - \Delta t \cdot \frac{1}{m} \cdot \frac{dV(\mathbf{r}(t))}{dr} \tag{15}$$

Therefore, we can solve $\mathbf{r}(t+\Delta t)$ as along as we know $\mathbf{r}(t)$ and $\mathbf{r}(t-\Delta t)$. In other words, if we know $\mathbf{r}(0)$ and $\mathbf{r}(-\Delta t)$, we can solve for all $\mathbf{r}(t_i)$ for $i = 1, 3, 4, \cdots$.

Question: Notice that to start the Verlet algorithm we need $\mathbf{r}(0)$ and $\mathbf{r}(-\Delta t)$. However, the initial condition of a simulation is usually given in $\mathbf{r}(0)$ and $\mathbf{v}(0)$. How do we start the simulation when this initial condition is specified?

References

1. Alan and Tildesley, *Computer Simulation of Liquids*, (Oxford University Press, 1987) pp.71-80.

2. Frenkel and Smit, *Understanding Molecular Simulation: From Algorithms to Applications*, 2nd ed. (Academic Press, 2002).

3. Bulatov and Cai, *Computer Simulation of Dislocations*, (Oxford University Press, 2006) pp.49-51.

4. Landau and Lifshitz, *Mechanics*, (Butterworth-Heinemann, 1976).

5. Kermit Sigmon, *Matlab Primer*, Third Edition, `http://ise.stanford.edu/Matlab/matlab-primer.pdf`

ME346 – Introduction to Molecular Simulations – Stanford University – Winter 2007

Handout 2. Numerical Integrators I

Wei Cai

January 12, 2007

Contents

1 Which integrator to use?

In the previous lecture we looked at a very simple simulation. The Newton's equation of motion is integrated numerically by the original Verlet algorithm. There are many algorithms that can be used to integrate an ordinary differential equation (ODE). Each has a its own advantages and disadvantages. In this lecture, we will look into more details at the numerical integrators. Our goal is to be able to make sensible choices when we need to select a numerical integrator for a specific simulation.

What questions should we ask when choosing an integrator? Obviously, we would like something that is both fast and accurate. But usually there are more issues we should care about. Here are a list of the most important ones (Allen and Tildesley 1987):

- Order of accuracy
- Range of stability
- Reversibility
- Speed (computation time per step)
- Memory requirement (as low as possible)
- Satisfying conservation law

- Simple form and easy to implement

Item 1 and 2 (especially 2) are important to allow the use of long time steps, which makes the simulation more efficient.

2 Several versions of Verlet algorithm

The Verlet algorithm used in the previous lecture can be written as,

$$\mathbf{r}(t+\Delta t) = 2\mathbf{r}(t) - \mathbf{r}(t-\Delta t) + \mathbf{a}(t)\cdot\Delta t^2 \tag{1}$$

where

$$\mathbf{a}(t) = -\frac{1}{m}\frac{dV(\mathbf{r}(t))}{d\mathbf{r}(t)} \tag{2}$$

While this is enough to compute the entire trajectory of the particle, it does not specify the velocity of the particle. Many times, we would like to know the particle velocity as a function of time as well. For example, the velocity is needed to compute kinetic energy and hence the total energy of the system. One way to compute velocity is to use the following approximation,

$$\mathbf{v}(t) \equiv \frac{d\mathbf{r}(t)}{dt} \approx \frac{\mathbf{r}(t+\Delta t) - \mathbf{r}(t-\Delta t)}{2\Delta t} \tag{3}$$

Question: if the initial condition is given in terms of $\mathbf{r}(0)$ *and* $\mathbf{v}(0)$*, how do we use the Verlet algorithm?*
Answer: The Verlet algorithm can be used to compute $\mathbf{r}(n\Delta t)$ for $n = 1, 2, \cdots$ provided $\mathbf{r}(-\Delta t)$ and $\mathbf{r}(0)$ are known. The task is to solve for $\mathbf{r}(-\Delta t)$ given $\mathbf{r}(0)$ and $\mathbf{v}(0)$. This is achieved from the following two equations,

$$\frac{\mathbf{r}(\Delta t) - \mathbf{r}(-\Delta t)}{2\Delta t} = \mathbf{v}(0) \tag{4}$$

$$\frac{\mathbf{r}(\Delta t) - 2\mathbf{r}(0) + \mathbf{r}(-\Delta t)}{\Delta t^2} = -\frac{1}{m}\left.\frac{dV(\mathbf{r}(t))}{d\mathbf{r}(t)}\right|_{t=0} \tag{5}$$

Exercise: express $\mathbf{r}(-\Delta t)$ *and* $\mathbf{r}(\Delta t)$ *in terms of* $\mathbf{r}(0)$ *and* $\mathbf{v}(0)$.

Therefore, $\mathbf{r}(-\Delta t)$ and $\mathbf{r}(\Delta t)$ are solved together. During the simulation, we only know $\mathbf{v}(t)$ after we have computed $(\mathbf{t}+\mathbf{\Delta t})$. These are the (slight) inconveniences of the (original) Verlet algorithm. As we will see later, in this algorithm the accuracy of velocity calculation is not very high (not as high as particle positions). Several modifications of the Verlet algorithms were introduced to give a better treatment of velocities.

The leap-frog algorithm works as follows,

$$\mathbf{v}(t + \Delta t/2) = \mathbf{v}(t - \Delta t/2) + \mathbf{a}(t) \cdot \Delta t \quad (6)$$

$$\mathbf{r}(t + \Delta t) = \mathbf{r}(t) + \mathbf{v}(t + \Delta t/2) \cdot \Delta t \quad (7)$$

Notice that the velocity and position are not stored at the same time slices. Their values are updated in alternation, hence the name "leap-frog". For a nice illustration see (Allen and Tildesley 1987). This algorithm also has the draw back that $\mathbf{v}$ and $\mathbf{r}$ are not known simultaneously. To get velocity at time t, we can use the following approximation,

$$\mathbf{v}(t) \approx \frac{\mathbf{v}(t - \Delta t/2) + \mathbf{v}(t + \Delta t/2)}{2} \quad (8)$$

The velocity Verlet algorithm solves this problem in a better way. The algorithm reads,

$$\mathbf{r}(t + \Delta t) = \mathbf{r}(t) + \mathbf{v}(t)\Delta t + \frac{1}{2}\mathbf{a}(t)\Delta t^2 \quad (9)$$

$$\mathbf{v}(t + \Delta t/2) = \mathbf{v}(t) + \frac{1}{2}\mathbf{a}(t)\Delta t \quad (10)$$

$$\mathbf{a}(t + \Delta t) = -\frac{1}{m}\frac{dV(\mathbf{r}(t + \Delta t))}{d\mathbf{r}(t + \Delta t)} \quad (11)$$

$$\mathbf{v}(t + \Delta t) = \mathbf{v}(t + \Delta t/2) + \frac{1}{2}\mathbf{a}(t + \Delta t)\Delta t \quad (12)$$

Exercise: show that both leap-frog and velocity Verlet algorithms gives identical results as the original Verlet algorithm (except for floating point truncation error).

3 Order of accuracy

How accurate are the Verlet-family algorithms? Let's take a look at the original Verlet first. Consider the trajectory of the particle as a continuous function of time, i.e. $\mathbf{r}(t)$. Let us Taylor expand this function around a given time t.

$$\mathbf{r}(t + \Delta t) = \mathbf{r}(t) + \frac{d\mathbf{r}(t)}{dt}\Delta t + \frac{1}{2}\frac{d^2\mathbf{r}(t)}{dt^2}\Delta t^2 + \frac{1}{3!}\frac{d^3\mathbf{r}(t)}{dt^3}\Delta t^3 + \mathcal{O}(\Delta t^4) \ , \quad (13)$$

where $\mathcal{O}(\Delta t^4)$ means that error of this expression is on the order of Δt^4. In other words, (when Δt is sufficiently small) if we reduce Δt by 10 times, the error term would reduce by 10^4 times. Replace Δt by $-\Delta t$ in the above equation, we have,

$$\mathbf{r}(t - \Delta t) = \mathbf{r}(t) - \frac{d\mathbf{r}(t)}{dt}\Delta t + \frac{1}{2}\frac{d^2\mathbf{r}(t)}{dt^2}\Delta t^2 - \frac{1}{3!}\frac{d^3\mathbf{r}(t)}{dt^3}\Delta t^3 + \mathcal{O}(\Delta t^4) \ , \quad (14)$$

Summing the two equations together, we have,

$$\begin{aligned}
\mathbf{r}(t+\Delta t)+\mathbf{r}(t-\Delta t) &= 2\mathbf{r}(t)+\frac{d^2\mathbf{r}(t)}{dt^2}\Delta t^2+\mathcal{O}(\Delta t^4) \\
&\equiv 2\mathbf{r}(t)+\mathbf{a}(t)\Delta t^2+\mathcal{O}(\Delta t^4) \qquad (15)\\
\mathbf{r}(t+\Delta t) &= 2\mathbf{r}(t)-\mathbf{r}(t-\Delta t)+\mathbf{a}(t)\Delta t^2+\mathcal{O}(\Delta t^4) \qquad (16)
\end{aligned}$$

Therefore, the local accuracy for the Verlet-family algorithms is to the order of $\mathcal{O}(\Delta t^4)$. This is quite accurate for such a simple algorithm! The trick here is that, by adding $t+\Delta t$ and $t-\Delta t$ terms, the third order term cancels out. Notice that the accuracy analysis here deals with the local error. That is, assuming $\mathbf{r}(t)$ is exact, how much error we make when computing $\mathbf{r}(t+\Delta t)$. In practice, the total error of computed $\mathbf{r}$ at time t is the accumulated (and possibly amplified) effect of all time steps before time t. Because for a smaller timestep Δt more steps is required to reach a pre-specified time t, the global order of accuracy is always local order of accuracy minus one. For example, the global order of accuracy for Verlet algorithms is 3.

Since all Verlet-family algorithms generate the same trajectory, they are all $\mathcal{O}(\Delta t^4)$ in terms of particle positions. But they differ in velocity calculations. How accurate is the velocity calculation in the original Verlet algorithm? Let us subtract Eq. (13) and (14),

$$\begin{aligned}
\mathbf{r}(t+\Delta t)-\mathbf{r}(t-\Delta t) &= 2\mathbf{v}(t)\Delta t+\frac{1}{3}\frac{d^3\mathbf{r}(t)}{dt^3}\Delta t^3+\mathcal{O}(\Delta t^4)\ , \qquad (17)\\
\mathbf{v}(t) &= \frac{1}{2\Delta t}\left[\mathbf{r}(t+\Delta t)-\mathbf{r}(t-\Delta t)-\frac{1}{6}\frac{d^3\mathbf{r}(t)}{dt^2}\Delta t^3\right]+\mathcal{O}(\Delta t^3) \qquad (18)\\
\mathbf{v}(t) &= \frac{\mathbf{r}(t+\Delta t)-\mathbf{r}(t-\Delta t)}{2\Delta t}+\mathcal{O}(\Delta t^2) \qquad (19)
\end{aligned}$$

Thus the velocity is only accurate to the order of $\mathcal{O}(\Delta t^2)$! This is much worse than $\mathcal{O}(\Delta t^4)$ of the positions. A reason for the lose of accuracy is that the velocities are computed by taking the difference between two large numbers, i.e. $\mathbf{r}(t+\Delta t)$ and $\mathbf{r}(t-\Delta t)$, and then divide by a small number.[1]

Intuitively, higher order algorithms allows the use of bigger time steps to achieve the same level of accuracy. However, the more important determining factor for the choice of time steps is usually not the order of accuracy, but instead is the algorithm's numerical stability (see next section).

4 Other integrators

Before closing this lecture, let us briefly look at two other well known integrators. Gear's predictor-corrector method is a high-order integrator. It keeps track of several time derivatives of the particle position. Define

$$\mathbf{r}_0(t) \equiv \mathbf{r}(t) \qquad (20)$$

[1]Strictly speaking, Eq. (17) is valid when we have exact values for $\mathbf{r}(t+\Delta t)$, $\mathbf{r}(t)$ and $\mathbf{r}(t-\Delta t)$. But in doing the order-of-accuracy analysis, we can only assume that we have exact values for $\mathbf{r}(t)$ and $\mathbf{r}(t-\Delta t)$ and we know that we are making an error in $\mathbf{r}(t+\Delta t)$. Fortunately, the error we make in $\mathbf{r}(t+\Delta t)$ is also $\mathcal{O}(\Delta t^4)$. Thus Eq. (17) still holds.

$$\mathbf{r}_1(t) \equiv \Delta t \frac{d\mathbf{r}(t)}{dt} \tag{21}$$

$$\mathbf{r}_2(t) \equiv \frac{\Delta t^2}{2!} \frac{d^2\mathbf{r}(t)}{dt^2} \tag{22}$$

$$\mathbf{r}_3(t) \equiv \frac{\Delta t^3}{3!} \frac{d^3\mathbf{r}(t)}{dt^3} \tag{23}$$

$$\cdots$$

Since

$$\begin{aligned}
\mathbf{r}(t+\Delta t) &= \mathbf{r}(t) + \Delta t \frac{d\mathbf{r}(t)}{dt} + \frac{\Delta t^2}{2!} \frac{d^2\mathbf{r}(t)}{dt^2} + \frac{\Delta t^3}{3!} \frac{d^3\mathbf{r}(t)}{dt^3} + \mathcal{O}(\Delta t^4) \\
&= \mathbf{r}(t) + \mathbf{r}_1(t) + \mathbf{r}_2(t) + \mathbf{r}_3(t) + \mathcal{O}(\Delta t^4) \\
\mathbf{r}_1(t+\Delta t) &= \mathbf{r}_1(t) + 2\mathbf{r}_2(t) + 3\mathbf{r}_3(t) + \mathcal{O}(\Delta t^4) \\
\mathbf{r}_2(t+\Delta t) &= \mathbf{r}_2(t) + 3\mathbf{r}_3(t) + \mathcal{O}(\Delta t^4) \\
\mathbf{r}_3(t+\Delta t) &= \mathbf{r}_3(t) + \mathcal{O}(\Delta t^4)
\end{aligned}$$

we can predict the values of $\mathbf{r}$ and $\mathbf{r}_i$ at time $t + \Delta t$ simply based on their values at time t,

$$\begin{aligned}
\mathbf{r}^{\mathrm{P}}(t+\Delta t) &= \mathbf{r}(t) + \mathbf{r}_1(t) + \mathbf{r}_2(t) + \mathbf{r}_3(t) \\
\mathbf{r}_1^{\mathrm{P}}(t+\Delta t) &= \mathbf{r}_1(t) + 2\mathbf{r}_2(t) + 3\mathbf{r}_3(t) \\
\mathbf{r}_2^{\mathrm{P}}(t+\Delta t) &= \mathbf{r}_2(t) + 3\mathbf{r}_3(t) \\
\mathbf{r}_3^{\mathrm{P}}(t+\Delta t) &= \mathbf{r}_3(t)
\end{aligned}$$

Notice that we have not even calculated the force at all! If we compute the force at time $t + \Delta t$ based on the predicted position $\mathbf{r}^{\mathrm{P}}(t + \Delta t)$, we will obtain the second derivative of $\mathbf{r}$ at time $t + \Delta t$ — let it be $\mathbf{r}^{\mathrm{C}}(t + \Delta t)$. Mostly likely, $\mathbf{r}^{\mathrm{C}}(t + \Delta t)$ will be different from the predicted value $\mathbf{r}^{\mathrm{P}}(t + \Delta t)$. The final results are obtained by adding a correction term to each predictor,

$$\mathbf{r}_n(t+\Delta t) = \mathbf{r}_n^{\mathrm{P}}(t+\Delta t) + C_n[\mathbf{r}_2^{\mathrm{C}}(t+\Delta t) - \mathbf{r}_2^{\mathrm{P}}(t+\Delta t)] \tag{24}$$

The Gear's 6th order scheme (uses $\mathbf{r}_0$ through $\mathbf{r}_5$) takes the following C_n values,

$$\begin{aligned}
C_0 &= \frac{3}{16} \\
C_1 &= \frac{251}{360} \\
C_2 &= 1 \\
C_3 &= \frac{11}{18} \\
C_4 &= \frac{1}{6} \\
C_5 &= \frac{1}{60}
\end{aligned}$$

The global accuracy is of the order $\mathcal{O}(\Delta t)^6$, hence the method is called the Gear's 6th order algorithm.

Exercise: show that the local truncation error of the above scheme is of the order of $\mathcal{O}(\Delta t^7)$.

In a way, the Runge-Kutta method is similar to predictor-corrector methods in that the final answer is produced by improving upon previous predictions. However, the Runge-Kutta method requires multiple evaluation of forces. The Runge-Kutta method is most conveniently represented when the equation of motion is written as a first order differential equation,

$$\dot{\boldsymbol{\eta}} = g(\boldsymbol{\eta}) \equiv \boldsymbol{\omega} \frac{\partial H(\boldsymbol{\eta})}{\partial \boldsymbol{\eta}} \tag{25}$$

where

$$\boldsymbol{\eta} \equiv (\mathbf{r}, \mathbf{p}) \tag{26}$$

and

$$\boldsymbol{\omega} = \begin{pmatrix} 0 & I \\ -I & 0 \end{pmatrix} \tag{27}$$

and I is the 3×3 identity matrix and H is the Hamiltonian.

The fourth-order Runge-Kutta method goes as (from `mathworld.wolfram.com`),

$$\begin{aligned} k_1 &= \Delta t \cdot g\left(\boldsymbol{\eta}(t)\right) \\ k_2 &= \Delta t \cdot g\left(\boldsymbol{\eta}(t) + \frac{1}{2}k_1\right) \\ k_3 &= \Delta t \cdot g\left(\boldsymbol{\eta}(t) + \frac{1}{2}k_2\right) \\ k_4 &= \Delta t \cdot g\left(\boldsymbol{\eta}(t) + k_3\right) \\ \boldsymbol{\eta}(t + \Delta t) &= \boldsymbol{\eta}(t) + \frac{1}{6}k_1 + \frac{1}{3}k_2 + \frac{1}{3}k_3 + \frac{1}{6}k_4 \end{aligned} \tag{28}$$

Exercise: show that the local truncation error of the above scheme is of the order of $\mathcal{O}(\Delta t^5)$ *and the global accuracy is of the order of* $\mathcal{O}(\Delta t^4)$.

Suggested reading

1. (Alan and Tildesley 1987) pp.71-84.

2. J. C. Butcher, *The numerical analysis of ordinary differential equations: Runge-Kutta and general linear methods*, (Wiley, 1987), pp. 105-151.

ME346 – Introduction to Molecular Simulations – Stanford University – Winter 2007

Handout 3. Symplectic Condition

Wei Cai

January 17, 2007

Contents

1 Conservation laws of Hamiltonian systems

The numerical integrators for simulating the Newton's equation of motion are solvers of ordinary differential equations (ODE). However, the Newton's equation of motion that can be derived from a Hamiltonian is a special type of ODE (not every ODE can be derived from a Hamiltonian). For example, a Hamiltonian system conserves it total energy, while an arbitrary ODE may not have any conserved quantity. Therefore, special attention is needed to select an ODE solver for Molecular Dynamics simulations. We need to pick those ODE solvers that obeys the conservation laws of a Hamiltonian system. For example, if an ODE solver predicts that the Earth will drop into the Sun after 100 cycles around the Sun, it is certainly the ODE solver to blame and we should not immediately start worrying about the fate of our planet based on this prediction.

A conservation law is a (time invariant) symmetry. A Hamiltonian system possess more symmetries than just energy conservation. Ideally the numerical integration scheme we pick should satisfy all the symmetries of the true dynamics of the system. We will look at these symmetries in this and following sections.

When discussing a Hamiltonian system, it is customary to use letter $\mathbf{q}$ to represent the particle position (instead of $\mathbf{r}$). Recall that the equation of motion for a system with Hamiltonian $H(\mathbf{q}, \mathbf{p})$ is,

$$\dot{\mathbf{q}} = \frac{\partial H(\mathbf{q}, \mathbf{p})}{\partial \mathbf{p}} \tag{1}$$

$$\dot{\mathbf{p}} = -\frac{\partial H(\mathbf{q},\mathbf{p})}{\partial \mathbf{q}} , \tag{2}$$

where $\dot{\mathbf{q}} \equiv d\mathbf{q}/dt$, $\dot{\mathbf{p}} \equiv d\mathbf{p}/dt$. If the system has N particles, then $\mathbf{q}$ is a $3N$-dimensional vector specifying its position and $\mathbf{p}$ is a $3N$-dimensional vector specifying its momentum. (In the above Earth orbiting example, $N = 1$.) Notice that in terms of $\mathbf{q}$ and $\mathbf{p}$, the equation of motion is a set of (coupled) first-order differential equations (whereas $\mathbf{F} = m\mathbf{a}$ is second order). The equation can be reduced to an even simpler form if we define a $6N$-dimensional vector

$$\boldsymbol{\eta} \equiv (\mathbf{q},\mathbf{p}) \tag{3}$$

Then the equation of motion becomes,

$$\dot{\boldsymbol{\eta}} = \boldsymbol{\omega}\frac{\partial H(\boldsymbol{\eta})}{\partial \boldsymbol{\eta}} \tag{4}$$

where

$$\boldsymbol{\omega} = \begin{pmatrix} 0 & I \\ -I & 0 \end{pmatrix} \tag{5}$$

and I is the 3×3 identity matrix. The $6N$-dimensional space which $\boldsymbol{\eta} \equiv (\mathbf{q},\mathbf{p})$ belongs to is called the *phase space*. The evolution of system in time can be regarded as the motion of a point $\boldsymbol{\eta}$ in the $6N$-dimensional phase space following the first-order differential equation(4).

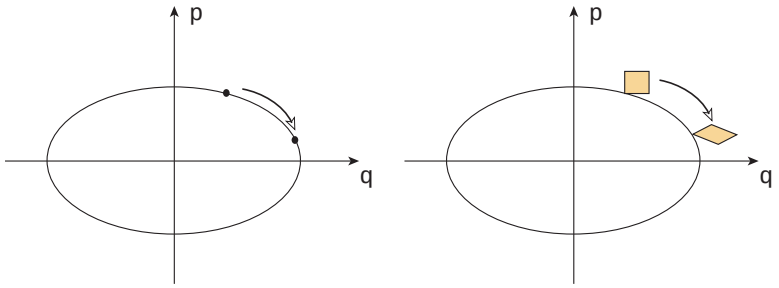

Figure 1: (a) Motion of a point $(\mathbf{q},\mathbf{p})$ in phase space is confined to a shell with constant energy. (b) Area of a phase space element (shaded) is conserved.

Because the Newton's equation of motion conserves total energy, the motion of a point in phase space must be confined to a subspace (or hyperplane) with constant energy, i.e. a constant energy shell, as illustrated in Fig. 1(a). Think about all the points in the constant energy shell. As time evolves, the entire volume that these points occupy remains the same — the points simply rearrange within the constant energy shell.

Let us now consider the evolution of a small element in phase space over time, as illustrated in Fig. 1(b). Think of this as the ensemble of trajectories of many Molecular Dynamics simulations with very similar initial conditions. We will show that the area enclosed by this element remains constant, even though the element inevitably experiences translation and

distortion.[1] Let the element at time t be a hypercube around point $\boldsymbol{\eta}$, whose area is,

$$|d\boldsymbol{\eta}| = |d\mathbf{q}| \cdot |d\mathbf{p}| = dq_1 \cdots dq_{3N} dp_1 \cdots dp_{3N} \tag{6}$$

For a point $\boldsymbol{\eta}$ at time t, let $\boldsymbol{\xi}$ be its new position at time $t + \delta t$. In the limit of $\delta t \to 0$, we have,

$$\boldsymbol{\xi} = \boldsymbol{\eta} + \dot{\boldsymbol{\eta}} \delta t = \boldsymbol{\eta} + \boldsymbol{\omega} \frac{\partial H(\boldsymbol{\eta})}{\partial \boldsymbol{\eta}} \delta t \tag{7}$$

Because the above equation is true only in the limit of $\delta t \to 0$, we will ignore any higher order terms (e.g. δt^2) in the following discussions. Let M be the Jacobian matrix of the transformation from $\boldsymbol{\eta}$ to $\boldsymbol{\xi}$, i.e.,

$$M \equiv \frac{\partial \boldsymbol{\xi}}{\partial \boldsymbol{\eta}} = 1 + \boldsymbol{\omega} \frac{\partial^2 H(\boldsymbol{\eta})}{\partial \boldsymbol{\eta} \partial \boldsymbol{\eta}} \delta t \tag{8}$$

For clarity, we write M explicitly in terms of $\mathbf{q}$ and $\mathbf{p}$,

$$M = 1 + \begin{pmatrix} 0 & I \\ -I & 0 \end{pmatrix} \cdot \begin{pmatrix} \frac{\partial^2 H}{\partial \mathbf{q} \partial \mathbf{q}} & \frac{\partial^2 H}{\partial \mathbf{q} \partial \mathbf{p}} \\ \frac{\partial^2 H}{\partial \mathbf{p} \partial \mathbf{q}} & \frac{\partial^2 H}{\partial \mathbf{p} \partial \mathbf{p}} \end{pmatrix} \cdot \delta t \tag{9}$$

$$= \begin{pmatrix} 1 + \frac{\partial^2 H}{\partial \mathbf{p} \partial \mathbf{q}} \delta t & \frac{\partial^2 H}{\partial \mathbf{p} \partial \mathbf{p}} \delta t \\ -\frac{\partial^2 H}{\partial \mathbf{q} \partial \mathbf{q}} \delta t & 1 - \frac{\partial^2 H}{\partial \mathbf{q} \partial \mathbf{p}} \delta t \end{pmatrix} \tag{10}$$

The area of the new element is related to the the determinant of the Jacobian matrix,

$$|d\boldsymbol{\xi}| = |d\boldsymbol{\eta}| \cdot |\det M| = |d\boldsymbol{\eta}| \cdot (1 + \mathcal{O}(\delta t^2)) \tag{11}$$

Because the first order term of δt in $\det M$ vanishes, we can show that the area of the element remains constant for an arbitrary period of time (i.e. forever).[2] This is an important property of a Hamiltonian system. Because the area of any element in phase space always remains constant, the evolution of phase space points is analogous to that in an incompressible fluid.

Exercise: Write down the explicit expression for the Jacobian matrix M for problem of the Earth orbiting around the Sun.

The Hamiltonian dynamics has even more symmetries. Notice that the transpose of M is,

$$M^T = 1 - \frac{\partial^2 H}{\partial \boldsymbol{\eta} \partial \boldsymbol{\eta}} \boldsymbol{\omega} \delta t \tag{12}$$

[1] It then follows that the area enclosed by an arbitrarily shaped element in the phase space also remains constant.

[2] To show that area remains constant after a finite period Δt, we only need to divide the time interval into N subintervals, each with $\delta t = \Delta t / N$. The area change per subinterval is of the order of $1/N^2$. The accumulated area change over time period Δt is then of the order of $1/N$, which vanishes as $N \to \infty$.

we have

$$\begin{aligned} M\boldsymbol{\omega}M^T &= \left(1+\boldsymbol{\omega}\frac{\partial^2 H}{\partial\boldsymbol{\eta}\partial\boldsymbol{\eta}}\delta t\right)\boldsymbol{\omega}\left(1-\frac{\partial^2 H}{\partial\boldsymbol{\eta}\partial\boldsymbol{\eta}}\boldsymbol{\omega}\delta t\right) \\ &= \boldsymbol{\omega}+\boldsymbol{\omega}\frac{\partial^2 H}{\partial\boldsymbol{\eta}\partial\boldsymbol{\eta}}\boldsymbol{\omega}\delta t-\boldsymbol{\omega}\frac{\partial^2 H}{\partial\boldsymbol{\eta}\partial\boldsymbol{\eta}}\boldsymbol{\omega}\delta t+\mathcal{O}(\delta t^2) \quad (13) \\ &= \boldsymbol{\omega}+\mathcal{O}(\delta t^2) \quad (14) \\ & \quad (15) \end{aligned}$$

Therefore the Jacobian matrix M thus satisfies the so called *symplectic* condition (up to $\mathcal{O}(\delta t^2)$) ,

$$M\boldsymbol{\omega}M^T=\boldsymbol{\omega} \quad (16)$$

Again, we can show that the *symplectic* condition is satisfied for an arbitrary period of time. To be specific, let $\boldsymbol{\xi}$ be the point in phase space at time t; at time 0 this point was at $\boldsymbol{\eta}$. $\boldsymbol{\xi}$ can then be regarded as a function of t and $\boldsymbol{\eta}$ (initial condition), i.e. $\boldsymbol{\xi}=\boldsymbol{\xi}(\boldsymbol{\eta},t)$. Define M as the Jacobian matrix between $\boldsymbol{\xi}$ and $\boldsymbol{\eta}$, we can show that M satisfies the *symplectic* condition Eq. (16).[3]

Obviously, the Hamiltonian dynamics is also time reversible. This means that if $\boldsymbol{\eta}$ evolves to $\boldsymbol{\xi}$ after time t. Another phase space point $\boldsymbol{\eta}'$ that has the same $\mathbf{q}$ as $\boldsymbol{\eta}$ but with reversed $\mathbf{p}$ (momentum) will exactly come to point $\boldsymbol{\xi}$ after time t. To summarize, the dynamics of a system that has a Hamiltonian has the following symmetry properties:

- Conserves total energy
- Conserves phase space area (incompressible flow in phase space)
- Satisfies *symplectic* condition Eq. (16)
- Is time reversible

Ideally, the numerical integrator we choose to simulate Hamiltonian system should satisfy all of these symmetries. In the following, let us take a look at how specific integrators are doing in this regard. In fact, if an algorithm satisfies the *symplectic* condition, it automatically conserves phase space area[4], is reversible, and should have good long-term energy conservation properties. This is why *symplectic* methods are good choices for simulating Hamiltonian systems.

2 Symplectic methods

What do we mean if we ask whether a numerical integrator satisfies the *symplectic* condition or not? For a numerical integrator, the system moves forward in time by discrete jumps. Let

[3]Again, we devide the time period t into N subintervals, each with $\delta t=\Delta t/N$. Let M_i be the Jacobian matrix from time $(i-1)\delta t$ to $i\delta t$. We have $M=\prod_{i=1}^{N}M_i$. We can show that $M^T\boldsymbol{\omega}M=\boldsymbol{\omega}$ in the limit of $N\to\infty$.

[4]Since $M^T\boldsymbol{\omega}M=\boldsymbol{\omega}$, $\det\boldsymbol{\omega}=\det(M^T\boldsymbol{\omega}M)=(\det M)^2\det\boldsymbol{\omega}$. Thus $\det M=\pm1$, which means area conservation.

$\boldsymbol{\eta}^{(i)} = (\mathbf{q}^{(i)}, \mathbf{p}^{(i)})$ be the place of the system in the phase space at time step i, i.e. $t_i = i\Delta t$. At the next time step, the algorithm brings the system to point $\boldsymbol{\eta}^{(i+1)} = (\mathbf{q}^{(i+1)}, \mathbf{p}^{(i+1)})$. Let M be the Jacobian matrix that connects $\boldsymbol{\eta}^{(i)}$ with $\boldsymbol{\eta}^{(i+1)}$. The method is *symplectic* if $M\boldsymbol{\omega}M^T = \boldsymbol{\omega}$.

The good news is that the Verlet-family algorithms are symplectic. To show this is the case, let us consider the leap-frog algorithm. Let $\mathbf{q}^{(i)}$ correspond to $\mathbf{q}(i \cdot \Delta t)$ and $\mathbf{p}^{(i)}$ correspond to $\mathbf{p}((i - \frac{1}{2}) \cdot \Delta t)$. Then the leap-frog algorithm is,

$$\mathbf{p}^{(i+1)} = \mathbf{p}^{(i)} - \frac{\partial V}{\partial \mathbf{q}^{(i)}}\Delta t \tag{17}$$

$$\mathbf{q}^{(i+1)} = \mathbf{q}^{(i)} + \frac{\mathbf{p}^{(i+1)}}{m}\Delta t = \mathbf{q}^{(i)} + \frac{1}{m}\left[\mathbf{p}^{(i)} - \frac{\partial V}{\partial \mathbf{q}^{(i)}}\Delta t\right]\Delta t \tag{18}$$

Thus,

$$M = \begin{pmatrix} \frac{\partial \mathbf{q}^{(i+1)}}{\partial \mathbf{q}^{(i)}} & \frac{\partial \mathbf{q}^{(i+1)}}{\partial \mathbf{p}^{(i)}} \\ \frac{\partial \mathbf{p}^{(i+1)}}{\partial \mathbf{q}^{(i)}} & \frac{\partial \mathbf{q}^{(i+1)}}{\partial \mathbf{p}^{(i)}} \end{pmatrix} = \begin{pmatrix} 1 - \frac{1}{m}\frac{\partial^2 V}{\partial \mathbf{q}^{(i)}\partial \mathbf{q}^{(i)}}\Delta t^2 & \frac{\Delta t}{m} \\ -\frac{\partial^2 V}{\partial \mathbf{q}^{(i)}\partial \mathbf{q}^{(i)}}\Delta t & 1 \end{pmatrix} \tag{19}$$

Thus M is symplectic.

Exercise: show that for M defined in Eq. (19), $M\boldsymbol{\omega}M^T = \boldsymbol{\omega}$ (symplectic) and $\det M = 1$ (area preserving).

Exercise: derive the Jacobian matrix M for velocity Verlet algorithm and show that it is symplectic and area preserving.

3 Reversibility and chaos

Because the Verlet-family algorithms (original Verlet, leap-frog and velocity Verlet) are symplectic, they are also time reversible. Nonetheless, it is instructive to show the time reversibility explicitly. If we run the leap-frog algorithm in reverse time, then the iteration can be written as,

$$\tilde{\mathbf{q}}^{(i+1)} = \tilde{\mathbf{q}}^{(i)} + \frac{\tilde{\mathbf{p}}^{(i)}}{m}\Delta t \tag{20}$$

$$\tilde{\mathbf{p}}^{(i+1)} = \tilde{\mathbf{p}}^{(i)} - \frac{\partial V}{\partial \tilde{\mathbf{q}}^{(i+1)}}\Delta t \tag{21}$$

$$\tag{22}$$

where i is the iteration number, $\tilde{\mathbf{q}}^{(i)} = \mathbf{q}(-i\Delta t)$, $\tilde{\mathbf{p}}^{(i)} = \mathbf{p}((-i - \frac{1}{2})\Delta t)$. It is not difficult to show that if $\tilde{\mathbf{q}}^{(i)} = \mathbf{q}^{(i+1)}$ and $\tilde{\mathbf{p}}^{(i)} = -\mathbf{p}^{(i+1)}$, then $\tilde{\mathbf{q}}^{(i+1)} = \mathbf{q}^{(i)}$ and $\tilde{\mathbf{p}}^{(i+1)} = -\mathbf{p}^{(i)}$.

Exercise: show that the leap-frog algorithm is reversible.

Exercise: show that the velocity Verlet algorithm is reversible.

Exercise: show that the Forward Euler method:
$\mathbf{q}^{(i+1)} = \mathbf{q}^{(i)} + \Delta t \cdot \mathbf{p}^{(i)}/m$,
$\mathbf{p}^{(i+1)} = \mathbf{p}^{(i)} - \Delta t \cdot \partial V/\partial \mathbf{q}^{(i)}$,
is not reversible and not symplectic.

Since every integration step using the Verlet algorithm is time reversible, then in principle an entire trajectory of Molecular Dynamics simulation using the Verlet algorithm should be time reversible. To be specific, let the initial condition of the simulation be $\mathbf{q}^{(0)}$ and $\mathbf{p}^{(0)}$. After N steps of integration, the system evolves to point $\mathbf{q}^{(N)}$ and $\mathbf{p}^{(N)}$. Time reversibility means that, if we run the reverse Verlet iteration starting from $\mathbf{q}^{(N)}$ and $-\mathbf{p}^{(N)}$, after N steps we should get exactly to point $\mathbf{q}^{(0)}$ and $-\mathbf{p}^{(0)}$.

In practice, however, we never have perfect reversibility. This is due to the combined effect of numerical round off error and the chaotic nature of trajectories of many Hamiltonian systems. The chaotic nature of many Hamiltonian system can be illustrated by considering the two trajectories with very close initial conditions. Let the distance between the two points in phase space at time 0 be $d(0)$. At sufficiently large t, the two phase space points will diverge exponentially, i.e. $d(t) \sim d(0)\mathrm{e}^{\lambda t}$, where λ is called the Lyapunov exponent and this behavior is called Lyapunov instability. Given that we can only represent a real number on a computer with finite precision, we are in effect introducing a small (random) perturbation at every step of the integration. Therefore, sooner or later, the numerical trajectory will deviate from the analytical trajectory (if the computer had infinite precision) significantly[5]. While the analytical trajectory is reversible, the one generated by a computer is not. This is why there exist a maximum number of iterations N, beyond which the original state cannot be recovered by running the simulation backwards. This by itself does not present too big a problem, since we seldom have the need to recover the initial condition of the simulation in this way. However, this behavior does mean that we will not be able to follow the "true" trajectory of the original system forever on a computer. Sooner or later, the "true" trajectory and the simulated one will diverge significantly. This is certainly a problem if we would like to rely entirely on simulations to tell us where is our satellite or space explorer. However, this usually does not present a problem in Molecular Simulations, in which we are usually not interested in the exact trajectories of every atom. We will return to this point in future lectures when we discuss Molecular Dynamics simulations involving many atoms.

[5]Notice that the analytical trajectory here is not the same as the "true" trajectory of the original system. The analytical trajectory is obtained by advancing the system in discrete jumps along the time axis.

Figure 2: Aleksandr Mikhailovich Lyapunov (1857-1918 Russia).

If we look at Lyapunov instability and area conservation of Hamiltonian systems together, there seems to be a problem here. The area conservation property states that an element in the phase space (containing points close to each other) will evolve while keeping its area constant. But the Lyapunov instability says that any two points, no matter how close they are, will eventually be separated into great distances. Wouldn't this mean that the points in the element now occupies a much larger volume? The answer is *no*. Both Lyapunov instability and area conservation occurs in a Hamiltonian system. The resolution to this paradox is that: while the element maintains its total area, its shape is continuously distorted, stretched and folded, so that any two points in this element no matter how close they are initially will be separated by great distances. The evolution of the element in phase space is similar to that of a dough from which you want to make thin noodles or flaky pastry for croissants.

4 Energy conservation

Due to inevitable approximations introduced, no integrators exactly conserves the original Hamiltonian H. Some high-order integrators (such as Gear's predictor-corrector scheme, see next section) may have a more impressive energy conservation in the short term than say Verlet algorithms, the energy in those high order schemes may drift significantly away from the original value if the schemes are not *symplectic*. At the same time, there exist evidence that symplectic methods exactly conserve another Hamiltonian $\tilde{H}$ (shadow Hamiltonian) that is slightly different from the original H. Because the constant energy shell of H and $\tilde{H}$ dance around each other in the phase space, the energy of a symplectic algorithm fluctuates around the initial energy and the difference does not grow as time goes to infinity. Therefore, symplectic methods have better long term stability than non-symplectic (even with higher order) methods.

Suggested reading

1. (Frenkel and Smit 2002) pp.488-494.
2. R. H. Miller, *A horror story about integration methods*, J. Comput. Phys. 93, 469 (1991).

ME346 – Introduction to Molecular Simulations – Stanford University – Winter 2007

Handout 4. Perfect Crystal Structures*

Wei Cai

January 17, 2007

1 Perfect crystal structures

Lattices and bases

A crystal is a collection of atoms arranged periodically in space. A crystal can be constructed from identical building blocks by replicating them periodically. This building block is called the *basis* (motif) and the way its replicas are repeated in space is specified by the *lattice* (scaffold). Thus, it is fair to say that,

$$\text{crystal structure} \;=\; \text{lattice} \;+\; \text{basis}. \tag{1}$$

A basis may consist of one or more atoms. For example, Fig. 1 illustrates a hypothetical 2-dimensional crystal structure made of two types of atoms. Its lattice is defined by two repeat vectors **a** and **b** and its basis consists of three atoms. In most crystal structures to be discussed in this book, the basis contains only one or two atoms. However, bases of protein crystals are macromolecules consisting of thousands of atoms. Obviously, an infinite variety of possible bases exist that can be used to build periodic crystal structures.

A lattice is an infinite array of mathematical points that form a periodic spatial arrangement. In 1948, French physicist Auguste Bravais proved that there are only 14 different types of lattices in three dimensions with distinct symmetry properties. These lattices have been called the *Bravais* lattices ever since.[1] For a more detailed account of the Bravais lattices, we refer to the standard textbooks on solid-state theory (e.g. [2, 3, 4]). In this book we will encounter only three Bravais lattice that all exhibit *cubic* symmetry.

A Bravais lattice is fully specified by its smallest repeat vectors, often called *primitive* lattice vectors, as shown in Fig. 1(b). In three dimensions, the position of every point in a Bravais lattice can be written as a linear combination of the *primitive* lattice vectors $\mathbf{e}_1$, $\mathbf{e}_2$, and $\mathbf{e}_3$,

$$\mathbf{R} = n_1\mathbf{e}_1 + n_2\mathbf{e}_2 + n_3\mathbf{e}_3 \;, \tag{2}$$

*This is Section 1.1 of `Computer Simulations of Dislocations`, V. V. Bulatov and W. Cai, (Oxford University Press, 2006). Website: `http://micro.stanford.edu`

[1] In two dimensions, there are only five *Bravais* lattices.

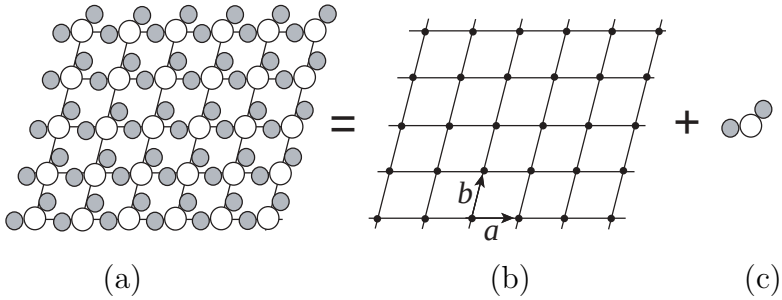

Figure 1: (a) A 2-dimensional crystal consisting of two types of atoms (white and gray). (b) The Bravais lattice is specified by two repeat vectors **a** and **b**. (c) The basis contains three atoms.

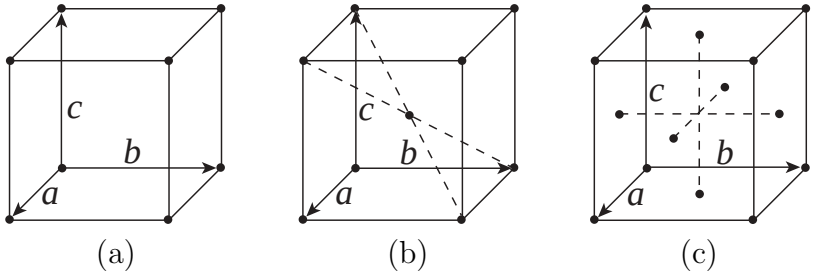

Figure 2: (a) The unit cell of a simple cubic Bravais lattice. (b) The unit cell of a body-centered-cubic Bravais lattice. (c) The unit cell of a face-centered-cubic Bravais lattice.

where n_1, n_2, n_3 are arbitrary integers. The smallest parallelepiped with a lattice point at each of its eight corners is called the *primitive* cell. Every edge of the primitive cell is a primitive lattice vector. Often, to better reflect the symmetries, certain types of Bravais lattices are specified by non-primitive lattice vectors **a**, **b** and **c**. The parallelepiped formed by these vectors is called the *unit* cell. Fig. 2(a) shows the unit cell of a simple-cubic (SC) lattice. In this case, the unit cell is also the primitive cell, i.e. $\mathbf{a} = \mathbf{e}_1$, $\mathbf{b} = \mathbf{e}_2$, $\mathbf{c} = \mathbf{e}_3$. In the SC lattice, the repeat vectors **a**, **b**, **c** are perpendicular to each other and have the same length. The positions of all lattice points in the SC lattice can be written as,

$$\mathbf{R} = i\,\mathbf{a} + j\,\mathbf{b} + k\,\mathbf{c}\ , \tag{3}$$

where i, j, k are integers.

In body-centered-cubic (BCC) and face-centered-cubic (FCC) lattices, the unit cell is larger than the primitive cell, as shown in Fig. 2(b) and (c).[2] In these two cases, the unit cell has lattice points either on its faces (FCC) or in its interior (BCC), in addition to the lattice points at its corners. The lattice points of a BCC lattice are,

$$\begin{aligned} \mathbf{R} &= i\,\mathbf{a} + j\,\mathbf{b} + k\,\mathbf{c}\ , \\ \text{and}\quad \mathbf{R} &= (i+1/2)\,\mathbf{a} + (j+1/2)\,\mathbf{b} + (k+1/2)\,\mathbf{c}\ , \end{aligned} \tag{4}$$

[2]The cube-shaped unit cell reveals the cubic symmetries more clearly than the primitive cells.

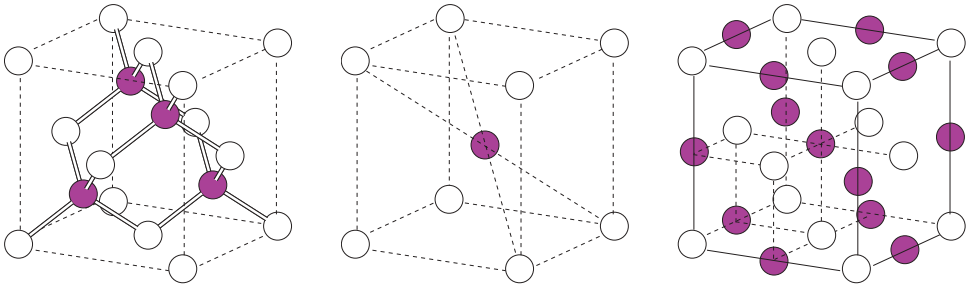

(a) (b) (c)

Figure 3: (a) The basis of a zinc-blend structure contains two atoms that are chemically distinct. When two atoms in the basis are chemically identical, the resulting structure is diamond-cubic. (b) The CsCl structure. (c) The NaCl structure.

and the lattice points of an FCC lattice are,

$$\begin{aligned} \mathbf{R} &= i\,\mathbf{a} + j\,\mathbf{b} + k\,\mathbf{c}\ , \\ \text{and}\ \ \mathbf{R} &= (i+1/2)\,\mathbf{a} + (j+1/2)\,\mathbf{b} + k\,\mathbf{c}\ , \\ \text{and}\ \ \mathbf{R} &= (i+1/2)\,\mathbf{a} + j\,\mathbf{b} + (k+1/2)\,\mathbf{c}\ , \\ \text{and}\ \ \mathbf{R} &= i\,\mathbf{a} + (j+1/2)\,\mathbf{b} + (k+1/2)\,\mathbf{c}\ . \end{aligned} \tag{5}$$

To obtain SC, BCC or FCC crystal structure, it suffices to associate a single atom of the same chemical species with every lattice point in the SC, BCC, and FCC lattices, respectively. In all these cases, the basis consists of only one atom. It is easy to see that, for a given crystal structure, the lattice and the basis are not uniquely defined. For example, the BCC crystal structure can be equally regarded as a combination of the SC Bravais lattice with a basis consisting of two atoms (see Problem 1.1.4). To avoid confusion, the adopted convention is to associate each crystal structure with the Bravais lattice of highest possible symmetry and with the basis containing the smallest number of atoms.

Starting from the same SC, BCC or FCC lattices, more complicated crystal structures can be built using bases containing several atoms, which may be chemically distinct. For example, the diamond-cubic (DC) crystal structure, i.e. the structure of Diamond, Silicon and Germanium crystals, is a combination of the FCC Bravais lattice with a two-atom basis. Separated by $\mathbf{a}/4 + \mathbf{b}/4 + \mathbf{c}/4$, the two atoms are shown in Fig. 3(a) in different colors. In the DC structure, two atoms of the basis are chemically identical (e.g. two Silicon atoms). On the other hand, when the atoms in this basis are chemically distinct, the zinc-blende crystal structure results. For example, if one atom in the basis is Gallium and the other is Arsenic, the resulting GaAs crystal has a zinc-blende structure.

Similarly, the CsCl structure shown in Fig. 3(b) is a cubic structure with two different types of atoms in its basis. It looks similar to the BCC structure, except that two atoms in its basis are different — one is Caesium and the other is Chlorine. The NaCl structure of kitchen salt is also cubic, as shown in Fig. 3(c). At a first glance, it looks very similar to the SC structure with two types of atoms on alternating lattice sites. However, a more careful analysis reveals that the CsCl structure does not have a BCC Bravais lattice and the NaCl structure does not have an SC Bravais lattice (see Problem 1.1.5).

Miller indices
It is common and convenient to express the positions of atoms in a crystal in the units of repeat vectors of its lattice. Miller indices are introduced for this purpose and are frequently used as a shorthand notation for line directions and plane orientations in the crystals. The Miller indices will be very useful in our subsequent discussions, to specify a dislocation's line direction and its glide plane.

A vector $\mathbf{l}$ that connects one point to another in a Bravais lattice can be written as a linear combination of repeat vectors, i.e.,

$$\mathbf{l} = i\,\mathbf{a} + j\,\mathbf{b} + k\,\mathbf{c}\ . \tag{6}$$

where i, j and k are integers. The Miller indices notation for this vector is $[ijk]$.[3] To specify a line direction that is parallel to $\mathbf{l}$, the convention is to select integer indices corresponding to the vector with the smallest length, among all vectors parallel to $\mathbf{l}$. For example, the line direction along vector $\mathbf{a}$ is simply [100]. By convention, a negative component is specified by placing a bar over the corresponding index. For example, $[1\bar{2}3]$ defines direction $\mathbf{l} = \mathbf{a} - 2\mathbf{b} + 3\mathbf{c}$. Sometimes, it is necessary to identify a family of line directions that are related to each other by crystal symmetry. Miller indices of a crystallographic family of directions are written in the angular brackets. For example, $\langle 112\rangle$ corresponds to the set of line directions that include [112], $[11\bar{2}]$, $[1\bar{1}2]$, [121], etc.

To specify a crystallographic plane, the Miller indices of the direction normal to the plane are used, but written between round brackets, i.e. (ijk). To identify a crystallographic family of planes related by symmetry, the Miller indices are written between the curly brackets, i.e. $\{ijk\}$.

Summary
• A crystal structure is a lattice plus a basis. The basis is the repeat pattern of atoms or molecules associated with every point of a Bravais lattice.
• Line directions and plane orientations in a crystal are conveniently specified by their Miller indices.

Problems

1.1.1. Define Bravais lattices and bases for Aluminum, Iron, and Silicon crystals and use `MD++` code to build and display their crystal structures (`MD++` can be downloaded from the book's web site [1].

1.1.2. Find the distances from a given atom to its first, second and third nearest neighbor atoms in SC, FCC and BCC crystal structures.

1.1.3. Find the spacing between adjacent (111) planes in SC, FCC and BCC crystal structures.

[3] Sometimes, fractional indices are used, such as $[\frac{1}{2}\,0\,0]$, which represents vector $\mathbf{a}/2$.

1.1.4. Defining the BCC (FCC) crystal structure by the SC Bravais lattice with a basis containing two (four) atoms, write the coordinates of each atom in the basis.

1.1.5. What are the Bravais lattices of the CsCl and NaCl structures shown in Fig. 3(b) and (c)? Write the coordinates of each basis atom for these two crystal structures.

References

[1] *MD++ simulation package is available from the book web site.* http://micro.stanford.edu.

[2] N. W. Ashcroft and N. D. Mermin. *Solid State Physics*. Saunders College, Philadelphia, 1976.

[3] A. Kelly, G. W. Groves, and P. Kidd. *Crystallography and crystal defects*. Wiley, Chichester; New York, revised edition, 2000.

[4] C. Kittel. *Introduction to Solid State Physics*. Wiley, New York, 7th edition, 1996.

ME346 – Introduction to Molecular Simulations – Stanford University – Winter 2007

Handout 5. Interatomic Interactions*

Wei Cai

January 19, 2007

Fundamentally, materials derive their properties from the interaction between their constituent atoms. These basic interactions make the atoms assemble in a particular crystalline structure. The same interactions also define how the atoms prefer to arrange themselves on the surface or around a vacancy. Therefore, to understand the behavior of a material, it is necessary and sufficient to study the collective behavior of atoms that constitutes the material. This handout discusses the basic features of the interactions between atoms and different models that describes them.

1 Interatomic interactions

When put close together, atoms interact by exerting forces on each other. Depending on the atomic species, some interatomic interactions are relatively easy to describe, while others can be very complicated. This variability stems from the quantum mechanical motion and interaction of electrons [19, 14]. Henceforth, rigorous treatment of interatomic interactions should be based on a solution of the Schrödinger's equation for interacting electrons, which is usually referred to as the first principles or *ab initio* theory. Numerical calculations based on first principles are computationally very expensive and can only deal with a relatively small number of atoms. However, we are often interested in systems that involve many thousands of atoms, which only be approached using much less sophisticated but more computationally efficient models. Even though we do not discuss it in this course, it is useful to bear in mind that the first principles theory provides a useful starting point for constructing approximate but efficient models that are needed to study large scale problems involving many atoms. The usual way to construct a model of interatomic interactions is to postulate a relatively simple, analytical functional form for the potential energy of a set of atoms,

$$V(\{\mathbf{r}_i\}) \equiv V(\mathbf{r}_1, \mathbf{r}_2, \cdots, \mathbf{r}_N) \tag{1}$$

*This handout is adapted from Section 2.1-2.3 of `Computer Simulations of Dislocations`, V. V. Bulatov and W. Cai, (Oxford University Press, 2006). Website: `http://micro.stanford.edu`

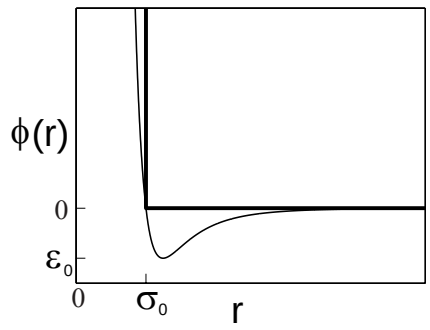

Figure 1: Interaction energy $\phi(r)$ as a function of the distance between two atoms. The thick line is the hard sphere model and the thin line is the Lennard-Jones model.

where $\mathbf{r}_i$ is the position vector of atom i and N is the total number of atoms. The force on an atom is the negative derivative of the potential function with respect to its position, i.e.,

$$\mathbf{f}_j = -\frac{\partial V(\{\mathbf{r}_i\})}{\partial \mathbf{r}_j} \tag{2}$$

The hope is that approximate forms can be developed that capture the most essential physical aspects of atom-atom interaction. Such functions are commonly called *interatomic potentials*. The parameters in the interatomic potential function are usually fitted to experimental or *ab initio* simulation data.

Interatomic potential models

The most obvious physical feature of interatomic interactions is that atoms do not like to get too close to each other. This is why all solid materials assume a certain volume and resist compression. While this effect is quantum mechanical in nature (due to repulsion between the electron clouds around each atom), it is simple to account for by making the potential energy increase when the distance between any two atoms becomes small. Probably the simplest model that accounts for the short range repulsion is the "hard-sphere" model, where the energy becomes infinite whenever the distance between two atoms gets smaller than σ_0 (the diameter of the spheres), i.e,

$$V(\{\mathbf{R}_i\}) = \sum_{i=1}^{N} \sum_{j=i+1}^{N} \phi(|\mathbf{R}_i - \mathbf{R}_j|) \tag{3}$$

where

$$\phi(r) = \begin{cases} +\infty, & r < \sigma_0 \\ 0, & r \geq \sigma_0 \end{cases}, \tag{4}$$

as shown in Fig. 1. Even though the hard sphere potential is not a very realistic model for atoms, computer simulations based on this model have contributed much to the understanding of the atomistic structure of liquids.

Figure 2: Sir John Edward Lennard-Jones (1894-1954 England).

The other important aspect of the interatomic interaction is that atoms attract each other at longer distances. This is why atoms aggregate into various bulk forms, such as a solid crystal of silicon or a liquid droplet of water. A well-known model that describes both long range attraction and short range repulsion between atoms is the Lennard-Jones (LJ) potential,

$$\phi(r) = 4\epsilon_0 \left[\left(\frac{r}{\sigma_0} \right)^{-12} - \left(\frac{r}{\sigma_0} \right)^{-6} \right] , \tag{5}$$

also plotted in Fig. 1. Here, ϵ_0 is the depth of the energy well and $2^{1/6}\sigma_0$ is the distance at which the interaction energy between two atoms reaches the minimum.

The two potential energy functions considered so far are constructed under the assumption that the potential energy can be written as a sum of interactions between pairs of atoms, Eq. (3). Model potential functions of this type are called *pair potentials*. Relatively few materials, among them the noble gases (He, Ne, Ar, etc.) and ionic crystals (e.g. NaCl), can be described by pair potentials with reasonable accuracy. For most other materials pair potentials do a poor job, especially in the solid state. For example, it is well known that all pair potential models are bound to produce equal values for C_{12} and C_{44}, which are two different elastic constants for cubic crystals,[1] This is certainly not true for most cubic semiconductors and metals.

There are several well established ways to go beyond pair potentials. One approach is to represent the many-body potential energy as a sum of two-body, three-body, four-body, and all the way up to N-body terms, i.e.,

$$\begin{aligned} V(\{\mathbf{r}_i\}) &= \sum_{i<j} \phi(|\mathbf{r}_i - \mathbf{r}_j|) + \sum_{i<j<k} V_3(\mathbf{r}_i, \mathbf{r}_j, \mathbf{r}_k) \\ &\quad + \sum_{i<j<k<l} V_4(\mathbf{r}_i, \mathbf{r}_j, \mathbf{r}_k, \mathbf{r}_l) + \cdots . \end{aligned} \tag{6}$$

The hope is that such a series converges fast enough to justify truncation of the expansion at some low-order term while retaining an accurate description of interatomic interactions.[2]

[1] Elastic properties of crystals with cubic symmetry are fully characterized by three elastic constants: C_{11}, C_{12} and C_{44}. The first two describe the response to tension while C_{44} describes the response to shear.

[2] A low order truncation is not always feasible for an arbitrary many-body function $V(\{\mathbf{r}_i\})$ [7].

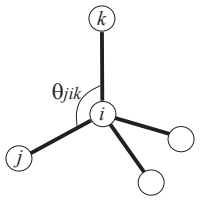

Figure 3: In the diamond cubic structure, every atom is bonded with four other atoms. The angle between any two bonds involving the same atom, such as θ_{jik}, equals 109.47°, i.e. $\cos\theta_{jik} = -1/3$.

As an example, the Stillinger-Weber (SW) potential [18] for semiconductor silicon contains two-body and three-body terms. The 3-body terms of the SW potential are proportional to,

$$(\cos\theta_{jik} + 1/3)^2 \tag{7}$$

where θ_{jik} is the angle between bond ij and bond ik, as shown in Fig. 3. Such terms penalize the deviation of the bond angle away from the tetrahedral angle (109.74°) and help to stabilize the diamond-cubic structure. Physically, this three-body term reflects the strong bond directionality of most tetrahedrally bonded covalent semiconductors.

While electrons in dielectric and semiconductor solids form well-localized covalent bonds, in metals they are more diffuse and shared by many atoms. This different behavior of bonding electrons suggests that many-body effects in the interatomic interactions in metals should be accounted for in a different manner. The embedded-atom model (EAM) is a simple and widely used interatomic potential for metals. Its functional form is

$$V(\{\mathbf{r}_i\}) = \sum_{i<j} \phi(|\mathbf{r}_i - \mathbf{r}_j|) + \sum_i F(\rho_i), \tag{8}$$

$$\rho_i = \sum_{j\neq i} f(r_{ij}). \tag{9}$$

The first term in Eq. (8) is the usual pairwise interaction accounting for the effect of core electrons. ρ_i is the local density of bonding electrons supplied by the atoms neighboring with atom i. Function $f(r)$ specifies the contribution of an atom to the electron density field. Finally, $F(\rho_i)$ is an embedding function defining the energy required to embed atom i into an environment with electron density ρ_i. For example, the form $F(\rho) = -A\sqrt{\rho}$ is used in the Finnis-Sinclair (FS) potential [8]. Other similar potentials, such as Effective-Medium-Theory (EMT) models, use somewhat different forms for the electron density contribution function $f(r)$ and the embedding function $F(\rho)$ [7].

Because the embedding function is non-linear, the EAM-like potentials include many-body effects that cannot be expressed by a superposition of pair-wise interactions. As a result, EAM potentials can be made more realistic than pair potentials. For example, EAM potentials give rise to non-zero values of the Cauchy pressure ($C_{12} - C_{44}$) and can be fitted to accurately reproduce the elastic constants of metals.

Numerous interatomic potentials have been developed for atomistic simulations of various types of materials. For some materials there is a choice of potentials of varying degrees of

accuracy and computational complexity. For example, there are more than 30 interatomic potentials for silicon alone and new potentials are likely to be developed in the future. In such a situation, it is not always obvious how to choose a potential that best fits the research objectives. In order to make reasonable choices, it is useful to appreciate what goes into the development of an interatomic potential.

Development of an interatomic potential is not a straightforward process. The first step is usually the selection of a functional form that can capture the underlying physics of interatomic interaction in the material of interest. Although inspired by physical considerations, this choice is often intuitive and hence subjective. The functional form should contain a sufficient number of adjustable parameters so that the potential can be fitted to reproduce a selected set of material properties. The fitting database of the material properties can include experimental data, or *ab initio* calculation results, or both. The selection of material properties to fit to is also a matter of subjective judgement and often reflects which material behaviors the developer is most interested in. Because fitting to empirical data is often involved in their development, the interatomic potential functions are sometimes referred to as *empirical potentials*, to reflect their less-than-rigorous physical foundation,

The key issue in developing a good interatomic potential is its *transferability*, the ability to accurately describe or predict a material's property that is *not* included in its fitting database. Transferability of an empirical potential is by no means guaranteed. As a rule of thumb, the further away from the fitted behavior the potential is used, the poorer the description it provides. It is not surprising that some users regard interatomic potentials as nothing more than interpolation functions between the data points they were fitted to. In general, it is wise to be cautious in the interpretation of simulation results obtained with the use of interatomic potentials, especially if the potential is used far from its demonstrated applicability range.

In the context of the mechanical properties of materials, the physical parameters that matter most are relative energies of most stable crystal structures (section 1.1), elastic constants, point defect energies, and stacking fault energies. An interatomic potential fitted to these parameters stands a better chance to describe the mechanical response of the material accurately.

Locality of interatomic interactions

Interatomic interactions are usually short ranged (exceptions include Coulomb interactions in ionic crystals such as NaCl). Intuitively, displacement of one atom from its initial position should only cause appreciable forces in a more or less localized neighborhood of this atom, even though the agents of this interactions, the electrons, could be completely delocalized in space. Take the Lennard-Jones (LJ) potential (Fig. 1) as an example. The magnitude of pair interaction energy already decreases down to $\sim 10^{-3}\epsilon_0$ when the distance between two atoms becomes larger than $4\sigma_0$. To improve numerical efficiency, it is common to truncate interatomic potentials, i.e. by setting the interaction energy to zero whenever the distance between two atoms exceeds a cut-off radius r_c. However, a simple truncation like this would lead to a (small) discontinuity of energy at $r = r_c$. This discontinuity can lead to undesirable artifacts in simulations. It is a simple matter to "smooth out" the LJ pair potential function so that both the energy and its derivative become zero at the cut-off distance (see Problem

2.1.1).

For short ranged potentials, calculation of the force on a given atom requires positions of its neighbors only within the cut-off radius. Taking the truncated LJ potential as an example, the force on atom i is,

$$\mathbf{f}_i = \sum_j -\frac{\partial \phi(|\mathbf{r}_i - \mathbf{r}_j|)}{\partial \mathbf{r}_i} \ , \tag{10}$$

where the sum is over all atoms within radius r_c around atom i. Depending on the potential model, the average number of interacting neighbors (per atom) within the cut-off sphere ranges from a few to a few hundred atoms. In solids, this is a relatively constant number which is related to the atomic density of the material. Hence, the time required to compute the potential energy and atomic forces for short ranged potentials scales as $\mathcal{O}(N)$, where N is the total number of atoms. This linear scaling is an important advantage of using the interatomic potentials.[3]

Another useful property of interatomic potential models is that it is usually straightforward to partition the potential energy into local energy contributions of each atom. Although largely artificial and somewhat arbitrary (only the potential energy of the entire system has physical meaning), this partitioning is useful in data analysis and visualization of localized lattice defects.For potentials constructed as cluster expansions, e.g. Eq. (6), the convention is to add half of every pair-wise interaction term (such as in the LJ potential) and one third of every three-body term (such as in the SW potential) to the local energy of each participating atom. For the EAM-like potentials, the local energy of atom i can be defined as

$$E_i = \sum_j \frac{1}{2}\phi(|\mathbf{r}_i - \mathbf{r}_j|) + F(\rho_i) \ . \tag{11}$$

It is easy to check that the sum of local energies of all atoms is equal to the total potential energy Eq. (8), as it should.

Computational cost of interatomic interaction models

As was already mentioned, the first principles theory describes the interatomic interactions more accurately than the interatomic potentials but at a much higher computational cost. Among first principles methods, those based on the Density Functional Theory (DFT) have become very popular in the computational materials science community [16]. The tight binding (TB) models present another popular alternative whose accuracy and efficiency lie somewhere between DFT and empirical potentials. In the following, we compare the computational cost among three models of silicon representative of DFT, TB and interatomic potential models. We hope that even a rough comparison will be helpful to better appreciate the computational limits of various models. For this estimate, we use reasonably optimized codes, specifically VASP [2] for DFT calculations, TBMD [20] for TB, and MD++ [1] with the SW potential for Si.

[3]In practice, we need to implement a *neighbor list* in order to achieve the $\mathcal{O}(N)$ scaling. A neighbor list provides the indices of all atoms that fall within the cut-off distance of any atom. To retain the overall $\mathcal{O}(N)$ scaling, the neighbor list itself should be constructed in $\mathcal{O}(N)$ time [4].

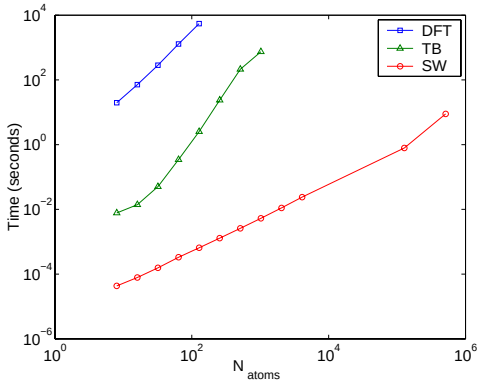

Figure 4: Computer time (in seconds) expended on evaluation of the total energy and atomic forces for a silicon crystal with different number of atoms using DFT, Tight Binding (TB) and Stillinger-Weber (SW) interatomic potential models.

The results of a series of benchmark calculations are presented in Fig. 4, showing the amount of time required in these three models to compute the potential energy and atomic forces for silicon crystals with various number of atoms. To avoid uncertainties associated with parallel machines, all calculations were performed on a single-processor Linux Alpha workstation, with 666 MHz clock speed and 1.33 GFlop peak performance.

As shown in Fig.4, for systems larger than a few hundred atoms DFT calculations become prohibitively expensive on our benchmark workstation. The feasibility limit for TB calculations is higher, over a thousand atoms.[4] On the other hand, the computing time for empirical potential model is not only much shorter but also scales linearly with the total number of atoms. Thus simulations of millions of atoms are feasible on a desktop workstation. Feasibility limits can be pushed significantly upward by using many processors in parallel. The gain due to parallel computing is again most impressive for the interatomic potential models because of their linear scaling. Molecular dynamics simulations of billions of atoms have been performed on parallel machines with thousands of processors [3].

To choose an appropriate model for atomistic simulations several factors need to be considered. The final selection is most often a compromise between computational expediency and theoretical rigor. If the problem of interest involves a large number of atoms far exceeding the feasibility limit of DFT and TB models, classical potential models may be the only choice. For some other materials, such as novel alloys for which no empirical potential or semi-empirical TB model exists, DFT becomes the method of choice. However, if the situation of interest demands both high accuracy and a large number of atoms simultaneously, one may need to develop a new potential, which is usually a very tedious task. The

[4]The actual time for one step in real simulations is likely to be different from this benchmark data. For examples, in DFT and TB methods, the electronic wave functions need to be relaxed to their ground states to compute potential energy and atomic forces. The relaxation of wave functions usually take more time in the first step (recorded here) than in subsequent steps because they do not change much from one step to the next. DFT usually scales as $\mathcal{O}(N^3)$ at large N on the more powerful parallel computers, whereas on single CPU workstations an $\mathcal{O}(N^2)$ scaling is usually observed. To extend their range of applicability, $\mathcal{O}(N)$ methods are being developed for DFT and TB calculations.

lack of computationally expedient approaches to modelling alloys and other "realistically dirty" materials is probably the greatest limitation for atomistic modelling in general and dislocation simulations in particular.

To improve the accuracy and to expedite atomistic simulations, different models, such as DFT and empirical potential, can be used in combinations. For example, a "cheap" empirical potential model can be used to screen a large family of crystal defect configurations and select candidates that are most likely to control the material behavior of interest. These observations often call for a "heavy artillery fire", suggesting targets for further calculations using more accurate and expensive methods such as TB and DFT. It is also possible to use inexpensive interatomic potential models to estimate and correct errors in TB and DFT calculations due to their limited number of atoms (chapter 5). Yet another very interesting possibility is to apply different models to different regions in the same simulation. For example, in atomistic simulations of cracks, a few atoms near the crack tip can be treated by more accurate DFT or TB methods, to obtain an accurate description of bond breaking process. At the same time, atoms farther away from the crack tip experience much smaller deformations and can be well described by an empirical potential model. How to handle interfaces between regions described by different models is a subject of active research (see [5] as an example). The models available for atomistic simulations are becoming more plentiful and their accuracy continues to improve. Along with the ever increasing computing power, this assures that atomistic simulations will be playing an increasingly important role in future materials research.

Summary

• The intricacies of interaction between atoms in molecules and solids are rooted in the quantum mechanics of electrons.

• First principles approaches, such as DFT, provide accurate descriptions of interatomic interactions but are computationally demanding.

• Empirical potential models are less accurate but allow simulations of a much larger number of atoms. These models are fitted to experimental data and/or first principles calculations.

• Models with different levels of complexity and accuracy can be combined to provide a more accurate description at a more reasonable computational cost.

Problems

1.1. It is easy to make the Lennard-Jones potential strictly short ranged by setting the energy to zero beyond the cut-off distance, $r > r_c$. However, the resulting modified LJ potential will be discontinuous at $r = r_c$. To avoid artifacts in atomistic simulations, it is best to make sure that both the energy and its first derivative vanish smoothly at $r = r_c$. Specifically, for the LJ potential this can be done by adding a linear term to $\phi(r)$ when $r < r_c$, i.e.,

$$\phi(r) \;=\; \begin{cases} 4\epsilon_0[(r/\sigma_0)^{-12} - (r/\sigma_0)^{-6}] + A + Br\ , & r < r_c \\ 0, & r \geq r_c \end{cases} \quad . \tag{12}$$

Find values for A and B such that the truncated LJ potential and its first derivative with respect to r become zero at $r = r_c$.

2 Equilibrium distribution

Consider a system containing N atoms of the same mass m interacting via an interatomic potential $V(\{\mathbf{r}_i\})$. The total energy of such a system is,

$$H(\{\mathbf{r}_i, \mathbf{p}_i\}) = \sum_{i=1}^{N} \frac{|\mathbf{p}_i|^2}{2m} + V(\{\mathbf{r}_i\}) \tag{13}$$

Function H is called the Hamiltonian. The first term on the right hand side is the sum of kinetic energies of all atoms in which $\mathbf{p}_i = m\mathbf{v}_i$ is the momentum vector of atom i, and $\mathbf{v}_i = d\mathbf{r}_i/dt$ is its velocity. In classical mechanics, the instantaneous state of the system is fully specified by the positions and momenta of all atoms $\{\mathbf{r}_i, \mathbf{p}_i\}$, and is usually called a *microstate*. In 3-dimension, this corresponds to $6N$ variables. Therefore, the state of the system can be regarded as a point in the $6N$ dimensional space spanned by $\{\mathbf{r}_i, \mathbf{p}_i\}$, called the *phase space*.

The theoretical basis of most atomistic simulation methods is the fundamental law of classical statistical mechanics — *Boltzmann's law* [6, 10]. It states that, when the system is in thermal equilibrium at temperature T, the probability density to find the system near a specific point $\{\mathbf{r}_i, \mathbf{p}_i\}$ in the phase space is $f(\{\mathbf{r}_i, \mathbf{p}_i\})$,

$$f(\{\mathbf{r}_i, \mathbf{p}_i\}) \;=\; \frac{1}{Z} \exp\left[-\frac{H(\{\mathbf{r}_i, \mathbf{p}_i\})}{k_B T}\right] \tag{14}$$

where

$$Z \;=\; \int \prod_{i=1}^{N} d\mathbf{r}_i d\mathbf{p}_i \exp\left[-\frac{H(\{\mathbf{r}_i, \mathbf{p}_i\})}{k_B T}\right] .$$

Here, $k_B = 8.6173 \times 10^{-5}$eV/K is Boltzmann's constant. Eq. (14) is the famous *Boltzmann's distribution* for classical particles at thermal equilibrium and Z is called the partition function. Z ensures the proper normalization of the probability density f. Boltzmann's distribution is suitable when the temperature is not too low so that quantum effects can be ignored[5] (see Problem 2.2.3).

An important concept in statistical mechanics is the *statistical ensemble* of systems. Consider a very large number of replicas of the system, each with N atoms and described by the same Hamiltonian. At any instance of time, each system's state is represented by a point $\{\mathbf{r}_i, \mathbf{p}_i\}$ in the $6N$-dimensional phase space. An *ensemble* is the collection of all these replicas, or equivalently, points in the $6N$-dimensional phase space. Each replica (a member of the ensemble) may evolve with time, which is reflected by the motion of a corresponding point in the phase space. The replicas do not interact, i.e., the points in the phase space move independently of each other. When the replicas are distributed according to Boltzmann's distribution, i.e. Eq. (14), the ensemble is called *canonical*.

Boltzmann's law makes it possible to express macroscopic quantities of the system at thermal equilibrium as a statistical average of microscopic functions over the canonical ensemble. Given a microscopic function $A(\{\mathbf{r}_i, \mathbf{p}_i\})$ that depends on the positions and momenta

[5] Quantum mechanical particles satisfy different types of distributions, such as Bose-Einstein and Fermi-Dirac distributions.

Figure 5: Ludwig Boltzmann (1844-1906 Austria).

of all atoms, its (canonical) ensemble average is,

$$\langle A \rangle \equiv \frac{1}{Z} \int \prod_{i=1}^{N} d\mathbf{r}_i d\mathbf{p}_i A(\{\mathbf{r}_i, \mathbf{p}_i\}) \exp\left[-\beta H(\{\mathbf{r}_i, \mathbf{p}_i\})\right] \tag{15}$$

where $\beta \equiv 1/(k_B T)$. For example, the average potential energy U of the system is,

$$\begin{aligned} U &= \langle V \rangle \equiv \frac{1}{Z} \int \prod_{i=1}^{N} d\mathbf{r}_i d\mathbf{p}_i V(\{\mathbf{r}_i\}) \exp\left[-\beta H(\{\mathbf{r}_i, \mathbf{p}_i\})\right] \\ &= \frac{\int \prod_{i=1}^{N} d\mathbf{r}_i V(\{\mathbf{r}_i\}) \exp\left[-\beta V(\{\mathbf{r}_i\})\right]}{\int \prod_{i=1}^{N} d\mathbf{r}_i \exp\left[-\beta V(\{\mathbf{r}_i\})\right]} \end{aligned} \tag{16}$$

Because the Hamiltonian has a simple dependence on atomic momenta, the momentum part of the integral for the Boltzmann's partition function Z can be separated out, i.e.,

$$f(\{\mathbf{r}_i, \mathbf{p}_i\}) = \frac{1}{Z} \prod_{i=1}^{N} \exp\left[-\frac{|\mathbf{p}_i|^2}{2mk_B T}\right] \exp\left[-\frac{V(\{\mathbf{r}_i\})}{k_B T}\right] \tag{17}$$

Physically, this means that at thermal equilibrium the momentum of each atom obeys an independent and identical distribution. The average kinetic energy of an atom j is,

$$\begin{aligned} \langle E_{\mathrm{kin},j} \rangle &= \left\langle \frac{|\mathbf{p}_j|^2}{2m} \right\rangle \equiv \frac{1}{Z} \int \prod_{i=1}^{N} d\mathbf{r}_i d\mathbf{p}_i \frac{|\mathbf{p}_j|^2}{2m} \exp\left[-\beta H(\{\mathbf{r}_i, \mathbf{p}_i\})\right] \\ &= \frac{\int d\mathbf{p}_j \frac{|\mathbf{p}_j|^2}{2m} \exp\left[-\frac{|\mathbf{p}_j|^2}{2mk_B T}\right]}{\int d\mathbf{p}_j \exp\left[-\frac{|\mathbf{p}_j|^2}{2mk_B T}\right]} = \frac{3}{2} k_B T \end{aligned} \tag{18}$$

The average kinetic energy of the entire system is,

$$\langle E_{\mathrm{kin}} \rangle = \sum_{j=1}^{N} \langle E_{\mathrm{kin},j} \rangle = \frac{3}{2} N k_B T \tag{19}$$

Notice that these results are independent of the atomic mass m. They are the direct consequence of the quadratic dependence of the Hamiltonian on atomic momentum. Similarly,

if the system is harmonic, meaning that the potential $V(\{\mathbf{r}_i\})$ is a quadratic function of atomic positions, the average potential energy of the system is $U = \frac{3}{2}Nk_BT$. Therefore, the average total energy of a harmonic system is $E_{\text{tot}} = E_{\text{kin}} + U = 3Nk_BT$, to which the kinetic and potential energies contribute equally. For a crystal well below its melting temperature, the potential energy function can be approximated by a set of harmonic (quadratic) terms through a Taylor expansion around the energy minimum (see section 6.2). In such a case, we would expect the total energy of the system to divide approximately equally between kinetic and potential energy parts.

Summary
• Boltzmann's distribution describes statistical properties of a classical system of atoms at thermal equilibrium.
• Some of the statistical averages over the canonical ensemble are particularly simple. The average kinetic energy of a system of N atoms is $\frac{3}{2}Nk_BT$. When the potential energy is a quadratic function of atomic coordinates, the average potential energy is also $\frac{3}{2}Nk_BT$.

Problems

2.1. The Hamiltonian of a one-dimensional harmonic oscillator is

$$H(x, p_x) = \frac{p_x^2}{2m} + \frac{1}{2}kx^2 \tag{20}$$

Assuming that an ensemble of such oscillators satisfies Boltzmann's distribution, find the average kinetic energy and the average total energy over this ensemble at temperature T.

2.2. The Hamiltonian of a three-dimensional Harmonic oscillator is

$$H(\mathbf{r}, \mathbf{p}) = \frac{|\mathbf{p}|^2}{2m} + \frac{1}{2}k|\mathbf{r}|^2. \tag{21}$$

Find the distribution function $f(E)$ for the energy of an ensemble of such oscillators in thermal equilibrium at temperature T.

2.3. In quantum mechanics, every particle possesses a de Broglie wavelength $\lambda = h/p$, where $h = 6.626068 \times 10^{-34}\text{m}^2 \cdot \text{kg} \cdot \text{s}^{-1}$ is Planck's constant, $p = mv$ is the momentum, and v is the velocity. The motion of interacting articles can be treated classically when the typical distance between them exceeds λ. In thermal equilibrium, the average kinetic energy of a classical particle is $\langle \frac{1}{2}m|\mathbf{v}|^2 \rangle = \frac{3}{2}k_BT$. Taking copper crystal as an example, estimate the temperature below which the motion of its atoms will have to be treated quantum mechanically. Copper has the FCC crystal structure with a lattice constant $a = 3.61\mathring{A}$ and atomic mass of $m = 63.546$a.u. (1a.u.=1.6604×10^{-27}kg).

3 Energy minimization

According to Boltzmann's distribution, the probability of finding the system at a microstate $\{\mathbf{r}_i, \mathbf{p}_i\}$ decreases exponentially with increasing energy $H(\{\mathbf{r}_i, \mathbf{p}_i\})$. In the low temperature

limit, this exponential dependence means that the system is most likely to be found in the neighborhood of the global minimum of $H(\{\mathbf{r}_i, \mathbf{p}_i\})$. From Eq. (13), the minimum of $H(\{\mathbf{r}_i, \mathbf{p}_i\})$ corresponds to $\mathbf{p}_i = 0$ for all i and $\{\mathbf{r}_i\}$ at the minimum of the potential function $V(\{\mathbf{r}_i\})$. Therefore, the minimum of the potential energy function $V(\{\mathbf{r}_i\})$ provides a good description of the atomic structure of the system at low temperatures. Searching for minima of a function of many variables is an extensively studied subject in computational sciences. Many algorithms exist [17], and the development of still more efficient methods remains an active area of research.

To simply notation for the following discussions, let us define a $3N$-dimensional vector $\mathbf{R} = (x_1, y_1, z_1, x_2, y_2, z_2, \cdots, x_N, y_N, z_N)^{\mathrm{T}}$, where x_i, y_i, z_i are the cartesian coordinates of atoms in a system of N atoms. The space spanned by $\mathbf{R}$ is called the *configurational space*. Now we can rewrite the potential energy $V(\{\mathbf{r}_i\})$ as $V(\mathbf{R})$. The $3N$-dimensional vector of force is then $\mathbf{F} = -\partial V(\mathbf{R})/\partial \mathbf{R}$ or, in the component form, $\mathbf{F} = (f_{x1}, f_{y1}, f_{z1}, \cdots, f_{xN}, f_{yN}, f_{zN})^{\mathrm{T}}$, where $f_{x_i} = -\partial V/\partial x_i$ is the force on atom i along the x direction. Let us define the magnitude of force $\mathbf{F}$ as $|\mathbf{F}| = (f_{x1}^2 + f_{y1}^2 + \cdots + f_{zN}^2)^{1/2}$. These definitions will simplify the following discussions.

The steepest descent method

Steepest descent is a simple, although not very efficient, iterative algorithm for finding a (local) minimum of $V(\mathbf{R})$ starting from an arbitrary initial configuration $\mathbf{R}$. At every iteration, the force vector $\mathbf{F}$ is computed and $\mathbf{R}$ is displaced by a small step along $\mathbf{F}$. The iterations continue until $|\mathbf{F}|$ becomes smaller than a prescribed tolerance ϵ. A simple steepest descent algorithm is given below, which requires the step size Δ to be specified as an input.

Algorithm 2.1

1. $\mathbf{F} := -\partial V(\mathbf{R})/\partial \mathbf{R}$
2. If $|\mathbf{F}| < \epsilon$, exit.
3. $\mathbf{R} := \mathbf{R} + \mathbf{F}\Delta$. Go to 1.

The idea of the steepest descent algorithm is that, as long as $|\mathbf{F}|$ is non-zero, $V(\mathbf{R})$ can be further reduced by displacing $\mathbf{R}$ in the direction of $\mathbf{F}$. This algorithm is equivalent to a numerical integration of an over-damped equation of motion,

$$\mathbf{f}_i - \gamma \mathbf{v}_i = 0 \ , \tag{22}$$

where $\mathbf{v}_i$ is the velocity of atom i, and γ is the friction coefficient. This equation describes the dynamics of a set of interacting particles in a highly viscous medium.[6] After a sufficiently long time, the particles will eventually arrive at a structure corresponding to a local energy minimum for which all forces vanish.

Although very simple, the *steepest descent* algorithm is rarely used in atomistic simulations because it is numerically inefficient, often requiring many steps to converge to a

[6]To make the analogy exact, Δ in Algorithm 2.1 corresponds to $\Delta t/\gamma$, where Δt is the time step for the numerical integration of Eq. (22).

minimum. The second problem with this method is that, even when a minimum energy state is found, it is not guaranteed to be the global minimum. In fact, potential energy functions constructed from the interatomic potentials typically have multiple local minima. A steepest descent search can converge to any one of them, depending on the initial atomic configuration. In the following, we discuss slightly more sophisticated approaches that address these two problems.

Conjugate gradient relaxation

Closely related to the steepest descent method is the *conjugate gradient relaxation* (CGR) algorithm. CGR relies on exactly the same information as steepest descent, i.e. atomic forces, but uses it in a more intelligent way. CGR goes through a series of search directions. The (local) minimum energy point along each search direction is reached before CGR proceeds to the next search direction. The search sequence is constructed in such a way that subsequent search directions "avoid" (i.e. are conjugate to) all previously searched directions. This is the key to the greater efficiency of the CGR algorithm compared to the steepest descent method.

The CGR algorithm works best in an idealized situation when the potential energy is a quadratic function, i.e., $V(\mathbf{R}) = \frac{1}{2}\mathbf{R}^{\mathrm{T}} \cdot \mathbf{G} \cdot \mathbf{R}$, where $\mathbf{G}$ is a $3N \times 3N$ symmetric matrix. The *conjugate* condition means that any two search directions $\mathbf{d}^{(n)}$ and $\mathbf{d}^{(m)}$ $(n \neq m)$ must satisfy

$$\mathbf{d}^{(n)\mathrm{T}} \cdot \mathbf{G} \cdot \mathbf{d}^{(m)} = 0 \tag{23}$$

One can prove that that the minimum (in this case it is $\mathbf{R} = 0$) is reached in no greater than $3N$ searches provided that the consecutive search directions are all conjugate to each other.[7] Making sure that the current search direction is conjugate to all previous search directions seems to be a daunting task, especially if the relaxation requires hundreds of search directions. The key to the success of CGR is to make sure that the current search direction $\mathbf{d}^{(n)}$ is conjugate to the previous one $\mathbf{d}^{(n-1)}$. Then, it is possible to show that $\mathbf{d}^{(n)}$ is also conjugate to all the previous search directions $\mathbf{d}^{(m)}$ [17]. The algorithm can be described as follows.

Algorithm 2.2

1. Initialize iteration counter $n := 1$
2. Compute forces $\mathbf{F} := -\partial V(\mathbf{R})/\partial \mathbf{R}$. If $|\mathbf{F}| < \epsilon$, exit.
3. If $n = 1$, $\mathbf{d}^{(n)} := \mathbf{F}^{(n)}$, i.e., the search direction is the same as the force direction; otherwise, $\gamma^{(n)} := [\mathbf{F}^{(n)} \cdot \mathbf{F}^{(n)}]/[\mathbf{F}^{(n-1)} \cdot \mathbf{F}^{(n-1)}]$,
   $\mathbf{d}^{(n)} := \mathbf{F}^{(n)} + \gamma^{(n)}\mathbf{d}^{(n-1)}$;
4. Find an energy minimum along direction $\mathbf{d}^{(n)}$, i.e. find x_0 that is a local minimum of the one-dimensional function $V(x) \equiv V(\mathbf{R} + x\mathbf{d}^{(n)})$.
5. $\mathbf{R} := \mathbf{R} + x_0\mathbf{d}$.

[7] In practice, the search bring the system close to the minimum much earlier than that.

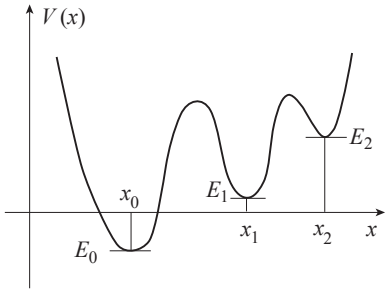

Figure 6: A function $V(x)$ with multiple local minima: E_0, E_1 and E_2. The lowest of the minima, E_0, is the global minimum.

6. $n := n + 1$. Go to 2.

Given its computational efficiency CGR is often used in atomistic simulations, including several examples in this book. The CGR algorithm has been implemented in MD++ [1], which works well in simulations of up to about half a million atoms.

Global minimization

Neither CGR nor the steepest descent algorithms guarantee to find the global minimum of an energy function. To better understand the nature of this problem, Fig. 6 illustrates the difference between local minima and the global minimum. Function $V(x)$ has three local minima, E_0, E_1 and E_2, at $x = x_0$, x_1 and x_2 respectively. Among the three, E_0 is the lowest or global minimum. Depending on the choice of the initial point, both minimization algorithms discussed so far can converge to one of the local minima E_1 or E_2. If the global minimum is the target, a brute-force approach is to run minimization many times starting from randomly selected initial configurations. Then, the lowest local minimum found from a series of relaxations provides an upper bound on the global minimum. Obviously, such an approach is very inefficient.[8]

Some of the more efficient methods for finding the global minimum of functions of many variables are motivated by processes occurring in Nature. For example, genetic algorithms invoke mutation and natural selection to evolve a collection of systems in search for the fittest (having the lowest energy) [11, 15, 9]. Another useful method is *simulated annealing* (SA), which mimics the thermal annealing of a material, as its name suggests [13, 12].

SA requires methods to simulate atomistic systems at non-zero temperatures. Both Monte Carlo (MC) and Molecular Dynamics (MD) methods described in following sections can be used for this purpose. At low temperatures, the system can become trapped in the neighborhood of a local energy minimum that depends on the choice of the initial configuration. To lessen this unwanted dependence, SA simulations starts at a high temperature, making it easier for the system to escape from the traps of local minima and explore a larger

[8]On the other hand, we are not always interested in the global energy minimum of the potential energy function in the entire configurational space. The global energy minimum state of a large collection of atoms is usually the perfect crystal. Thus the system is by definition not in its global energy minimum if we are studying dislocations. Therefore, what we are usually interested in is a "global" minimum within a certain domain of the configurational space, such as the minimum energy structure of a dislocation (chapter 3).

volume in the configurational space. The SA search then slowly reduces the temperature to zero. At the end of this procedure, the system converges to a local minimum that is likely to be less dependent on the initial configuration, and is more likely to be the global minimum. To further reduce the statistical uncertainty, it is advisable to run SA for several times, starting from different initial configurations. In this way a tight upper bound on the global minimum can be obtained, provided that the temperature varies with time sufficiently slowly. How long the SA simulation runs is usually dictated by the available computing resources. At the same time, there should exist an optimal annealing schedule, i.e. temperature T as a function of time t, for a given total annealing time. The optimal form of $T(t)$ is system dependent and generally not known in advance. In practice, annealing functions of the form $T(t) = T_0 \exp(-t/\tau)$ are commonly used where τ is a prescribed time scale of temperature reduction.

While the MC and MD methods can be combined with SA to search for global minimum of the potential function, they are often used by themselves to study the finite temperature properties of atomistic systems. The relaxed atomistic configuration from local minimization algorithms described in this section (such as CGR) is usually used as initial conditions for MC and MD simulations.

Summary

• An atomistic configuration with the lowest possible potential energy is the most likely state in the limit of zero temperature.

• The steepest descent and the conjugate gradient relaxation algorithms are used for finding local energy minima. Finding the global energy minimum is a much more difficult task. The method of simulated annealing can provide a tight upper bound on the global minimum.

References

[1] *MD++ simulation package is available from the book web site.* http://micro.stanford.edu.

[2] *Vienna Ab initio Simulation Package (VASP).* http://cms.mpi.univie.ac.at/vasp.

[3] F. F. Abraham, R. Walkup, H. J. Gao, M. Duchaineau, T. D. De la Rubia, and M. Seager. Simulating materials failure by using up to one billion atoms and the world's fastest computer: Work-hardening. *Proceedings of the National Academy of Sciences of the United States of America*, 99(9):5783–5787, 2002.

[4] M. P. Allen and D. J. Tildesley. *Computer Simulation of Liquids.* Oxford University Press, Oxford, 1989.

[5] J. Q. Broughton, F. F. Abraham, N. Bernstein, and E. Kaxiras. Concurrent coupling of length scales: Methodology and application. *Physical Review B (Condensed Matter)*, 60:2391–403, 1999.

[6] D. Chandler. *Introduction to Modern Statistical Mechanics*. Oxford University Press, Oxford, 1987.

[7] M. W. Finnis. *Interatomic Forces in Condensed Matter*. Oxford University Press, Oxford, 2003.

[8] M. W. Finnis and J. E. Sinclair. A simple empirical n-body potential for transition metals. *Philosophical Magazine A (Physics of Condensed Matter, Defects and Mechanical Properties)*, 50(1):45–55, 1984.

[9] R. L. Haupt and S. E. Haupt. *Practical Genetic Algorithms*. Wiley, 2nd edition, 2004.

[10] T. L. Hill. *An Introduction to Statistical Thermodynamics*. Dover, New York, 1986.

[11] J. H. Holland. *Adaptation in natural and artificial systems : an introductory analysis with applications to biology, control, and artificial intelligence*. MIT Press, Cambridge, Mass., 1992.

[12] S. Kirkpatrick. Optimization by simulated annealing: quantitative studies. *Journal of Statistical Physics*, 34(5/6):975–86, 1984.

[13] S. Kirkpatrick, C. D. Gelatt, and M. P. Vecchi. Optimization by simulated annealing. *Science*, 220(4598):671–680, 1983.

[14] R. M. Martin. *Electronic Structure: Basic Theory and Practical Methods*. Cambridge University Press, Cambridge, 2003.

[15] M. Mitchell. *Introduction to Genetic Algorithms*. Bradford Book, 1998.

[16] M. C. Payne, M. P. Teter, D. C. Allan, T. A. Arias, and J. D. Joannopoulos. Iterative minimization techniques for ab initio total-energy calculations: molecular dynamics and conjugate gradients. *Reviews of Modern Physics*, 64(4):1045–97, 1992.

[17] W. H. Press, B. P. Flannery, S. A. Teukolsky, and W. T. Vetterling. *Numerical Recipies in C: The Art of Scientific Computing*. Cambridge University Press, Cambridge, 1992.

[18] F. H. Stillinger and T. A. Weber. Computer simulation of local order in condensed phases of silicon. *Physical Review B (Condensed Matter)*, 31(8):5262–71, 1985.

[19] A. P. Sutton. *Electronic Structure of Solids*. Oxford University Press, Oxford, 1996.

[20] C. Z. Wang, C. T. Chan, and K. M. Ho. Empirical tight-binding force model for molecular-dynamics simulation of si. *Physical Review B (Condensed Matter)*, 39(12):8586–92, 1989.

ME346 – Introduction to Molecular Simulations – Stanford University – Winter 2007

Handout 6. Periodic Boundary Conditions*

Wei Cai

January 24, 2007

1 Boundary conditions

Suitable boundary conditions are key to a successful atomistic simulation. To appreciate the importance of boundary conditions for atomistic simulations, consider Avogadro's number, $N_A = 6.022 \times 10^{23}$, which is the number of molecules in one mole of any substance.[1] Roughly speaking, the number of atoms contained in a cubic-centimeter of solid or liquid is on the order of N_A. In comparison, a typical simulation on a desktop workstation can only handle 10^3 to 10^6 atoms. Even in the billion-atom simulations on massively parallel computers [3], the total number of atoms is still very small compared with Avogadro's number. Therefore, unless one is specifically interested in isolated nano-sized atomic clusters, the actual simulation volume is only a very small portion of the material of interest. The behavior of atoms in the simulation volume is affected by a large number ($\sim 10^{23}$) of surrounding atoms, which cannot be explicitly included in the simulation. The influence of these surrounding atoms can only be accounted for implicitly and approximately, through special treatment of boundary conditions discussed below and external couplings to be discussed later.

Unless a different boundary condition is specifically defined, "no-boundary" boundary condition or, equivalently, "free-surface" boundary condition means that there is no constrain on the motion of any atom. In such cases, the atoms usually form a compact cluster in which some of the atoms are exposed to vacuum. Such a boundary condition is not a good description of bulk materials since it completely ignores the effects of atoms outside the simulation volume and introduces unnecessary surfaces. One way to reduce the unwanted surface effects is to fix atoms on the periphery of the simulation volume in equilibrium positions that they would occupy in an infinite solid. Such a fixed boundary condition is relatively simple to implement but has its own artifacts, especially in dynamical simulations since in a real material all atoms should be able to move. As an improvement, flexible boundary conditions allow the atoms in the boundary layer to adjust their positions in

*This handout is adapted from Section 3.2 of `Computer Simulations of Dislocations`, V. V. Bulatov and W. Cai, (Oxford University Press, 2006). Website: `http://micro.stanford.edu`

[1] N_A is formally defined as the number of atoms in 12 gram of Carbon-12.

response to the motion of inner atoms [7, 6]. The search for better boundary conditions continues to the present day. The goal is to reduce surface artifacts as much as possible, while maximizing the numerical efficiency by not including too many atoms explicitly in the simulation. Periodic Boundary Condition (PBC) is a special case among many types of boundary conditions available. The idea of PBC has a long history, but it remains a very competitive method today. The particular advantage of PBC is that it completely eliminates surface effects and maintains translational invariance of the simulation volume which is especially important in simulations of crystals. PBC can be applied along one, two, or three directions of the simulation cell. In the following, we describe how to implement PBC along all three directions.

2 Periodic boundary conditions

Figure 1: Left: Max Born (1882-1970), Nobel Prize in Physics 1954. Right: Theodore von Karman (1881-1963).

The idea of (Born-von Karman) periodic boundary conditions (PBC) is to embed the simulation volume or simulation *cell* into an infinite, periodic array of replicas or *images*. This is illustrated in Fig. 2 for a 2-dimensional simulation. The atoms in the replicas are assumed to behave exactly in the same way as the atoms in the original or *primary* simulation cell [4]. Because the primary and image cells are identical, it is irrelevant which one of them is regarded as primary and which ones are the images. This type of periodic arrangement of atoms is fully specified by a set of repeat vectors, $\mathbf{c}_i$, $i = 1, 2$ in 2-dimension and $i = 1, 2, 3$ in 3-dimension. The repeat vectors relate positions of atoms in the periodic replicas. Whenever there is an atom at position $\mathbf{r}$ there are also atoms at positions $\mathbf{r} + n_1\mathbf{c}_1 + n_2\mathbf{c}_2 + n_3\mathbf{c}_3$, where n_1, n_2 and n_3 are arbitrary integers.[2]

A remarkable property of PBC is that no point in space is treated any more specially than others. To better understand this feature, let us first consider a simulation under free-surface boundary condition. In this case, the atoms closer to the surface experience a different environment than the atoms further away from the surface. In other words, the

[2] An atomistic model under 3-dimensional PBC is equivalent to a crystal structure whose primitive vectors are the same as the PBC repeat vectors and whose basis is the total collection of atoms inside the primary cell (see section 1.1 for the definition of crystal structures). The unit cell of such a super-crystal is sometimes called *supercell*.

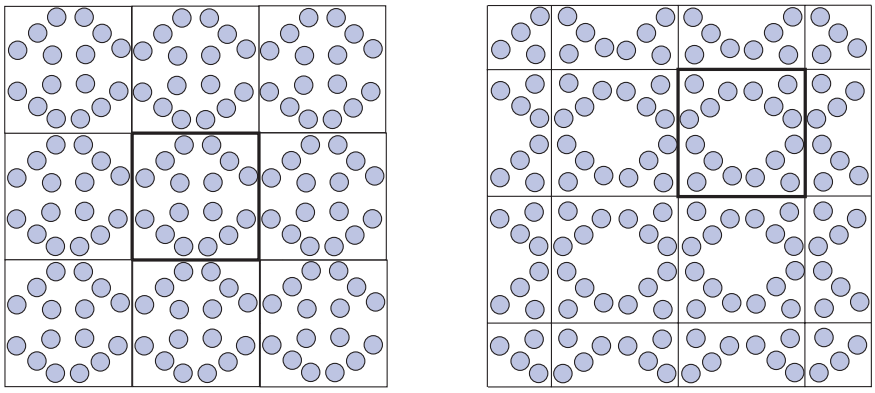

(a) (b)

Figure 2: (a) A simulation supercell with 16 atoms replicated periodically in 2D space. (b) Shifting supercell boundaries produces a different set of atoms in each supercell but does not alter the overall periodic arrangement.

presence of the surface breaks the translational invariance. At a first glance, even when PBC is applied one might think that the border of the simulation supercell (solid line in Fig. 2(a)) creates artificial interfaces that break the translational invariance. But this is not the case. The boundary of the primary cell can be shifted arbitrarily, such shown as in Fig. 2(b). Such a shift has no effect on the dynamics of any atom, even though each periodic replica now apparently contains a different arrangement of atoms. In other words, translational invariance of space is fully preserved.[3] Hence, there are no boundaries and no artificial surface effects to speak of when PBC is used. This fundamental property has made PBC a very popular boundary condition for simulations of condensed matter systems. In particular, PBC is a standard boundary condition for first principles calculations that rely on the plane-wave basis functions requiring translational invariance of space.

In an atomistic simulation with only short-ranged interactions, implementation of PBC is straighforward. All it takes is a careful enforcement of the *minimum image convention* that states that the relative displacement vector between atoms i and j is taken to be the shortest of all vectors that connect atom i to all periodic replicas of atom j. Since the energy and forces depend only on the relative positions between the atoms, this convention avoids any ambiguity provided that the potential cut-off distance is sufficiently small so that no more than one replica of atom j falls within the cut-off radius of atom i (see Problem 6.1).

Enforcement of the minimum image convention is simplest in *scaled coordinates*. For an atom at $\mathbf{r} = (x, y, z)^{\mathrm{T}}$, its scaled coordinates $s = (s_x, s_y, s_z)^{\mathrm{T}}$ are defined through,

$$\mathbf{s} = \mathbf{h}^{-1} \cdot \mathbf{r} \,, \tag{1}$$

$$\mathbf{r} = \mathbf{h} \cdot \mathbf{s} \,, \tag{2}$$

where $\mathbf{h}$ is a 3×3 matrix whose columns are the repeat vectors of the simulation cell,

[3] If PBC is applied only in one direction, then the translational invariance in that direction is preserved.

$\mathbf{h} \equiv (\mathbf{c}_1|\mathbf{c}_2|\mathbf{c}_3)$. Or, in the component form,

$$\begin{pmatrix} x \\ y \\ z \end{pmatrix} = \begin{pmatrix} c_{1x} & c_{2x} & c_{3x} \\ c_{1y} & c_{2y} & c_{3y} \\ c_{1z} & c_{2z} & c_{3z} \end{pmatrix} \cdot \begin{pmatrix} s_x \\ s_y \\ s_z \end{pmatrix} . \tag{3}$$

The manifestation of PBC in scaled coordinates is that, whenever there is an atom at position $\mathbf{s} = (s_x, s_y, s_z)$, there are also atoms at positions $\mathbf{s} = (s_x + n_1, s_y + n_2, s_z + n_3)$, where n_1, n_2 and n_3 are arbitrary integers. That is, in the space of scaled coordinates periodic images of every atom in the supercell form a simple cubic lattice with the unit lattice constant. Under the minimum image convention, the distance between two atoms with scaled coordinates $\mathbf{s}_1 = (s_{x1}, s_{y1}, s_{z1})$ and $\mathbf{s}_2 = (s_{x2}, s_{y2}, s_{z2})$ is, $\Delta\mathbf{s} = (\Delta s_x, \Delta s_y, \Delta s_z)$, where

$$\begin{aligned} \Delta s_x &= f(s_{x1} - s_{x2}) , \qquad (4) \\ \Delta s_y &= f(s_{y1} - s_{y2}) , \\ \Delta s_z &= f(s_{z1} - s_{z2}) . \\ f(t) &\equiv t - [t] \qquad (5) \end{aligned}$$

Here, function $[t]$ returns the nearest integer to t and is called `rint()` in `C` language, `dnint()` in `Fortran` and `round()` in `Matlab`. The useful property of $f(t)$ is that its values lie within $[-0.5, 0.5)$, meaning that the nearest image of atom j is certain to stay within a unit cube with atom i at its center. Therefore, the separation vector in the real space can be calculated simply as[4]

$$\Delta\mathbf{r} = \mathbf{h} \cdot \Delta\mathbf{s} . \tag{6}$$

Even though in PBC the simulation cell has no boundaries, it has finite physical dimensions and occupies volume

$$\Omega = \det(\mathbf{h}) . \tag{7}$$

The use of PBC does not completely eliminate the artifacts caused by the inevitably small number of atoms. Not surprisingly, the only way to reduce the unwanted small-size effects is by increasing the size of the simulation cell. In fact, PBC can bring in its own artifacts. One relevant example is when the simulation cell contains a crystal defect and is subjected to PBC. Such a simulation does not exactly reproduce the behavior of a single defect in an infinite crystal. Instead, it will be more representative of an infinite periodic array of defects. Unless the simulation domain is sufficiently large, the interaction between primary and image defects may "pollute" the simulation results. This is an important issue given the wide applicability and robustness of PBC in atomistic simulations of materials. Some techniques have been developed to eliminate or mitigate the artifacts introduced by PBC when modeling defects in crystals [5].

[4]Because the transformation between the real and the scaled coordinates does not necessarily preserve the relative length of segments in different orientations, it is possible that two images that are nearest in the real space are not nearest images in the scaled space. This will not create a problem if the cut-off distance of the interatomic potential is sufficiently small so that, whenever this situation occurs, atoms i and j are separated by a distance larger than the cut-off radius.

Due to the prevalence of PBC, many simulation codes, such as *ab initio* codes [2] and MD++ [1], have PBC built into them as a default boundary condition. Other types of boundary conditions can still be constructed "inside" PBC. For example, consider a simulation cell contains a nano-cluster whose size is less than the length of the simulation cell minus the cut-off radius of the interatomic potential. Even though our model correspond to a periodic array of nano-clusters, the periodic images of the cluster do not interact with each other. Hence the simulation is equivalent to an isolated nano-cluster under free-surface boundary condition.

Summary

• The total number of atoms in a simulation is typically many orders of magnitude smaller than required in most situations of interest for materials modelling. Well chosen boundary conditions mimic the effects of atoms outside the simulation volume and help to eliminate or mitigate the unwanted artifacts associated with the unavoidably small size of the simulation domain.

• Periodic boundary conditions remove artificial surface effects and preserve translational invariance in atomistic simulations.

Problems

6.1. The minimum image convention states that an atom interacts with at most one image of any other atom. To be able to enforce this convention, the size and shape of the periodic box under PBC should be selected with some care. The allowable size and shape can be deduced from the condition that no two images of the same atom can fit inside a sphere with a radius equal to the cut-off radius of the potential. Given three periodicity vectors $\mathbf{c}_1$, $\mathbf{c}_2$, $\mathbf{c}_3$ and a cut-off radius r_{cut} and assuming pairwise interactions, derive inequalities that determine when the box becomes too small or two skewed for the minimum image convention to work safely. (Hint: Consider a sphere of radius r_{cut} inscribed in the supercell.)

6.2. If the PBC vectors $\mathbf{c}_1$, $\mathbf{c}_2$, and $\mathbf{c}_3$ are not orthogonal to each other, the procedure given in Eqs. (4)-(6) does not necessarily leads to the image of atom 2 that is physically the closest to atom 1 in the real coordinate space. This would not cause any problem, if all images of atom 2 are beyond the cut-off sphere centered on atom 1. This condition puts further constraints on the admissible size and shape of the periodic box. Derive the inequalities that have to be in place for Eqs. (4)-(6) to work properly. Are the conditions described in Problem 6.1 automatically satisfied if the conditions obtained here are met?

References

[1] *MD++ simulation package is available from the book web site.* http://micro.stanford.edu.

[2] *Vienna Ab initio Simulation Package (VASP).* http://cms.mpi.univie.ac.at/vasp.

[3] F. F. Abraham, R. Walkup, H. J. Gao, M. Duchaineau, T. D. De la Rubia, and M. Seager. Simulating materials failure by using up to one billion atoms and the world's fastest

computer: Work-hardening. *Proceedings of the National Academy of Sciences of the United States of America*, 99(9):5783–5787, 2002.

[4] M. P. Allen and D. J. Tildesley. *Computer Simulation of Liquids*. Oxford University Press, Oxford, 1989.

[5] W. Cai, V. V. Bulatov, J. Chang, J. Li, and S. Yip. Periodic image effects in dislocation modelling. *Philosophical Magazine*, 83(5):539–567, 2003.

[6] W. Cai, V. V. Bulatov, J. F. Justo, A. S. Argon, and S. Yip. Intrinsic mobility of a dissociated dislocation in silicon. *Physical Review Letters*, 84(15):3346–3349, 2000.

[7] J. E. Sinclair, P. C. Gehlen, R. G. Hoagland, and J. P. Hirth. Flexible boundary-conditions and non-linear geometric effects in atomic dislocation modeling. *Journal of Applied Physics*, 49(7):3890–3897, 1978.

ME346 – Introduction to Molecular Simulations – Stanford University – Winter 2007

Handout 7. Constant Stress Molecular Dynamics

Keonwook Kang, Christopher R. Weinberger and Wei Cai

February 8, 2007

1 Microcanonical (NVE) Ensemble

Consider a Molecular Dynamics (MD) simulation of a system of N atoms, interacting with each other through the potential function $U(\{\mathbf{r}_i\})$, subjected to periodic boundary conditions (PBC), specified by three repeat vectors $\mathbf{c}_1$, $\mathbf{c}_2$, $\mathbf{c}_3$. Usually, the repeat vectors remain fixed during the simulation, hence the simulation volume $V = (\mathbf{c}_1 \times \mathbf{c}_2) \cdot \mathbf{c}_3$ remain constant.[1] In this case, the simulation corresponds to a closed system, for which the total energy also remains constant along the trajectory, i.e. $\mathcal{H}(\{\mathbf{r}_i, \mathbf{p}_i\}) = E$, where

$$\mathcal{H}(\{\mathbf{r}_i, \mathbf{p}_i\}) = \sum_{i=1}^{N} \frac{|\mathbf{p}_i|^2}{2m} + U(\{\mathbf{r}_i\}) \tag{1}$$

is the Hamiltonian.[2] The simulation is said to sample the microcanonical, or (NVE), ensemble, because the number of atoms N, volume V and total energy E are all conserved. Assuming the dynamics is *ergodic*, the equilibrium distribution of the system should satisfy the microcanonical ensemble, i.e.

$$f_{NVE}(\{\mathbf{r}_i, \mathbf{p}_i\}) = \begin{cases} \text{const.} & \mathcal{H}(\{\mathbf{r}_i, \mathbf{p}_i\}) \in [E, E + \delta E] \\ 0 & \text{otherwise} \end{cases} \tag{2}$$

where δE is a small parameter of which we will take the limit to zero, so that energy distribution will become a delta function. The long-time average of an arbitrary function, $\alpha(\{\mathbf{r}_i, \mathbf{p}_i\})$, equals to the ensemble average, i.e.

$$\overline{\alpha} = \langle \alpha \rangle_{NVE} \tag{3}$$

where

$$\overline{\alpha} \equiv \lim_{\tau \to \infty} \frac{1}{\tau} \int_0^{\tau} dt \; \alpha(\{\mathbf{r}_i(t), \mathbf{p}_i(t)\}) \tag{4}$$

$$\langle \alpha \rangle_{NVE} \equiv \frac{\int_V d^N\mathbf{r} \int_{-\infty}^{\infty} d^N\mathbf{p} \; \alpha(\{\mathbf{r}_i, \mathbf{p}_i\}) \, \delta\left(\mathcal{H}(\{\mathbf{r}_i, \mathbf{p}_i\}) - E\right)}{\int_V d^N\mathbf{r} \int_{-\infty}^{\infty} d^N\mathbf{p} \; \delta\left(\mathcal{H}(\{\mathbf{r}_i, \mathbf{p}_i\}) - E\right)} \tag{5}$$

[1] $V = \det(\mathbf{h})$, where $\mathbf{h}$ is a 3×3 matrix formed by column vectors $\mathbf{c}_1$, $\mathbf{c}_2$, $\mathbf{c}_3$.

[2] If we use a symplectic integrator with an adequately small time step, the numerical values of the Hamiltonian fluctuates around a constant but there is no long-term drift.

The (NVE) ensemble average is simply the average within the constant energy shell $\mathcal{H} = E$ in the phase space. Notice that atom positions are limited to volume V in the integration, while atom momenta are not limited at all.

2 Constant Pressure (NPH) Ensemble

Now consider a system that can exchange volume with its environment, which exerts a pressure P on the system. As an example, we may imagine gas contained in a cylindrical vessel that has a movable piston. If the system volume changes by ΔV, then the environment does work $\Delta W = -P\Delta V$ to the system. On the other hand, assume the system does not exchange heat with its environment, $\Delta Q = 0$. In our example, this means that the material of the vessel and the piston are ideal heat insulators. The first law of thermodynamics [1] states that the change of internal energy of a system equals to the sum of work done and heat flux to the system, i.e. $\Delta E = \Delta W + \Delta Q$. In this case, we have

$$\Delta E = -P\Delta V \tag{6}$$

Define enthalpy

$$H \equiv E + PV \tag{7}$$

Because P is a constant, the change of H during a volume change ΔV must be zero, i.e.

$$\Delta H = \Delta(E + PV) = \Delta E + P\Delta V = 0 \tag{8}$$

The thermodynamics considerations above motivate us to construct the following statistical ensemble, i.e. the *isobaric-isoenthalpic* or (NPH) ensemble. Imagine that the system, with energy $E = \mathcal{H}(\{\mathbf{r}_i, \mathbf{p}_i\})$, is coupled to a *barostat*, which does work to the system $\Delta W = -P\Delta V$ when the volume of the system changes by ΔV. Because of energy conservation, the energy of the barostat changes by $\Delta E_{\rm bs} = P\Delta V$. This means that the energy of the barostat can be described by $E_{\rm bs} = PV + E_0$, where E_0 is a constant which will be ignored in the following discussions by redefining the reference energy point. Therefore, we can represent the environment surrounding the system by a single variable, V, whose energy is simply $E_{\rm bs} = PV$.

The system and the barostat together can be considered as a closed system, whose total energy is conserved, i.e., $E + E_{\rm bs} = H$. Therefore, its equilibrium distribution should satisfy the microcanonical ensemble,

$$f(\{\mathbf{r}_i, \mathbf{p}_i\}, V) = \begin{cases} \text{const.} & \mathcal{H}(\{\mathbf{r}_i, \mathbf{p}_i\}) + PV \in [H, H + \delta H] \\ 0 & \text{otherwise} \end{cases} \tag{9}$$

Eq. (9) can also be considered as a distribution function for the system itself. It then looks different from the microcanonical distribution, Eq. (2). To make the coupling between V and the energy of the system more explicit, consider the example of an MD simulation under periodic boundary conditions (PBC). Consider the matrix $\mathbf{h}$ formed by three column vectors, $\mathbf{h} = (\mathbf{c}_1|\mathbf{c}_2|\mathbf{c}_3)$, where $\mathbf{c}_1$, $\mathbf{c}_2$, $\mathbf{c}_3$ are the three repeat vectors of PBC. Define scaled coordinates $\mathbf{s}_i$ so that,

$$\mathbf{r}_i = \mathbf{h} \cdot \mathbf{s}_i \tag{10}$$

$$\mathbf{s}_i = \mathbf{h}^{-1} \cdot \mathbf{r}_i \tag{11}$$

In the following we will rewrite V as Ω (to avoid confusion between V and potential energy function U), i.e. $\Omega = V = \det(\mathbf{h})$. The Hamiltonian of the system can thus be rewritten as

$$\mathcal{H}(\{\mathbf{s}_i, \mathbf{p}_i\}, \mathbf{h}) \tag{12}$$

Here we only allow the simulation box to change its volume without changing its shape.[3] Hence $\mathbf{h} = \mathbf{h}_0\Omega^{1/3}$, where $\mathbf{h}_0$ is a constant matrix with unit volume. In this case, we can rewrite the Hamiltonian as

$$\mathcal{H}(\{\mathbf{s}_i, \mathbf{p}_i\}, \Omega) \tag{13}$$

The dependence on the constant matrix $\mathbf{h}_0$ is omitted for brevity. The (NPH) ensemble for the system thus defined can be rewritten from Eq. (9) as,

$$f_{NPH}(\{\mathbf{s}_i, \mathbf{p}_i\}, \Omega) = \begin{cases} \text{const.} & \mathcal{H}(\{\mathbf{s}_i, \mathbf{p}_i\}, \Omega) + P\Omega \in [H, H + \delta H] \\ 0 & \text{otherwise} \end{cases} \tag{14}$$

The (NPH) ensemble average of any function $\alpha(\{\mathbf{s}_i, \mathbf{p}_i\}, \Omega)$ is,

$$\begin{aligned} \langle\alpha\rangle_{NPH} &\equiv \frac{\int_0^\infty d\Omega \int_\Omega d^N\mathbf{r} \int_{-\infty}^\infty d^N\mathbf{p}\ \alpha(\{\mathbf{s}_i, \mathbf{p}_i\}, \Omega)\, \delta\left(\mathcal{H}\left(\{\mathbf{s}_i, \mathbf{p}_i\}, \Omega\right) + P\Omega - H\right)}{\int_0^\infty d\Omega \int_\Omega d^N\mathbf{r} \int_{-\infty}^\infty d^N\mathbf{p}\ \delta\left(\mathcal{H}\left(\{\mathbf{s}_i, \mathbf{p}_i\}, \Omega\right) + P\Omega - H\right)} \\ \langle\alpha\rangle_{NPH} &\equiv \frac{\int_0^\infty d\Omega\, \Omega^N \int d^N\mathbf{s} \int_{-\infty}^\infty d^N\mathbf{p}\ \alpha(\{\mathbf{s}_i, \mathbf{p}_i\}, \Omega)\, \delta\left(\mathcal{H}\left(\{\mathbf{s}_i, \mathbf{p}_i\}, \Omega\right) + P\Omega - H\right)}{\int_0^\infty d\Omega\, \Omega^N \int d^N\mathbf{s} \int_{-\infty}^\infty d^N\mathbf{p}\ \delta\left(\mathcal{H}\left(\{\mathbf{s}_i, \mathbf{p}_i\}, \Omega\right) + P\Omega - H\right)} \end{aligned} \tag{15}$$

The factor Ω^N appears because of the change of integration variables from $d^N\mathbf{r}$ to $d^N\mathbf{s}$. The integration domain for each component of $\mathbf{s}$ is $[-0.5, 0.5]$.[4]. Our task now is to develop an MD simulation whose long time average equals to the (NPH) ensemble average defined above (analogous to Eq. (3)).

3 Andersen's Method

To develop a Molecular Dynamics simulation to sample the (NPH) ensemble, the simulation cell volume Ω must be included in the equations of motion so that it can fluctuate. For this purpose, Andersen[5] proposed the following Lagrangian for the extended system that includes the volume Ω and its time derivative $\dot{\Omega}$, [2]

$$\mathcal{L}_A = \frac{1}{2}\sum_i^N m_i|\Omega^{1/3}\dot{\mathbf{s}}_i|^2 - U\left(\{\Omega^{1/3}\mathbf{s}_i\}\right) + \frac{1}{2}M\dot{\Omega}^2 - P\Omega \tag{16}$$

From Legendre transform, the following Hamiltonian $\mathcal{H}_A$ is obtained.[6]

$$\mathcal{H}_A = \frac{1}{2}\sum_i^N m_i|\Omega^{1/3}\dot{\mathbf{s}}_i|^2 + U\left(\{\Omega^{1/3}\mathbf{s}_i\}\right) + \frac{1}{2}M\dot{\Omega}^2 + P\Omega. \tag{17}$$

[3]Shape change is considered in the following section, Parrinello-Rahman method.

[4]The integration domain can also be $[0, 1]$ or any other interval with unit width due to PBC.

[5]Hans Andersen is Professor and Chair of the Chemistry Department at Stanford University.

[6]The final result for $\mathcal{H}_A$ should be expressed in terms of the momenta, as in Appendix A.

where M is a fictitious mass for the simulation box. In Andersen's Lagrangian, we have made the simplified assumption that the periodic simulation cell is a cube, i.e. the matrix $\mathbf{h}$ is a constant times an identity matrix,

$$\mathbf{h} = \begin{pmatrix} \Omega^{1/3} & 0 & 0 \\ 0 & \Omega^{1/3} & 0 \\ 0 & 0 & \Omega^{1/3} \end{pmatrix} \tag{18}$$

$$\mathbf{r}_i = \Omega^{1/3}\,\mathbf{s}_i \tag{19}$$

The Lagrange's equations of motion

$$\frac{d}{dt}\left(\frac{\partial \mathcal{L}_A}{\partial\,\dot{\mathbf{s}}_i}\right) - \frac{\partial \mathcal{L}_A}{\partial\,\mathbf{s}_i} = 0 \tag{20}$$

$$\frac{d}{dt}\left(\frac{\partial \mathcal{L}_A}{\partial\,\dot{\Omega}}\right) - \frac{\partial \mathcal{L}_A}{\partial\,\Omega} = 0 \tag{21}$$

become

$$\ddot{\mathbf{s}}_i = -\frac{2}{3}\Omega^{-1}\dot{\Omega}\dot{\mathbf{s}}_i - \frac{1}{m_i\Omega^{2/3}}\frac{\partial U\left(\{\Omega^{1/3}\mathbf{s}_i\}\right)}{\partial \mathbf{s}_i} \tag{22}$$

$$\ddot{\Omega} = \frac{1}{M}\left(\frac{1}{3\Omega}\sum_i m_i|\Omega^{1/3}\dot{\mathbf{s}}_i|^2 - \frac{\partial U\left(\{\Omega^{1/3}\mathbf{s}_i\}\right)}{\partial\Omega} - P\right) \tag{23}$$

The above expressions for the Hamiltonian and the equations of motion below are derived in detail in Appendix A. It is interesting to note that the right hand side of Eq. (23) is simply proportional to the difference in the internal Virial pressure and the external pressure. The Virial stress is defined as,

$$\sigma_{\alpha\beta} = \frac{1}{\Omega}\sum_i -m_i v_\alpha^i\, v_\beta^i + r_\alpha^i\,\frac{\partial U}{\partial r_\beta^i} \tag{24}$$

where $\alpha, \beta = x, y, z$, r_α^i is the α-component of the cartesian coordinate of atom i and v_α^i is the α-component of the velocity of atom i. The Virial pressure is defined as,

$$P_{\text{Virial}} \equiv -\frac{1}{3}\left(\sigma_{xx} + \sigma_{yy} + \sigma_{zz}\right) \tag{25}$$

In terms of the Virial pressure, Eq. (23) can be rewritten as

$$\ddot{\Omega} = \frac{1}{M}\left(P_{\text{Virial}} - P\right) \tag{26}$$

Therefore, the volume Ω will tend to enlarge if the internal Virial pressure is greater than the external pressure P. The Andersen's equations of motion thus contains a feedback loop to adjust the simulation volume so that the internal Virial pressure fluctuate around the external pressure.

Along the trajectory of Andersen's dynamics, Andersen's Hamiltonian, Eq. (17), is conserved. When we use a symplectic integrator, the numerical value of $\mathcal{H}_A$ has good long-term

stability (it stays close to a constant value). However, Andersen's Hamiltonian $\mathcal{H}_A$ is not the same as the enthalpy, $H = \mathcal{H}(\{\mathbf{s}_i, \mathbf{p}_i\}, \Omega) + P\Omega$, which should be conserved in the (NPH) ensemble. Therefore, Andersen's dynamics does not exactly sample the (NPH) ensemble. However, Andersen showed that it becomes very close to the (NPH) ensemble in the limit of large N. Let $\overline{\alpha}_A$ be the long-time average of the function $\alpha(\{\mathbf{s}_i, \mathbf{p}_i\}, \Omega)$ along the trajectory of Andersen's dynamics. Then

$$\overline{\alpha}_A = \langle \alpha \rangle_{\mathrm{NPH}} + \mathcal{O}(N^{-2}) \tag{27}$$

The difference is of the order $\mathcal{O}(N^{-2})$ and becomes negligible for simulations with a large number of particles.

4 Parrinello-Rahman's method

Andersen's method allows the simulation volume to change by enlarging or shrinking the simulation cell length in all directions isotropically. This is adequate for simulation of liquids which is subjected to either zero or non-zero pressure, because the liquid molecules can rearrange themselves to relax all deviatoric stress components to zero. However, solids can sustain a non-zero deviatoric stress. Therefore, Andersen's method may be insufficient if we wish to apply zero deviatoric stress to a simulation of solids (while the pressure may or may not be zero).[7] We need to allow the simulation cell to change its *shape*, in addition to its volume, in order to relax the deviatoric stress components. In the Parrinello-Rahman (PR) method, this is done by allowing all 9 components of the $\mathbf{h}$ matrix to change during the simulation. For simplicity, we will first discuss the PR method when the simulation cell is subjected to a pressure (which may or may not be zero) and zero deviatoric stress. We will then discuss the most general case in which the simulation cell is subjected to an arbitrary stress tensor $\boldsymbol{\sigma}$. In both cases, the simulation conserves a quantity that is close to the enthalpy H in the thermodynamic limit ($N \to \infty$). In the latter case, it is more appropriate to say that the simulation samples the $(N\sigma H)$ ensemble instead of the (NPH) ensemble.

4.1 PR method under hydrostatic pressure

The Lagrangian in Parinello-Rahman's method [4, 5] is a generalization to that in Andersen's method.

$$\mathcal{L}_{\mathrm{PR}} = \frac{1}{2}\sum_i^N m_i |\mathbf{h}\dot{\mathbf{s}}_i|^2 - U\left(\{\mathbf{h}\mathbf{s}_i\}\right) + \frac{1}{2}M\left(|\dot{\mathbf{c}}_1|^2 + |\dot{\mathbf{c}}_2|^2 + |\dot{\mathbf{c}}_3|^2\right) - P\Omega, \tag{28}$$

where $(|\dot{\mathbf{c}}_1|^2 + |\dot{\mathbf{c}}_2|^2 + |\dot{\mathbf{c}}_3|^2)M/2$ represents the fictitious kinetic energy of the "simulation box", and $P\Omega$ presents the potential energy of the barostat. Because $\mathbf{h} = (\mathbf{c}_1|\mathbf{c}_2|\mathbf{c}_3)$, $|\dot{\mathbf{c}}_1|^2 +$

[7] The stress σ_{ij} is a symmetric tensor with 6 independent components. Pressure $P = -\frac{1}{3}\sigma_{kk}$ is also called the hydrostatic component of the stress tensor. Here we use Einstein's convention in which repeated indices are summed over from 1 to 3 (i.e. x to z). The deviatoric part of the stress tensor is defined as $\sigma'_{ij} = \sigma_{ij} + P$. Similarly, the strain ϵ_{ij} is also a symmetric tensor with 6 independent components. $\epsilon_{\mathrm{d}} = \frac{1}{3}\epsilon_{kk}$ is called the dilatational strain and $\epsilon'_{ij} = \epsilon_{ij} - \epsilon_{\mathrm{d}}$ is the deviatoric part of the strain.

$|\dot{\mathbf{c}}_2|^2 + |\dot{\mathbf{c}}_3|^2$ is simply the sum of the square of the time derivatives of all 9 elements of the $\mathbf{h}$ matrix, and can be written as $\dot{\mathbf{h}} : \dot{\mathbf{h}}$. Also notice that $\Omega = \det(\mathbf{h})$. Hence the Lagrangian can be rewritten as

$$\mathcal{L}_{\rm PR} = \frac{1}{2}\sum_i^N m_i \dot{\mathbf{s}}_i^T \mathbf{G} \dot{\mathbf{s}}_i - U\left(\{\mathbf{h}\mathbf{s}_i\}\right) + \frac{1}{2} M \dot{\mathbf{h}} : \dot{\mathbf{h}} - P \det\left(\mathbf{h}\right), \tag{29}$$

where $\mathbf{G} = \mathbf{h}^T\mathbf{h}$ is called the metric tensor. The Lagrange's equations of motion for $\mathbf{s}_i$ and $\mathbf{h}$ are

$$\ddot{\mathbf{s}}_i = -\mathbf{G}^{-1}\dot{\mathbf{G}}\dot{\mathbf{s}}_i - \frac{\mathbf{G}^{-1}}{m_i}\frac{\partial U\left(\{\mathbf{h}\mathbf{s}_i\}\right)}{\partial \mathbf{s}_i} \tag{30}$$

$$\begin{aligned}\ddot{\mathbf{h}} &= \frac{1}{M}\left(\sum_i m_i \mathbf{h}\,\dot{\mathbf{s}}_i \otimes \dot{\mathbf{s}}_i - \frac{\partial U\left(\{\mathbf{h}\mathbf{s}_i\}\right)}{\partial \mathbf{h}} - P\boldsymbol{\Xi}\right) \\ &= -\frac{1}{M}\left(\boldsymbol{\sigma}_{Virial} + P\mathbf{I}\right)\boldsymbol{\Xi}\end{aligned} \tag{31}$$

where $\boldsymbol{\Xi} = \partial \det(\mathbf{h})/\partial \mathbf{h} = \det(\mathbf{h})\left(\mathbf{h}^{-1}\right)^T = \Omega\left(\mathbf{h}^{-1}\right)^T$. Detailed derviation of the equations of motion and the conserved quantity $\mathcal{H}_{\rm PR}$ is given in Appendix B. Notice that in Eq. (31), the box will change its shape if the internal Virial stress contains non-zero deviatoric components.

4.2 PR method under arbitrary stress

When the applied stress has zero deviatoric component, the environment does work to the system only when it changes its volume. Therefore in the previous subsection, the potential energy of the environment only includes the $P\Omega$ term. When the simulation cell is subjected to arbitrary stress, the potential energy of the environment needs to include one more term that accounts for the work done by the deviatoric stress during shape change of the simulation cell. In the PR method, this term is

$$\frac{\Omega_0}{2}\,\mathrm{Tr}(\boldsymbol{\Sigma}\mathbf{G}) \tag{32}$$

where $\boldsymbol{\Sigma} = -\mathbf{h}_0^{-1}(\boldsymbol{\sigma} + P\mathbf{I})(\mathbf{h}_0^{-1})^T$. $\mathbf{h}_0$ is a reference matrix that specifies the coordinate system in which the stress components are defined. It is usually taken to be the value of $\mathbf{h}$ at the beginning of the simulation or the average value of $\mathbf{h}$ during the simulation. $\boldsymbol{\sigma}$ is the applied stress tensor and P is the corresponding pressure, $P = -\frac{1}{3}(\sigma_{xx} + \sigma_{yy} + \sigma_{zz})$. $\boldsymbol{\sigma} + P\mathbf{I}$ is the deviatoric part of the stress tensor.[8] The justification of this term is given in Appendix B. The new Lagrangian now becomes

$$\begin{aligned}\mathcal{L}'_{\rm PR} &= \mathcal{L}_{\rm PR} - \frac{\Omega_0}{2}\,\mathrm{Tr}(\boldsymbol{\Sigma}\mathbf{G}) \\ &= \frac{1}{2}\sum_i^N m_i \dot{\mathbf{s}}_i^T \mathbf{G} \dot{\mathbf{s}}_i - U\left(\{\mathbf{h}\mathbf{s}_i\}\right) + \frac{1}{2} M \dot{\mathbf{h}} : \dot{\mathbf{h}} - P\det\left(\mathbf{h}\right) - \frac{\Omega_0}{2}\,\mathrm{Tr}(\boldsymbol{\Sigma}\mathbf{G})\end{aligned} \tag{33}$$

[8] There is a sign difference between the stress tensor $\boldsymbol{\sigma}$ here and that in the original PR paper, in which $P = \frac{1}{3}(\sigma_{xx} + \sigma_{yy} + \sigma_{zz})$. The implementation of PR method in MD++ follows PR's sign convention.

The equation of motion for $\mathbf{s}_i$ stays the same as Eq. (30). The equation of motion for $\mathbf{h}$ now contains an addition term and becomes

$$\begin{aligned}\ddot{\mathbf{h}} &= \frac{1}{M}\left(\sum_i m_i \mathbf{h}\,\dot{\mathbf{s}}_i \otimes \dot{\mathbf{s}}_i - \frac{\partial U\left(\{\mathbf{h}\mathbf{s}_i\}\right)}{\partial \mathbf{h}} - P\boldsymbol{\Xi} - \Omega_0\,\mathbf{h}\,\boldsymbol{\Sigma}\right) \\ &= -\frac{1}{M}\left[\left(\boldsymbol{\sigma}_{Virial} + P\mathbf{I}\right)\boldsymbol{\Xi} + \Omega_0\,\mathbf{h}\,\boldsymbol{\Sigma}\right] \end{aligned} \tag{34}$$

A Derivation of Anderson's dynamics

A.1 Lagrange's equation of motion

From the Andersen's Lagrangian, defined in Eq.(16), we have,

$$\frac{\partial \mathcal{L}_A}{\partial \dot{\mathbf{s}}_i} = m_i \Omega^{2/3} \dot{\mathbf{s}}_i \tag{35}$$

$$\frac{\partial \mathcal{L}_A}{\partial \dot{\Omega}} = M\dot{\Omega} \tag{36}$$

$$\frac{\partial \mathcal{L}_A}{\partial \mathbf{s}_i} = -\frac{\partial U\left(\{\Omega^{1/3}\mathbf{s}_i\}\right)}{\partial \mathbf{s}_i} \tag{37}$$

$$\frac{\partial \mathcal{L}_A}{\partial \Omega} = \frac{1}{3\Omega^{1/3}}\sum_i m_i |\dot{\mathbf{s}}_i|^2 - \frac{\partial U\left(\{\Omega^{1/3}\mathbf{s}_i\}\right)}{\partial \Omega} - P \tag{38}$$

The Lagrange's equation of motion for the scaled coordinates of particle i is

$$\begin{aligned} &\frac{d}{dt}\left(m_i \Omega^{2/3}\dot{\mathbf{s}}_i\right) + \frac{\partial U\left(\{\Omega^{1/3}\mathbf{s}_i\}\right)}{\partial \mathbf{s}_i} = 0 \\ \Longrightarrow\quad &\boxed{\ddot{\mathbf{s}}_i = -\frac{2}{3}\Omega^{-1}\dot{\Omega}\dot{\mathbf{s}}_i - \frac{1}{m_i\Omega^{2/3}}\frac{\partial U\left(\{\Omega^{1/3}\mathbf{s}_i\}\right)}{\partial \mathbf{s}_i}} \end{aligned} \tag{39}$$

The Lagrange's equation for the volume is

$$\begin{aligned} &\frac{d}{dt}\left(M\dot{\Omega}\right) - \frac{1}{3\Omega^{1/3}}\sum_i m_i|\dot{\mathbf{s}}_i|^2 + \frac{\partial U\left(\{\Omega^{1/3}\mathbf{s}_i\}\right)}{\partial \Omega} + P = 0 \\ \Longrightarrow\quad &\boxed{\ddot{\Omega} = \frac{1}{3M\Omega}\left(\sum_i m_i \Omega^{2/3}|\dot{\mathbf{s}}_i|^2 - 3\Omega\frac{\partial U\left(\{\Omega^{1/3}\mathbf{s}_i\}\right)}{\partial \Omega} - 3P\Omega\right)} \end{aligned} \tag{40}$$

These equations can be expressed in terms of real coordinates as

$$\ddot{\mathbf{r}}_i = -\frac{2\dot{\Omega}}{3\Omega}\dot{\mathbf{r}}_i - \frac{1}{m_i}\frac{\partial U\left(\{\mathbf{r}_i\}\right)}{\partial \mathbf{r}_i} \tag{41}$$

$$\begin{aligned}\ddot{\Omega} &= \frac{1}{M}\left\{\frac{1}{3\Omega}\left[\sum_i m_i|\dot{\mathbf{r}}_i|^2 - \sum_i \mathbf{r}_i \cdot \frac{\partial U\left(\{\mathbf{r}_i\}\right)}{\partial \mathbf{r}_i}\right] - P\right\} \\ &= \frac{1}{M}\left(P_{Virial} - P\right) \end{aligned} \tag{42}$$

When going from Eq. (40) to Eq. (42), we have used the following identities.

$$\begin{aligned}\frac{\partial U\left(\{\Omega^{1/3}\mathbf{s}_i\}\right)}{\partial\Omega} &= \sum_i \frac{\partial U\left(\{\Omega^{1/3}\mathbf{s}_i\}\right)}{\partial\left(\Omega^{1/3}\mathbf{s}_i\right)}\cdot\frac{\partial\left(\Omega^{1/3}\mathbf{s}_i\right)}{\partial\Omega} \\ &= \frac{1}{3\Omega^{2/3}}\sum_i \mathbf{s}_i\cdot\frac{\partial U\left(\{\Omega^{1/3}\mathbf{s}_i\}\right)}{\partial\left(\Omega^{1/3}\mathbf{s}_i\right)} = \sum_i \frac{\mathbf{r}_i}{3\Omega}\cdot\frac{\partial U\left(\{\mathbf{r}_i\}\right)}{\partial\mathbf{r}_i}\end{aligned}$$

A.2 Hamilton's equations of motion

The momenta $\mathbf{p}_i^s$ and Π, conjugate to $\mathbf{s}_i$ and Ω, are defined as the following.

$$\mathbf{p}_i^s \equiv \frac{\partial\mathcal{L}_A}{\partial\dot{\mathbf{s}}_i} = m_i\Omega^{2/3}\,\dot{\mathbf{s}}_i \tag{43}$$

$$\Pi \equiv \frac{\partial\mathcal{L}_A}{\partial\dot{\Omega}} = M\,\dot{\Omega} \tag{44}$$

Andersen's Hamiltonian $\mathcal{H}_A$ is then obtained through Legendre's transform.

$$\begin{aligned}\mathcal{H}_A &= \sum_i \mathbf{p}_i^s\cdot\dot{\mathbf{s}}_i + \Pi\dot{\Omega} - \mathcal{L} \\ &= \sum_i \mathbf{p}_i^s\cdot\frac{\mathbf{p}_i^s}{m_i\Omega^{2/3}} + \Pi\frac{\Pi}{M} - \mathcal{L} \\ &= \frac{1}{2}\sum_i \frac{|\mathbf{p}_i^s|^2}{m_i\Omega^{2/3}} + U(\{\Omega^{1/3}\mathbf{s}_i\}) + \frac{\Pi^2}{2M} + P\Omega\end{aligned} \tag{45}$$

The Hamilton's equations of motion are

$$\dot{\mathbf{p}}_i^s = -\frac{\partial\mathcal{H}_A}{\partial\mathbf{s}_i} = -\frac{\partial U(\{\Omega^{1/3}\mathbf{s}_i\})}{\partial\mathbf{s}_i} \tag{46}$$

$$\dot{\mathbf{s}}_i = \frac{\partial\mathcal{H}_A}{\partial\mathbf{p}_i^s} = \frac{\mathbf{p}_i^s}{m_i\Omega^{2/3}} \tag{47}$$

$$\dot{\Pi} = -\frac{\partial\mathcal{H}_A}{\partial\Omega} = \frac{1}{3\Omega^{5/3}}\sum_i\frac{|\mathbf{p}_i^s|^2}{m_i} - \frac{\partial U\left(\{\Omega^{1/3}\mathbf{s}_i\}\right)}{\partial\Omega} - P \tag{48}$$

$$\dot{\Omega} = \frac{\partial\mathcal{H}_A}{\partial\Pi} = \frac{\Pi}{M} \tag{49}$$

Defining the conjugate momenta for $\mathbf{r}_i$ as

$$\mathbf{p}_i \equiv \frac{\partial\mathcal{L}_A}{\partial\dot{\mathbf{r}}_i} = m_i\dot{\mathbf{r}}_i = \frac{\mathbf{p}_i^s}{\Omega^{1/3}} \tag{50}$$

we can express the above equations of motion in terms of real coordinates.

$$\dot{\mathbf{p}}_i = -\frac{1}{3}\frac{d(\ln\Omega)}{dt}\mathbf{p}_i - \frac{\partial U(\{\mathbf{r}_i\})}{\partial\mathbf{r}_i} = -\frac{\Pi}{3M\Omega}\mathbf{p}_i - \frac{\partial U(\{\mathbf{r}_i\})}{\partial\mathbf{r}_i} \tag{51}$$

$$\dot{\mathbf{r}}_i = \frac{1}{3}\frac{d(\ln\Omega)}{dt}\mathbf{r}_i + \frac{\mathbf{p}_i}{m_i} = \frac{\Pi}{3M\Omega}\mathbf{r}_i + \frac{\mathbf{p}_i}{m_i} \tag{52}$$

$$\dot{\Pi} = \frac{1}{3\Omega}\left(\sum_i \frac{|\mathbf{p}_i|^2}{m_i} - \sum_i \mathbf{r}_i \cdot \frac{\partial U\left(\{\mathbf{r}_i\}\right)}{\partial \mathbf{r}_i} - 3\Omega P\right) \tag{53}$$

$$\dot{\Omega} = \frac{\Pi}{M} \tag{54}$$

Eqs. (46)-(49) are Hamilton's equations of motion, but Eqs. (51)-(54) are not. Nonetheless, if we express $\mathcal{H}_A$ as a function of $\mathbf{r}_i$, $\mathbf{p}_i$, Ω, Π, it is still a conserved quantity. The following identity can be easily verified by plugging in Eqs. (51)-(54).

$$\frac{d\mathcal{H}_A\left(\mathbf{r}_i, \mathbf{p}_i, \Omega, \Pi\right)}{dt} = \sum_i \frac{\partial \mathcal{H}_A}{\partial \mathbf{r}_i} \cdot \dot{\mathbf{r}}_i + \sum_i \frac{\partial \mathcal{H}_A}{\partial \mathbf{p}_i} \cdot \dot{\mathbf{p}}_i + \frac{\partial \mathcal{H}_A}{\partial \Omega}\dot{\Omega} + \frac{\partial \mathcal{H}_A}{\partial \Pi}\dot{\Pi} = 0. \tag{55}$$

B Derivation of Parrinello-Rahman's Dynamics

B.1 Pure hydrostatic pressure

B.1.1 Lagrange's equations of motion

From Parrinello-Rahman's Lagrangian $\mathcal{L}_{\mathrm{PR}}$, defined in Eq. (29), we have

$$\frac{\partial \mathcal{L}_{\mathrm{PR}}}{\partial \dot{\mathbf{s}}_i} = m_i \mathbf{G}\dot{\mathbf{s}}_i \tag{56}$$

$$\frac{\partial \mathcal{L}_{\mathrm{PR}}}{\partial \dot{\mathbf{h}}} = M\dot{\mathbf{h}} \tag{57}$$

$$\frac{\partial \mathcal{L}_{\mathrm{PR}}}{\partial \mathbf{s}_i} = -\frac{\partial U\left(\{\mathbf{h}\mathbf{s}_i\}\right)}{\partial \mathbf{s}_i} \tag{58}$$

$$\frac{\partial \mathcal{L}_{\mathrm{PR}}}{\partial \mathbf{h}} = \sum_i^N m_i \mathbf{h}\,\dot{\mathbf{s}}_i \otimes \dot{\mathbf{s}}_i - \frac{\partial U\left(\{\mathbf{h}\mathbf{s}_i\}\right)}{\partial \mathbf{h}} - P\boldsymbol{\Xi} \tag{59}$$

where $\boldsymbol{\Xi} \equiv \partial \det(\mathbf{h})/\partial \mathbf{h} = (\det \mathbf{h})\,\mathbf{h}^{-T}$. The first term on the right hand side of Eq. (59) is obtained from the following derivation.

$$\begin{aligned}
\frac{\partial \dot{\mathbf{s}}_i^T \mathbf{G}\dot{\mathbf{s}}_i}{\partial \mathbf{h}} &= \frac{\partial \dot{\mathbf{s}}_i^T \mathbf{h}^T \mathbf{h}\dot{\mathbf{s}}_i}{\partial \mathbf{h}} = \frac{\partial\left(\left(\mathbf{h}\dot{\mathbf{s}}_i\right)^T \mathbf{h}\mathbf{s}_i\right)}{\partial \mathbf{h}} \\
&= \frac{\partial H_{\alpha\beta}\left(\dot{\mathbf{s}}_i\right)_\beta H_{\alpha\gamma}\left(\dot{\mathbf{s}}_i\right)_\gamma}{\partial H_{pq}}\mathbf{e}_p \otimes \mathbf{e}_q \\
&= \left(\delta_{\alpha p}\delta_{\beta q}\left(\dot{\mathbf{s}}_i\right)_\beta H_{\alpha\gamma}\left(\dot{\mathbf{s}}_i\right)_\gamma + \delta_{\alpha p}\delta_{\gamma q}\left(\dot{\mathbf{s}}_i\right)_\beta H_{\alpha\beta}\left(\dot{\mathbf{s}}_i\right)_\gamma\right)\mathbf{e}_p \otimes \mathbf{e}_q \\
&= \left(\left(\dot{\mathbf{s}}_i\right)_q H_{p\gamma}\left(\dot{\mathbf{s}}_i\right)_\gamma + H_{p\beta}\left(\dot{\mathbf{s}}_i\right)_\beta \left(\dot{\mathbf{s}}_i\right)_q\right)\mathbf{e}_p \otimes \mathbf{e}_q \\
&= 2H_{p\beta}\left(\dot{\mathbf{s}}_i\right)_\beta \left(\dot{\mathbf{s}}_i\right)_q \mathbf{e}_p \otimes \mathbf{e}_q = \left(\mathbf{h}\dot{\mathbf{s}}_i\right) \otimes \dot{\mathbf{s}}_i
\end{aligned}$$

The Lagrange's equation of motion for the scaled coordinate $\mathbf{s}_i$ is

$$\frac{d}{dt}\left(m_i \mathbf{G}\dot{\mathbf{s}}_i\right) + \frac{\partial U\left(\{\mathbf{h}\mathbf{s}_i\}\right)}{\partial \mathbf{s}_i} = 0$$

$$\Longrightarrow \quad \boxed{\ddot{\mathbf{s}}_i = -\mathbf{G}^{-1}\dot{\mathbf{G}}\dot{\mathbf{s}}_i - \frac{\mathbf{G}^{-1}}{m_i}\frac{\partial U\left(\{\mathbf{h}\mathbf{s}_i\}\right)}{\partial \mathbf{s}_i}} \tag{60}$$

The Lagrange's equation of motion for matrix $\mathbf{h}$ is

$$\frac{d}{dt}\left(M\dot{\mathbf{h}}\right) - \sum_i m_i \mathbf{h}\,\dot{\mathbf{s}}_i \otimes \dot{\mathbf{s}}_i + \frac{\partial U\left(\{\mathbf{h}\mathbf{s}_i\}\right)}{\partial \mathbf{h}} + P\boldsymbol{\Xi} = 0$$

$$\Longrightarrow \quad \boxed{\ddot{\mathbf{h}} = \frac{1}{M}\left(\sum_i m_i \mathbf{h}\,\dot{\mathbf{s}}_i \otimes \dot{\mathbf{s}}_i - \frac{\partial U\left(\{\mathbf{h}\mathbf{s}_i\}\right)}{\partial \mathbf{h}} - P\boldsymbol{\Xi}\right)} \tag{61}$$

These two equations can be rewritten in terms of real space coordinates $\mathbf{r}_i$ and Virial stress tensor $\boldsymbol{\sigma}_{Virial}$ as,

$$\ddot{\mathbf{r}}_i = -\left(\mathbf{h}^T\right)^{-1}\dot{\mathbf{G}}\mathbf{h}^{-1}\dot{\mathbf{r}}_i - \frac{1}{m_i}\frac{\partial U\left(\{\mathbf{r}_i\}\right)}{\partial \mathbf{r}_i} \tag{62}$$

$$\ddot{\mathbf{h}} = -\frac{1}{M}\left(\boldsymbol{\sigma}_{Virial} + P\mathbf{I}\right)\boldsymbol{\Xi} \tag{63}$$

where $\ddot{\mathbf{r}}_i = \mathbf{h}\ddot{\mathbf{s}}_i$, $\dot{\mathbf{r}}_i = \mathbf{h}\dot{\mathbf{s}}_i$ and

$$\begin{aligned}
\boldsymbol{\sigma}_{Virial} &\equiv \frac{1}{\Omega}\sum_i \left\{-m_i\dot{\mathbf{r}}_i \otimes \dot{\mathbf{r}}_i + (-\mathbf{r}_i)\otimes \mathbf{f}_i\right\} \\
&= \frac{1}{\Omega}\sum_i \left\{-m_i\dot{\mathbf{r}}_i \otimes \dot{\mathbf{r}}_i + \mathbf{f}_i \otimes (-\mathbf{r}_i)\right\} \\
&= \frac{1}{\Omega}\sum_i \left(-m_i\dot{\mathbf{r}}_i \otimes \dot{\mathbf{r}}_i + \frac{\partial U\left(\{\mathbf{r}_i\}\right)}{\partial \mathbf{r}_i}\otimes \mathbf{r}_i\right).
\end{aligned}$$

($\because$ $\sum_i \mathbf{r}_i \otimes \mathbf{f}_i$ is symmetric due to angular momentum conservation.)

For the derivation of Eq. (62) and (63), the following identities have been used.

$$\begin{aligned}
\frac{\partial U\left(\{\mathbf{h}\mathbf{s}_i\}\right)}{\partial \mathbf{s}_i} &= \left\{\frac{\partial U}{\partial H_{\alpha\beta}\left(\mathbf{s}_i\right)_\beta}\frac{\partial H_{\alpha\gamma}\left(\mathbf{s}_i\right)_\gamma}{\left(\mathbf{s}_i\right)_m}\right\}\mathbf{e}_m = \frac{\partial U}{\partial r_\alpha}H_{\alpha m}\mathbf{e}_m = \mathbf{h}^T\frac{\partial U\left(\{\mathbf{r}_i\}\right)}{\partial \mathbf{r}_i} \\
\frac{\partial U\left(\{\mathbf{h}\mathbf{s}_i\}\right)}{\partial \mathbf{h}} &= \sum_i^N \frac{\partial U}{\partial H_{ab}(\mathbf{s}_i)_b}\frac{\partial H_{ac}(\mathbf{s}_i)_c}{\partial H_{\alpha\beta}}\mathbf{e}_\alpha \otimes \mathbf{e}_\beta = \sum_i^N \frac{\partial U}{\partial (\mathbf{r}_i)_a}\delta_{a\alpha}\delta_{c\beta}(\mathbf{s}_i)_c\mathbf{e}_\alpha \otimes \mathbf{e}_\beta \\
&= \sum_i^N \frac{\partial U}{\partial (\mathbf{r}_i)_\alpha}(\mathbf{s}_i)_\beta\mathbf{e}_\alpha \otimes \mathbf{e}_\beta = \sum_i^N \frac{\partial U\left(\{\mathbf{r}_i\}\right)}{\partial \mathbf{r}_i}\otimes\left(\mathbf{h}^{-1}\mathbf{r}_i\right) \\
&= \sum_i^N \left(\frac{\partial U\left(\{\mathbf{r}_i\}\right)}{\partial \mathbf{r}_i}\otimes \mathbf{r}_i\right)\left(\mathbf{h}^{-1}\right)^T \\
\mathbf{h}\dot{\mathbf{s}}_i \otimes \dot{\mathbf{s}}_i &= \left(\mathbf{h}\dot{\mathbf{s}}_i\right)\otimes\left(\mathbf{h}^{-1}\mathbf{h}\dot{\mathbf{s}}_i\right) = \left(\mathbf{h}\dot{\mathbf{s}}_i\right)\otimes\left(\mathbf{h}\dot{\mathbf{s}}_i\right)\mathbf{h}^{-T} = \dot{\mathbf{r}}_i \otimes \dot{\mathbf{r}}_i\left(\mathbf{h}^{-1}\right)^T
\end{aligned}$$

B.1.2 Hamilton's equations of motion

The conjugate momenta $\mathbf{p}_i$ and $\mathbf{\Pi}$ for $\mathbf{s}_i$ and $\mathbf{h}$ are

$$\begin{aligned} \mathbf{p}_i &\equiv \frac{\partial \mathcal{L}_{\mathrm{PR}}}{\partial \dot{\mathbf{s}}_i} = m_i \mathbf{G} \dot{\mathbf{s}}_i \\ \mathbf{\Pi} &\equiv \frac{\partial \mathcal{L}_{\mathrm{PR}}}{\partial \dot{\mathbf{h}}} = M \dot{\mathbf{h}}. \end{aligned}$$

From this we obtain Parrinello-Rahman's Hamiltonian $\mathcal{H}_{\mathrm{PR}}$ by Legendre transform

$$\begin{aligned} \mathcal{H}_{\mathrm{PR}} &\equiv \sum_i^N \mathbf{p}_i \cdot \dot{\mathbf{s}}_i + \mathbf{\Pi} : \dot{\mathbf{h}} - \mathcal{L}_{\mathrm{PR}} \\ &= \frac{1}{2} \sum_i \frac{\mathbf{p}_i^T \mathbf{G}^{-1} \mathbf{p}_i}{m_i} + \frac{1}{2M} \mathbf{\Pi} : \mathbf{\Pi} + U\left(\{\mathbf{h}\mathbf{s}_i\}\right) + P \det \mathbf{h}. \end{aligned} \tag{64}$$

The Hamilton's equations of motion are

$$\dot{\mathbf{p}}_i \equiv -\frac{\partial \mathcal{H}_{\mathrm{PR}}}{\partial \mathbf{s}_i} = -\frac{\partial U\left(\{\mathbf{h}\mathbf{s}_i\}\right)}{\partial \mathbf{s}_i} = -\mathbf{h}^T \frac{\partial U\left(\{\mathbf{r}_i\}\right)}{\partial \mathbf{r}_i} \tag{65}$$

$$\dot{\mathbf{s}}_i \equiv \frac{\partial \mathcal{H}_{\mathrm{PR}}}{\partial \mathbf{p}_i} = \frac{1}{m_i} \mathbf{G}^{-1} \mathbf{p}_i \tag{66}$$

$$\begin{aligned} \dot{\mathbf{\Pi}} &\equiv -\frac{\partial \mathcal{H}_{\mathrm{PR}}}{\partial \mathbf{h}} = -\left[\frac{1}{\Omega} \sum_{i=1}^N \left(\frac{\partial U}{\partial \mathbf{r}_i} \otimes \mathbf{r}_i - \frac{\mathbf{p}_i \otimes \mathbf{p}_i}{m_i}\right) + P\mathbf{I}\right] \mathbf{\Xi} \\ &= -\left(\boldsymbol{\sigma}_{Virial} + P\mathbf{I}\right) \mathbf{\Xi} \end{aligned} \tag{67}$$

$$\dot{\mathbf{h}} \equiv \frac{\partial \mathcal{H}_{\mathrm{PR}}}{\partial \mathbf{\Pi}} = \frac{\mathbf{\Pi}}{M} \tag{68}$$

B.2 Arbitrary applied stress

Here we justify the term proposed by Parrinello and Rahman to describe the work done by the deviatoric (shear) components of the applied stress tensor. It amounts to the definition of the (average) strain $\boldsymbol{\epsilon}$ in the simulation cell. Once the strain is defined, the work done by the environment is simply

$$\Delta W = \boldsymbol{\sigma} : \boldsymbol{\epsilon}\, \Omega_0 \equiv \sigma_{ij} \epsilon_{ij}\, \Omega_0 \tag{69}$$

where Ω_0 is the volume of the simulation cell in a reference state, $\Omega_0 = \det \mathbf{h}_0$. $-\Delta W$ should replace $P\Omega$ in the PR Lagrangian defined in Eq. (29) to account for the general applied stress.

Consider an arbitrary point in the simulation cell with scaled coordinate $\mathbf{s}$. Its real coordinate at the reference state is $\mathbf{r}_0 = \mathbf{h}_0 \mathbf{s}$. When the matrix changes to $\mathbf{h}$, its real coordinate becomes $\mathbf{r} = \mathbf{h}\mathbf{s}$. Hence the displacement vector is

$$\mathbf{u} \equiv \mathbf{r} - \mathbf{r}_0 = \left(\mathbf{h} - \mathbf{h}_0\right) \mathbf{s} = \left(\mathbf{h}\mathbf{h}_0^{-1} - \mathbf{I}\right) \mathbf{r}_0 \tag{70}$$

The strain tensor is defined in the continuum mechanics as follows,[9]

$$\begin{aligned}
\boldsymbol{\epsilon} &\equiv \frac{1}{2}\left\{\nabla\mathbf{u} + (\nabla\mathbf{u})^T + (\nabla\mathbf{u})^T\nabla\mathbf{u}\right\} \\
&= \frac{1}{2}\left\{(\mathbf{h}\mathbf{h}_0^{-1} - \mathbf{I}) + (\mathbf{h}\mathbf{h}_0^{-1} - \mathbf{I})^T + (\mathbf{h}\mathbf{h}_0^{-1} - \mathbf{I})^T(\mathbf{h}\mathbf{h}_0^{-1} - \mathbf{I})\right\} \\
&= \frac{1}{2}\left(\mathbf{h}_0^{-T}\mathbf{h}^T\mathbf{h}\mathbf{h}_0^{-1} - \mathbf{I}\right) = \frac{1}{2}\left(\mathbf{h}_0^{-T}\mathbf{G}\mathbf{h}_0^{-1} - \mathbf{I}\right) \qquad (71)
\end{aligned}$$

Hence the energy term describing the environment should be

$$\begin{aligned}
-\Delta W &= -\boldsymbol{\sigma} : \boldsymbol{\epsilon}\ \Omega_0 \\
&= -(\boldsymbol{\sigma} + P\mathbf{I}) : \boldsymbol{\epsilon}\ \Omega_0 + P\mathbf{I} : \boldsymbol{\epsilon}\ \Omega_0 \\
&= -\mathrm{Tr}\left[(\boldsymbol{\sigma} + P\mathbf{I})\,\boldsymbol{\epsilon}\right]\ \Omega_0 + \mathrm{Tr}\left[\boldsymbol{\epsilon}\right]\ P\,\Omega_0 \\
&= -\mathrm{Tr}\left[(\boldsymbol{\sigma} + P\mathbf{I})\boldsymbol{\epsilon}\right]\Omega_0 + P\left(\frac{\Omega}{\Omega_0} - 1\right)\Omega_0 \\
&= -\mathrm{Tr}\left[(\boldsymbol{\sigma} + P\mathbf{I})\boldsymbol{\epsilon}\right]\Omega_0 + P\left(\Omega - \Omega_0\right) \\
&= -\frac{1}{2}\mathrm{Tr}\left[(\boldsymbol{\sigma} + P\mathbf{I})\left(\mathbf{h}_0^{-T}\mathbf{G}\mathbf{h}_0^{-1} - \mathbf{I}\right)\right]\Omega_0 + P\left(\Omega - \Omega_0\right) \\
&= P\Omega - \frac{\Omega_0}{2}\mathrm{Tr}\left[(\boldsymbol{\sigma} + P\mathbf{I})\mathbf{h}_0^{-T}\mathbf{G}\mathbf{h}_0^{-1}\right] - P\Omega_0 \\
&= P\Omega - \frac{\Omega_0}{2}\mathrm{Tr}\left[\mathbf{h}_0^{-1}(\boldsymbol{\sigma} + P\mathbf{I})\mathbf{h}_0^{-T}\mathbf{G}\right] - P\Omega_0 \\
&= P\Omega + \frac{\Omega_0}{2}\mathrm{Tr}\left(\boldsymbol{\Sigma}\mathbf{G}\right) - P\Omega_0 \qquad (72)
\end{aligned}$$

where $\boldsymbol{\Sigma} = -\mathbf{h}_0^{-1}(\boldsymbol{\sigma} + P\mathbf{I})\,\mathbf{h}_0^{-T}$. Then the new Parrinello and Rahman's Lagrangian $\mathcal{L}'_{\mathrm{PR}}$ becomes

$$\begin{aligned}
\mathcal{L}'_{\mathrm{PR}} &= \frac{1}{2}\sum_i^N m_i\dot{\mathbf{s}}_i^T\mathbf{G}\dot{\mathbf{s}}_i - U\left(\{\mathbf{h}\mathbf{s}_i\}\right) + \frac{1}{2}M\dot{\mathbf{h}} : \dot{\mathbf{h}} - P\Omega - \frac{\Omega_0}{2}\mathrm{Tr}\left(\boldsymbol{\Sigma}\mathbf{G}\right) \\
&= \mathcal{L}_{\mathrm{PR}} - \frac{\Omega_0}{2}\mathrm{Tr}\left(\boldsymbol{\Sigma}\mathbf{G}\right) \qquad (73)
\end{aligned}$$

where the constant term $-P\Omega_0$ is dropped, because it has no effect on the equations of motion. The additional term $\frac{\Omega_0}{2}\mathrm{Tr}\left(\boldsymbol{\Sigma}\mathbf{G}\right)$ produces the following changes to the derivative of Lagrangian, Hamiltonian and equations of motion

$$\frac{\partial\mathcal{L}'_{\mathrm{PR}}}{\partial\mathbf{h}} = \frac{\partial\mathcal{L}_{\mathrm{PR}}}{\partial\mathbf{h}} - \frac{\Omega_0}{2}\frac{\partial\left(\mathrm{Tr}\left(\boldsymbol{\Sigma}\mathbf{G}\right)\right)}{\partial\mathbf{h}} = \frac{\partial\mathcal{L}_{\mathrm{PR}}}{\partial\mathbf{h}} - \Omega_0\mathbf{H}\boldsymbol{\Sigma} \qquad (74)$$

$$\mathcal{H}'_{\mathrm{PR}} = \mathcal{H}_{\mathrm{PR}} + \frac{\Omega_0}{2}\mathrm{Tr}\left(\boldsymbol{\Sigma}\mathbf{G}\right) \qquad (75)$$

$$\dot{\boldsymbol{\Pi}} = -\frac{\partial\mathcal{H}'_{\mathrm{PR}}}{\partial\mathbf{h}} = -\frac{\partial\mathcal{H}_{\mathrm{PR}}}{\partial\mathbf{h}} - \frac{\Omega_0}{2}\frac{\partial\mathrm{Tr}\left(\boldsymbol{\Sigma}\mathbf{G}\right)}{\partial\mathbf{h}} = -\frac{\partial\mathcal{H}_{\mathrm{PR}}}{\partial\mathbf{h}} - \Omega_0\mathbf{h}\boldsymbol{\Sigma}. \qquad (76)$$

[9] $\mathbf{h}_0^{-T} \equiv (\mathbf{h}_0^{-1})^T$.

References

[1] R. E. Sonntag and G. J. Van Wylen "Introduction to Thermodynamics", John Wiley & Sons 3rd ed.

[2] Hans C. Andersen "Molecular dynamics simulations at constant pressures and/or temperature", *J. Chem. Phys* **72** 2384–2393 1980

[3] J. R. Ray and A. Rahman "Statistical ensembles and molecular dynamics studies of aniosotropic solids", *J. Chem. Phys* **80** 4423–4428 1984

[4] M. Parrinello and A. Rahman "Crystal structure and pair potentials: a molecular-dynamics study", *Physical Review Letters* **45** 1196–1199 1980

[5] M. Parrinello and A. Rahman "Polymorphic transition in single crystals: a new molecular dynamics method", *J. Appl. Phys.* **52** 7182–7190 1981

ME346 – Introduction to Molecular Simulations – Stanford University – Winter 2007

Handout 8. Constant Temperature Molecular Dynamics

Keonwook Kang and Wei Cai

February 10, 2007

1 Microcanonical (NVE) ensemble and entropy

The dynamical trajectory of a closed Hamiltonian system samples the microcanonical (NVE) ensemble (assuming the dynamics is ergodic), which corresponds to the following density distribution in phase space,

$$f_{NVE}(\{\mathbf{r}_i, \mathbf{p}_i\}) = \begin{cases} \frac{1}{\Omega(E,\delta E)} & \mathcal{H}(\{\mathbf{r}_i, \mathbf{p}_i\}) \in [E - \delta E, E] \\ 0 & \text{otherwise} \end{cases} \tag{1}$$

where δE is a small parameter and $\Omega(E, \delta E)$ is the normalization constant,

$$\Omega(E, \delta E) = \int_{E-\delta E \le \mathcal{H}(\{\mathbf{r}_i, \mathbf{p}_i\}) \le E} d^N\mathbf{r}\, d^N\mathbf{p} \tag{2}$$

which is the volume of the phase space covered by the microcanonical ensemble.

In thermodynamics, the number of particles N, volume V, and internal energy E always remain constants for a closed system (regardless of whether or not it is in equilibrium). As the system approaches equilibrium, its entropy S reaches a maximum. This maximum value of entropy S is a function of N, V and E. The function $S(N, V, E)$ itself depends on the nature of the system (e.g. whether it consists of hydrogen or water molecules) and is called the (equilibrium) *equation of state*.

Statistical mechanics provides the following microscopic expression for the entropy and hence for the equation of state.[1]

$$S(N, V, E) = k_B \ln \tilde{\Omega}(N, V, E) \tag{3}$$

$$\tilde{\Omega}(N, V, E) = \frac{\Omega(E, \delta E)}{N!\, h^{3N}} \tag{4}$$

where $k_B = 1.381 \times 10^{-23}\text{J} \cdot \text{K}^{-1} = 8.617 \times 10^{-5}\text{eV} \cdot \text{K}^{-1}$ is Boltzmann's constant, $h = 6.626 \times 10^{-34}\text{J}\cdot\text{s} = 4.136 \times 10^{-15}\text{eV}\cdot\text{s}$ is Planck's constant. $\tilde{\Omega}$ is the number of distinguishable

[1] This is consistent with the definition of entropy (as lack of information) in information theory.

microscopic states in the phase space volume Ω.[2] Here for simplicity we assume that the system consists of N particles of the same species. The factor $N!$ accounts for the fact that one cannot distinguish these particles, i.e. exchanging the positions of two identical particles does not lead to a new microscopic state.

In the limit of large N, $\ln \Omega(E, \delta E)$ is insensitive to the choice of δE. Hence we have ignored the dependence of S on δE. There is a geometric interpretation for the insensitivity of S on δE. Consider a sphere with radius R in N-dimensional space.[3] For very large N, the volume of the entire sphere $r \leq R$ is very close to the volume of a very skin layer near its surface, $R - \delta R \leq r \leq R$. Therefore, it will not make a big difference in the value of S even if we redefine Ω to be the volume of all the phase space that satisfies $\mathcal{H}(\{\mathbf{r}_i, \mathbf{p}_i\}) \leq E$, i.e.

$$S(N, V, E) = k_B \ln \left[\frac{1}{N!\, h^{3N}} \int_{\mathcal{H}(\{\mathbf{r}_i, \mathbf{p}_i\}) \leq E} d^N \mathbf{r}\, d^N \mathbf{p} \right] \tag{5}$$

In this case, the dependence on δE is completely removed.

2 Canonical (NVT) ensemble and free energy

In thermodynamics, temperature T is defined through the derivative of the equation of state $S(N, V, E)$,

$$\frac{1}{T} \equiv \left(\frac{\partial S}{\partial E} \right)_{N,V} \tag{6}$$

We can also rewrite the equation of state as $E(N, V, S)$ and temperature can be written as

$$T \equiv \left(\frac{\partial E}{\partial S} \right)_{N,V} \tag{7}$$

The physical meaning of function $E(N, V, S)$ is the following. Imagine a system with a fixed number of particles N, and a constant volume V. The system can exchange heat with its environment in such a way that its entropy S remains constant (which is very difficult to do in practice). The second law of thermodynamics states that, as the system approaches equilibrium under such a constraint, its internal energy goes to a minimum. The internal energy at equilibrium is a function of N, V, and S. The function $E(N, V, S)$ depends on the nature of the system and is the equation of state of the system.

In practice, it is impossible to keep the entropy of a system at a constant. It is much easier to control the temperature of the system. Therefore, the equation of state will be easier to use if it is expressed in terms of the temperature T. This can be done by Legendre transformation,

$$A = E - TS \tag{8}$$

[2] Heisenberg's uncertainty principle in quantum mechanics states that one cannot measure the position x and the momentum p_x of a particle with infinite accuracy. The minimum value for the product of the standard deviations, $\Delta x \Delta p_x$ is on the order of h.

[3] A specific example is the constant energy shell of a system consisting of N harmonic oscillators, $H(\{x_i, p_i\}) = \sum_{i=1}^{N} \frac{1}{2} k x_i^2 + \frac{1}{2m} p_i^2$, with $k = 1$ and $m = 1$.

where A is called the Helmholtz free energy. Because E is a function of N, V and S,

$$dE = \left(\frac{\partial E}{\partial N}\right)_{V,S} dN + \left(\frac{\partial E}{\partial N}\right)_{N,S} dV + \left(\frac{\partial E}{\partial N}\right)_{N,V} dS \tag{9}$$

Define chemical potential μ and pressure P as

$$\mu \equiv \left(\frac{\partial E}{\partial N}\right)_{V,S} \tag{10}$$

$$P \equiv -\left(\frac{\partial E}{\partial V}\right)_{N,S} \tag{11}$$

we have

$$dE = \mu dN - PdV + TdS \tag{12}$$

$$dA = dE - (TdS + SdT) = \mu dN - PdV - SdT \tag{13}$$

This means that A is a function of N, V and T. The function $A(N, V, T)$ is the equation of state we are looking for.

The transform from $E(N, V, S)$ to $A(N, V, T)$ in thermodynamics corresponds to the construction of the canonical (NVT) ensemble from the microcanonical (NVE) ensemble in statistical mechanics. Statistical mechanics also gives a microscopic expression for the Helmholtz free energy A and hence for the equation of state.

To construct the canonical (NVT) ensemble, imagine a system with fixed number of particles N and constant volume V that can exchange heat ΔQ with its environment, which is a large heat reservoir (thermostat). The environment cannot do any work to the system, i.e. $\Delta W = 0$. From the first law of thermodynamics, the change of internal energy of the system is $\Delta E = \Delta Q$. The system and the reservoir together can be considered as a closed system, which can be described by the microcanonical ensemble when they have reached equilibrium.

We will use the $\hat{}$ symbol to represent the variables for the thermostat. For example, $\hat{S}(\hat{N}, \hat{V}, \hat{E})$ is the equation of state for the thermostat, and $\hat{S} \gg S$, $\hat{N} \gg N$, $\hat{E} \gg E$. The total energy of the system and the thermostat together is $E_0 = E + \hat{E}$, which remains a constant. The joint distribution in the phase space of the system and the thermostat at equilibrium is

$$f(\{\mathbf{r}_i, \mathbf{p}_i\}, \{\hat{\mathbf{r}}_i, \hat{\mathbf{p}}_i\}) = \begin{cases} \text{const.} & \mathcal{H}(\{\mathbf{r}_i, \mathbf{p}_i\}) + \hat{E} \in [E_0 - \delta E, E_0] \\ 0 & \text{otherwise} \end{cases} \tag{14}$$

To find the distribution of the system itself, we need to integrate over all the thermostat variables,

$$f(\{\mathbf{r}_i, \mathbf{p}_i\}) \propto \int d^{\hat{N}}\mathbf{r}_i \, d^{\hat{N}}\mathbf{p}_i \; \delta(E_0 - \mathcal{H}(\{\mathbf{r}_i, \mathbf{p}_i\}) - \hat{E}) \tag{15}$$

$$\propto \hat{\Omega}(\hat{N}, \hat{V}, E_0 - \mathcal{H}(\{\mathbf{r}_i, \mathbf{p}_i\})) \tag{16}$$

$$\propto \exp\left[\frac{1}{k_B}\hat{S}(\hat{N}, \hat{V}, E_0 - \mathcal{H}(\{\mathbf{r}_i, \mathbf{p}_i\}))\right] \tag{17}$$

where $\hat{\Omega}$ is the volume occupied by thermostat variables in the phase space that satisfies the constraint $\hat{E} = E_0 - \mathcal{H}(\{\mathbf{r}_i, \mathbf{p}_i\})$.

The temperature of the thermostat is

$$T = \left[\left(\frac{\partial \hat{S}}{\partial \hat{E}} \right)_{\hat{N},\hat{V}} \right]^{-1} \tag{18}$$

Because the thermostat is much bigger than the system, putting it in contact with the system will not change its temperature.[4] We can Taylor expand $\hat{S}$ with respect to $\hat{E}$ around E_0 and only keep the first two terms,

$$\hat{S}(\hat{N}, \hat{V}, \hat{E}) = \hat{S}(\hat{N}, \hat{V}, E_0) - \frac{\mathcal{H}(\{\mathbf{r}_i, \mathbf{p}_i\})}{T} \tag{19}$$

Plug this expression into Eq. (17), we have

$$f(\{\mathbf{r}_i, \mathbf{p}_i\}) \;\propto\; \exp\left[-\frac{\mathcal{H}(\{\mathbf{r}_i, \mathbf{p}_i\})}{k_B T} \right] \tag{20}$$

The proportional constant can be determined by the normalization condition,

$$\int d^N\mathbf{r}_i \, d^N\mathbf{p}_i \, f(\{\mathbf{r}_i, \mathbf{p}_i\}) = 1 \tag{21}$$

The final expression for the canonical (NVT) ensemble is

$$f_{NVT}(\{\mathbf{r}_i, \mathbf{p}_i\}) = \frac{1}{Z(N,V,T)} \exp\left[-\frac{\mathcal{H}(\{\mathbf{r}_i, \mathbf{p}_i\})}{k_B T} \right] \tag{22}$$

$$Z(N,V,T) = \int d^N\mathbf{r}_i \, d^N\mathbf{p}_i \exp\left[-\frac{\mathcal{H}(\{\mathbf{r}_i, \mathbf{p}_i\})}{k_B T} \right] \tag{23}$$

This is also called Boltzmann's distribution. It is characterized by a single parameter T, which is a property of the thermostat defined through Eq. (18). We can also obtain the microscopic expression for the Helmholtz free energy A in terms of N, V, T (derivation omitted here).

$$\exp\left[-\frac{A(N,V,T)}{k_B T} \right] = \frac{1}{N!\, h^{3N}} Z(N,V,T) \tag{24}$$

$$\begin{aligned} A(N,V,T) &= -k_B T \, \ln\left[\frac{1}{N!\, h^{3N}} Z(N,V,T) \right] \\ &= -k_B T \, \ln\left\{ \frac{1}{N!\, h^{3N}} \int d^N\mathbf{r}_i \, d^N\mathbf{p}_i \exp\left[-\frac{\mathcal{H}(\{\mathbf{r}_i, \mathbf{p}_i\})}{k_B T} \right] \right\} \end{aligned} \tag{25}$$

This is the (NVT) counterpart of Eq. (5) in the (NVE) ensemble.

[4] Instead, the system will go to temperature T when it reaches equilibrium.

3 Nosé's Thermostat

Shūichi Nosé proposed an extended Lagrangian from which we can derive a set of equations of motion which will sample the canonical (NVT) ensemble [2]. The basic idea is to introduce a new (thermostat) variable s that can exchange heat with the system by scaling its velocities. The extended Lagrangian is

$$\mathcal{L} = \sum_i \frac{m_i}{2} s^2 \dot{\mathbf{r}}_i^2 - U(\{\mathbf{r}_i\}) + \frac{Q}{2}\dot{s}^2 - g k_B T_{\mathsf{obj}} \ln s. \tag{26}$$

where Q is the "thermal mass" associated to s, $g = dN+1$ and d is the number of dimensions (d=3 for 3-dimension),[5] and T_{obj} is the temperature we wish to apply to the simulation cell. We can show that Nosé's dynamics samples the canonical ensemble if the total energy (system plus thermostat) is the only conserved quantity along the trajectory (i.e. the trajectory is ergodic).

3.1 Scaling the time axis

Nosé stated that [2] it is conceptually more appropriate to interpret s as a time scaling variable, i.e.,

$$\Delta t' = \Delta t / s \tag{27}$$

where $\Delta t'$ is the real time step and Δt is the scaled time step.[6] From now on, we will denote a physical quantity expressed in real time axis with a prime ($'$) and that expressed in scaled time axis without the prime. For example, $\dot{\mathbf{r}}_i' \equiv d\mathbf{r}_i/dt'$ and $\dot{\mathbf{r}}_i \equiv d\mathbf{r}_i/dt$ are velocities of particle i in real time frame and scaled time frames respectively and they are related by $\dot{\mathbf{r}}_i' = \dot{\mathbf{r}}_i \cdot s$. $\mathbf{p}_i'$ is the momentum of particle i in real time frame and $\mathbf{p}_i$ is the momentum in real time frame. They are related by $\mathbf{p}_i' = \mathbf{p}_i/s$. The equation of motion directly obtained from the Nosé Lagrangian exists in the scaled time frame. The distribution of real-time-frame quantities satisfy the canonical distribution. The potential energy term $g k_B T_{\mathsf{obj}} \ln s$ is a clever choice because it is essential to the proof that the Nosé dynamics samples the canonical ensemble [2].

3.2 Lagrange's equations of motion

From the Nosé Lagrangian in Eq.(26), we have

$$\frac{\partial \mathcal{L}}{\partial \dot{\mathbf{r}}_i} = m_i s^2 \dot{\mathbf{r}}_i \tag{28}$$

$$\frac{\partial \mathcal{L}}{\partial \dot{s}} = Q\dot{s} \tag{29}$$

$$\frac{\partial \mathcal{L}}{\partial \mathbf{r}_i} = -\frac{U(\{\mathbf{r}_i\})}{\mathbf{r}_i} \tag{30}$$

[5] When the total momentum is conserved, g should be replaced with $g = d(N-1)+1$. In this case the canonical ensemble is generated only if the center-of-mass momentum is zero, see Appendix B.2 of Ref.[4].

[6] The idea of scaling traces back to Andersen's 1980 paper [3], in which he introduced a length scaling variable to achieve constant pressure.

$$\frac{\partial \mathcal{L}}{\partial s} = \sum_i m_i s \, |\dot{\mathbf{r}}_i|^2 - \frac{g}{\beta s} \tag{31}$$

where $\beta = 1/(kT_{\mathsf{obj}})$. Lagrange's equation of motion for particles is,

$$\begin{aligned} & \frac{d}{dt}\Big(\frac{\partial \mathcal{L}}{\partial \dot{\mathbf{r}}_i}\Big) - \frac{\partial \mathcal{L}}{\partial \mathbf{r}_i} = 0 \\ \Longrightarrow \quad & \boxed{\ddot{\mathbf{r}}_i = -\frac{2}{s}\dot{s}\,\dot{\mathbf{r}}_i - \frac{1}{m_i s^2}\frac{\partial U(\{\mathbf{r}_i\})}{\partial \mathbf{r}_i}} \end{aligned} \tag{32}$$

Eq. (32) can be rewritten in real time axis as,[7]

$$\ddot{\mathbf{r}}'_i = -\frac{2}{s}\frac{ds}{dt'}\dot{\mathbf{r}}'_i - \frac{1}{m_i}\frac{\partial U(\{\mathbf{r}'_i\})}{\partial \mathbf{r}'_i} \tag{33}$$

Similarly, Lagrange's equation of motion for s is

$$\begin{aligned} & \frac{d}{dt}\Big(\frac{\partial \mathcal{L}}{\partial \dot{s}}\Big) - \frac{\partial \mathcal{L}}{\partial s} = 0 \\ \Longrightarrow \quad & \boxed{Q\ddot{s} = \sum_i m_i s \, \dot{\mathbf{r}}_i^2 - \frac{g}{\beta s}} \end{aligned} \tag{34}$$

Eq. (34) can be rewritten in real time axis as,

$$\frac{d^2 s}{dt'^2} = \frac{1}{Q}\left(\sum_i m_i s |\dot{\mathbf{r}}'_i|^2 - \frac{gs}{\beta}\right) \tag{35}$$

3.3 Hamilton's equation of motion

The conjugate momentua $\mathbf{p}_i$ and p_s for $\mathbf{r}_i$ and s are

$$\mathbf{p}_i \equiv \frac{\partial \mathcal{L}}{\partial \dot{\mathbf{r}}_i} = m_i s^2 \dot{\mathbf{r}}_i \tag{36}$$

$$p_s \equiv \frac{\partial \mathcal{L}}{\partial \dot{s}} = Q\dot{s} \tag{37}$$

The Nosé Hamiltonian $\mathcal{H}$ is

$$\begin{aligned} \mathcal{H} &= \sum_i \mathbf{p}_i \cdot \dot{\mathbf{r}}_i + p_s \dot{s} - \mathcal{L} \\ &= \frac{1}{2}\sum_i \frac{|\mathbf{p}_i|^2}{m_i s^2} + U(\{\mathbf{r}_i\}) + \frac{p_s^2}{2Q} + \frac{g \ln s}{\beta} \end{aligned} \tag{38}$$

[7] $\dot{\mathbf{r}}'_i \equiv d\mathbf{r}_i/dt' = s d\mathbf{r}_i/dt = s\dot{\mathbf{r}}_i$, $\ddot{\mathbf{r}}'_i \equiv d^2\mathbf{r}_i/dt'^2 = s^2 d^2\mathbf{r}_i/d^2 t = s^2\ddot{\mathbf{r}}_i$.

Hamilton's equations of motion are

$$\dot{\mathbf{p}}_i \equiv -\frac{\partial \mathcal{H}}{\partial \mathbf{r}_i} = -\frac{\partial U(\{\mathbf{r}_i\})}{\partial \mathbf{r}_i} \tag{39}$$

$$\dot{\mathbf{r}}_i \equiv \frac{\partial \mathcal{H}}{\partial \mathbf{p}_i} = \frac{\mathbf{p}_i}{m_i s^2} \tag{40}$$

$$\dot{p}_s \equiv -\frac{\partial \mathcal{H}}{\partial s} = \sum_i \frac{|\mathbf{p}_i|^2}{m_i s^3} - \frac{g}{\beta s} \tag{41}$$

$$\dot{s} \equiv \frac{\partial \mathcal{H}}{\partial p_s} = \frac{p_s}{Q} \tag{42}$$

We can also express Eqs. (39)–(42) in real time frame. First, let us define the conjugate momenta $\mathbf{p}'_i$ and p'_s in real time frame are defined as

$$\mathbf{p}'_i \equiv \frac{\partial \mathcal{L}'}{\partial \dot{\mathbf{r}}'_i} = m_i \dot{\mathbf{r}}'_i = \mathbf{p}_i / s \tag{43}$$

$$p'_s \equiv \frac{\partial \mathcal{L}'}{\partial \dot{s}'} = \frac{Q}{s^2}\frac{ds}{dt'} = p_s / s, \tag{44}$$

Using Eqs. (39)–(42), the following equations of motion in terms of real-time quantities can be obtained.

$$\frac{d\mathbf{p}'_i}{dt'} = -\frac{s p'_s \mathbf{p}'_i}{Q} - \frac{\partial U(\{\mathbf{r}'_i\})}{\partial \mathbf{r}'_i} \tag{45}$$

$$\frac{d\mathbf{r}'_i}{dt'} = \frac{\mathbf{p}'_i}{m_i} \tag{46}$$

$$\frac{dp'_s}{dt'} = \left(\sum_i \frac{|\mathbf{p}'_i|^2}{m_i} - \frac{g}{\beta}\right)\frac{1}{s} - \frac{s {p'_s}^2}{Q} \tag{47}$$

$$\frac{ds}{dt'} = \frac{s^2 p'_s}{Q} \tag{48}$$

Eqs. (45)–(48) are no longer Hamilton's equations of motion. Nonetheless, they are preferred in Molecular Dynamics simulations than Eqs. (39)–(42), which require us to rescale the time step when computing time averages of physical quantities. Furthermore, the Hamiltonian defined in Eq. (38) can be written as a function of real-time variables,

$$\mathcal{H}'(\{\mathbf{r}_i, \mathbf{p}'_i\}, s, p'_s) = \frac{1}{2}\sum_i \frac{|\mathbf{p}'_i|^2}{m_i} + U(\{\mathbf{r}_i\}) + \frac{s^2 {p'_s}^2}{2Q} + \frac{g \ln s}{\beta} \tag{49}$$

It can be easily shown that $\mathcal{H}'$ is still conserved, i.e.,

$$\frac{d\mathcal{H}'}{dt'} = \sum_i \left\{ \frac{\partial \mathcal{H}'}{\partial \mathbf{p}'_i}\frac{d\mathbf{p}'_i}{dt'} + \frac{\partial \mathcal{H}'}{\partial \mathbf{r}'_i}\frac{d\mathbf{r}'_i}{dt'} \right\} + \frac{\partial \mathcal{H}'}{\partial p'_s}\frac{dp'_s}{dt'} + \frac{\partial \mathcal{H}'}{\partial s}\frac{ds}{dt'} = 0 \tag{50}$$

by plugging in Eqs. (45)–(48). However, we stress that function $\mathcal{H}'(\{\mathbf{r}_i, \mathbf{p}'_i\}, s, p'_s)$ is not a Hamiltonian, because it cannot be used to derive equations of motion. For example,

$$\frac{d\mathbf{p}'_i}{dt'} \neq -\frac{\partial \mathcal{H}'}{\partial \mathbf{r}_i} \tag{51}$$

4 Hoover's modification

Hoover [6] further simplified Eqs. (45)–(48) by introducing a new variable

$$\zeta \equiv p_s/Q = sp'_s/Q = \dot{s} = \frac{d(\ln s)}{dt'} \tag{52}$$

The real-time equations of motion now become

$$\frac{d\mathbf{p}'_i}{dt'} = -\frac{\partial U(\{\mathbf{r}'_i\})}{\partial \mathbf{r}'_i} - \zeta \mathbf{p}'_i \tag{53}$$

$$\frac{d\mathbf{r}'_i}{dt'} = \frac{\mathbf{p}'_i}{m_i} \tag{54}$$

$$\frac{d\zeta}{dt'} = \frac{1}{Q}\left(\sum_i \frac{|\mathbf{p}'_i|^2}{m_i} - \frac{g}{\beta}\right) \tag{55}$$

$$\frac{d(\ln s)}{dt'} = \zeta \tag{56}$$

The value for g now changes to $g = dN$ [8] (from $g = dN + 1$ in the original formulation of Nosé). Eqs. (53)–(55) are sufficient to generate the trajectory of the particles. However, Eq.(56) is still included in numerical implementations of the Nosé-Hoover thermostat, because $\ln s$ is needed to compute the conserved quantity $\mathcal{H}$, which is an important check for the self-consistency of the code. In summary, the equations of motion for the Nosé-Hoover dynamics can be written as,

$$\ddot{\mathbf{r}}'_i = -\frac{\partial U(\{\mathbf{r}_i\})}{m_i \partial \mathbf{r}_i} - \zeta \dot{\mathbf{r}}'_i \tag{57}$$

$$\dot{\zeta}' = \frac{1}{Q}\left(\sum_i m_i \, |\dot{\mathbf{r}}'_i|^2 - \frac{g}{\beta}\right) \tag{58}$$

and the quantity

$$\mathcal{H}' = \frac{1}{2}\sum_i m_i |\dot{\mathbf{r}}'_i|^2 + U(\{\mathbf{r}_i\}) + \frac{1}{2}Q\zeta^2 + \frac{g \ln s}{\beta} \tag{59}$$

is conserved. Eqs. (57) and (58) have a very simple interpretation. Define instantaneous temperature T_{inst} through the kinetic energy of the particles,

$$\frac{g}{2}k_B T_{\mathsf{inst}} = \sum_i \frac{1}{2} m_i \, |\dot{\mathbf{r}}'_i|^2 \tag{60}$$

Then Eq. (58) becomes,

$$\dot{\zeta}' = \frac{g k_B}{Q}\left(T_{\mathsf{inst}} - T_{\mathsf{obj}}\right) \tag{61}$$

This means that when T_{inst} is higher than the target temperature T_{obj}, it will cause ζ to increase. When ζ becomes positive, it will produce a viscous drag to the particle velocities. This is a feedback mechanism to make T_{inst} fluctuate around the target temperature T_{obj}.

[8] $g = d(N-1)$ when the center of mass motion is prohibited.

A Implementing Nosé-Hoover Algorithms in MD++

Here we present the implementation details of the Nosé-Hoover thermostat in MD++. For simplicity, we omit the prime symbol here even though we are discussing the real-time quantities. The equations of motion are

$$\ddot{\mathbf{r}}_i = \frac{\mathbf{F}_i}{m_i} - \zeta\,\dot{\mathbf{r}}_i \tag{62}$$

$$\dot{\zeta} = \frac{gk_B}{Q}(T_{\mathsf{inst}} - T_{\mathsf{obj}}) \tag{63}$$

$\ln s$, ζ, $\dot{\zeta}$ and Q corresponds to the following variables in MD++.

$$\ln s = \texttt{zeta} \tag{64}$$

$$\zeta = \frac{\texttt{zetav}}{\texttt{dt}} \tag{65}$$

$$\dot{\zeta} = \frac{2\,\texttt{zetaa}}{\texttt{dt}^2} \tag{66}$$

$$Q = \frac{gk_BT_{\mathsf{obj}}}{\texttt{vt2}} \tag{67}$$

In other words, the input variable `vt2` of MD++ corresponds to $\texttt{vt2} = gk_BT_{\mathsf{obj}}/Q$ (in s^{-2}). A typical setting is `vt2 = 1e28` (in s^{-2}), i.e. $10^4(\mathrm{ps}^{-2})$. This corresponds to a characteristic time for temperature fluctuation, $t_c = 1/\sqrt{\texttt{vt2}} = 0.01$ ps. The following quantity is computed by MD++ and should be conserved

$$\texttt{HELMP} = \frac{1}{2}\sum_i m_i|\dot{\mathbf{r}}_i|^2 + U(\{\mathbf{r}_i\}) + \frac{gk_BT_{\mathsf{obj}}}{2\,\texttt{vt2}}\frac{\texttt{zetav}^2}{\texttt{dt}^2} + gk_BT_{\mathsf{obj}}\;\texttt{zeta} \tag{68}$$

To use Nosé-Hoover thermostat in MD++, set `ensemble_type = NVT` in the input file before calling `run`. We can use either `integrator_type = Gear6` or `integrator_type = VVerlet`. There are three different implementations [8] for the Velocity-Verlet integrator in MD++, so we need to select `implementation_type` (see `integrators.cpp`). By default, `implementation_type = 0`, which corresponds to an implicit method. Define $G(t) \equiv \left[\sum_i m_i|\mathbf{v}_i(t)|^2 - 3Nk_BT_{\mathsf{obj}}\right]/Q$. The algorithm for `implementation_type = 0` is the following.

$$\begin{aligned}
\mathbf{v}_i(t+\Delta t/2) &= \mathbf{v}_i(t) + \left[\frac{\mathbf{F}_i(t)}{m_i} - \zeta(t)\mathbf{v}_i(t)\right]\Delta t/2 \\
\mathbf{r}_i(t+\Delta t) &= \mathbf{r}_i(t) + \mathbf{v}_i(t+\Delta t/2)\Delta t \\
\zeta(t+\Delta t/2) &= \zeta(t) + G(t)\,\Delta t/2 \\
\ln s(t+\Delta t) &= \ln s(t) + \zeta(t+\Delta t/2)\,\Delta t \\
\mathbf{v}_i(t+\Delta t) &= \mathbf{v}_i(\Delta t/2) + \left[\frac{\mathbf{F}_i(t+\Delta t)}{m_i} - \zeta(t+\Delta t)\,\mathbf{v}_i(t+\Delta t)\right]\Delta t/2 \\
\zeta(t+\Delta t) &= \zeta(t+\Delta t/2) + G(t+\Delta t)\,\Delta t/2
\end{aligned} \tag{69}$$

The last two equations has to be solved simultaneously, because $G(t+\Delta t)$ depends on the values of $\mathbf{v}_i(t+\Delta t)$. The solution is obtained by an iterative procedure.

`implementation_type = 1` corresponds to an explicit method

$$\begin{aligned}
\mathbf{v}_i(t+\Delta t/2) &= \mathbf{v}_i(t) + \left[\frac{\mathbf{F}_i(t)}{m_i} - \zeta(t)\,\mathbf{v}_i(t+\Delta t/2)\right]\Delta t/2 \\
\mathbf{r}_i(t+\Delta t) &= \mathbf{r}_i(t) + \mathbf{v}_i(t+\Delta t/2)\Delta t \\
\ln s(t+\Delta t) &= \ln s(t) + \zeta(t)\,\Delta t + G(t+\Delta t/2)\,\Delta t^2/2 \\
\zeta(t+\Delta t) &= \zeta(t) + G(t+\Delta t/2)\,\Delta t \\
\mathbf{v}_i(t+\Delta t) &= \mathbf{v}_i(\Delta t/2) + \left[\frac{\mathbf{F}_i(t+\Delta t)}{m_i} - \zeta(t+\Delta t)\,\mathbf{v}_i(t+\Delta t/2)\right]\Delta t/2
\end{aligned} \tag{70}$$

The first line looks like an implicit equation but it can be solved very easily (without any iteration).

`implementation_type = 2` corresponds to another explicit method.

$$\begin{aligned}
\zeta(t+\Delta t/2) &= \zeta(t) + G(t)\,\Delta t/2 \\
\ln s(t+\Delta t) &= \ln s(t) + \zeta(t+\Delta t/2)\,\Delta t \\
\mathbf{v}_i(t+\Delta t/2) &= \mathbf{v}_i(t)\exp\left[-\zeta(t+\Delta t/2)\,\Delta t/2\right] + \frac{\mathbf{F}_i(t)}{m_i}\,\Delta t/2 \\
\mathbf{r}_i(t+\Delta t) &= \mathbf{r}_i(t) + \mathbf{v}_i(t+\Delta t/2)\Delta t \\
\mathbf{v}_i(t+\Delta t) &= \left[\mathbf{v}_i(t+\Delta t/2) + \frac{\mathbf{F}_i(t+\Delta t)}{m_i}\Delta t/2\right]\exp\left[-\zeta(t+\Delta t/2)\Delta t/2\right] \\
\zeta(t+\Delta t) &= \zeta(t+\Delta t/2) + G(t+\Delta t)\,\Delta t/2
\end{aligned} \tag{71}$$

All three algorithms are time-reversible.

References

[1] David Chandler, "Introduction to Modern Statistical Mechanics", Oxford University Press, 1987.

[2] Shūichi Nosé "A molecular dynamics method for simulations in the canonical ensemble", *Molecular Physics* **52** 255–268 1984

[3] Hans C. Andersen "Molecular dynamics simulations at constant pressures and/or temperature", *J. Chem. Phys* **72** 2384–2393 1980

[4] Daan Frenkel and Berend Smit "Understanding Molecular Simulation from Algorithm to Applications", Academic Press 2002

[5] Shuichi Nosé "A unified formulation of the constant temperature molecular dynamics methods", *J. Chem. Phys.* **81** 511–519 1984

[6] William G. Hoover "Canonical dynamics: Equilibrium phase-space distributions", *Physical Review A*, **31** 1695–1697 1985

[7] MD++ code can be download from a link on *http://micro.stanford.edu/*

[8] Stephen D. Bond, Benedict J. Leimkuhler, and BrianB Laird "The Nosé–Poincaré method for constant temperature molecular dynamics", *Journal of Computational Physics* **151** 114–134 1999